NASA TECHNICAL REPORT

NASA TR R-366

EFFECTS OF THE ATMOSPHERIC-LITHOSTATIC PRESSURE RATIO ON EXPLOSIVE CRATERS IN DRY SOIL

by Robert W. Herr

Langley Research Center
Hampton, Va. 23365

NATIONAL AERONAUTICS AND SPACE ADMINISTRATION • WASHINGTON, D. C. • SEPTEMBER 1971

1. Report No.	2. Government Accession No.	3. Recipient's Catalog No.
NASA TR R-366		

4. Title and Subtitle	5. Report Date
EFFECTS OF THE ATMOSPHERIC-LITHOSTATIC PRESSURE RATIO ON EXPLOSIVE CRATERS IN DRY SOIL	September 1971
	6. Performing Organization Code
7. Author(s)	8. Performing Organization Report No.
Robert W. Herr	L-7380
	10. Work Unit No.
9. Performing Organization Name and Address	114-08-13-03
NASA Langley Research Center Hampton, Va. 23365	11. Contract or Grant No.
	13. Type of Report and Period Covered
12. Sponsoring Agency Name and Address	Technical Report
National Aeronautics and Space Administration Washington, D.C. 20546	14. Sponsoring Agency Code

15. Supplementary Notes

Technical Film Supplement L-1105 available on request.

16. Abstract

The effects of the atmospheric pressure on the size of explosive craters was experimentally investigated by detonating small spherical high-explosive charges at various depths in a bed of dry, particulate soil contained within a vacuum cylinder. The results indicate that for surface explosions atmospheric pressure has little effect on crater dimensions, but for charges buried beneath the surface, the dimensionless ratio of atmospheric pressure to lithostatic pressure can be of major importance. For a constant value of this pressure ratio and a range of charge masses of nearly 11 orders of magnitude, crater dimensions were found to vary as the fourth root of the charge mass and inversely as the fourth root of the product of the soil density and gravitational acceleration. Soil permeability was found to have an appreciable effect on crater dimensions.

For cratering experiments conducted under standard atmospheric pressure and gravity conditions, the atmosphere had a relatively greater effect on the small explosions than on the large ones at a given value of the charge-depth parameter.

17. Key Words (Suggested by Author(s))	18. Distribution Statement
Explosive craters Atmospheric-lithostatic pressure ratio	Unclassified – Unlimited

19. Security Classif. (of this report)	20. Security Classif. (of this page)	21. No. of Pages	22. Price*
Unclassified	Unclassified	88	$3.00

*For sale by the National Technical Information Service, Springfield, Virginia 22151

EFFECTS OF THE ATMOSPHERIC-LITHOSTATIC PRESSURE RATIO ON EXPLOSIVE CRATERS IN DRY SOIL

By Robert W. Herr
Langley Research Center

SUMMARY

The effects of the atmospheric pressure on the size of explosive craters was experimentally investigated by detonating small spherical high-explosive charges at various depths in a bed of dry, particulate soil contained within a vacuum cylinder. The results indicate that for surface explosions atmospheric pressure has little effect on crater dimensions, but for charges buried beneath the surface the dimensionless ratio of atmospheric pressure to lithostatic pressure can be of major importance. For a constant value of this pressure ratio and a range of charge masses of nearly 11 orders of magnitude, crater dimensions were found to vary as the fourth root of the charge mass and inversely as the fourth root of the product of the soil density and gravitational acceleration. Soil permeability was found to have an appreciable effect on crater dimensions.

For cratering experiments conducted under standard atmospheric pressure and gravity conditions, the atmosphere had a relatively greater effect on the small explosions than on the large ones at a given value of the charge-depth parameter.

INTRODUCTION

In future lunar or planetary operations, it may prove expedient to utilize the high-energy density of high explosives to blast craters for such purposes as geological experiments, mining operations, or site alteration for shelter construction. In view of the high transportation costs to the extraterrestrial test site, it is desirable that a given mass of high-explosive charge be detonated at the burial depth which will result in the largest possible crater. To achieve this goal, it is necessary that any effects of gravity or atmospheric pressure on the craters formed by explosives be taken into account.

As noted in reference 1, early attempts to correlate terrestrial explosive-crater dimensions were based on cube-root scaling in which the crater dimensions are assumed to vary as the cube root of the explosive energy. When identical charge materials and soils are used in cratering experiments, the principle deficiency associated with this direct dimensional scaling is the nonscaling of the viscous and gravity dependent forces.

To simulate the gravity forces, the effective acceleration must be increased by the same factor that the burial depth is reduced (i.e., gd = Constant). See references 2 and 3. The use of cube-root scaling to compare 1-g cratering experiments implies that gravity has no effect on crater dimensions. For small explosions in rock or soils of appreciable strength, this implication is approximately correct if, as is generally assumed, most of the energy is used in fragmenting the rock and a relatively small amount is required to lift the ejecta from the crater. As the explosive energy is increased and the burial depth is increased correspondingly, however, a larger fraction of the available energy must be devoted to lifting the ejecta from the crater. For extremely large events, it is probable that gravity forces become all important while soil strength is of little consequence. Thus, when crater dimensions from 1-g field experiments are compared by means of cube-root scaling, the larger explosions produce relatively small-scaled crater dimensions.

When it became apparent that cube-root scaling would not adequately scale the larger terrestrial explosive craters it was suggested that these larger craters might correlate better by fourth-root scaling (ref. 2). Although gravity dependent forces are taken into account by fourth-root scaling, its use gives rise to several violations of similarity when, as is usually the case, the strength and sonic velocity of the soil and the pressure and viscosity of the atmosphere remain constant for experiments of different magnitude. The charge radius is also a source of similarity violation when the same explosive is used in experiments of different magnitude. As noted in references 1 and 2, the qualitative effect of any or all of these violations of similarity is to produce larger fourth-root scaled crater dimensions for the larger explosions.

In view of these results, it would appear that improved correlation of terrestrial explosive-crater dimensions might result if a scaling exponent between 1/4 and 1/3 were used. This empirical approach has been taken by many investigators (refs. 4 to 9) and some have found an exponent of approximately 3/10 to best fit terrestrial cratering data. As noted in reference 1 Chabai and Hankins suggest an overburden scaling which is, in effect, a sliding exponent varying from 1/3 for small charges to 1/4 for the largest. While terrestrial crater dimensions can be predicted reasonably well by these approaches, such empirical scaling is of questionable value for predicting crater dimensions on the lunar or planetary surfaces where the atmospheric pressure and gravitational acceleration are radically different from those on earth.

Although correlation of terrestrial craters by means of fourth-root scaling is poor due to several violations of similitude, it may prove possible to minimize some of these effects in the simulation of lunar explosive craters in the laboratory. Of the variables noted previously as contributing to lack of similitude in terrestrial field tests, nonscaling of the soil strength is generally held to be the most serious and has received the most attention from investigators. If the lunar cratering experiments are restricted to the soil above the bedrock, the effects of nonscaling of the soil strength as well as the sonic velocity could be held to a minimum by conducting laboratory experiments in a cohesionless soil which rapidly dissipates the energy of a shock wave. Simulation of the lunar atmospheric pressure would require the laboratory experiments to be conducted in a vacuum chamber.

Perhaps the least appreciated of the similitude violations occurring in all terrestrial field tests and in most laboratory cratering experiments is that caused by the nearly constant atmospheric pressure. For any given subsurface explosion it is apparent that any pressure in addition to that due to the weight of the soil (lithostatic pressure) will retard the expansion of the gases and result in smaller crater dimensions. For similarity of experiments at any given value of the charge-depth parameter, the dimensionless ratio of the atmospheric to lithostatic pressures $p/\rho gd$ must be constant. The magnitude of this scaling violation for large-scale field tests is evident in cratering data obtained from reference 1 and shown in figure 1 in which the fourth-root crater-radius parameter is plotted as a function of the scaled depth of burial in Nevada desert alluvium (a lightly cemented mixture of sand and gravel). The ratio $p/\rho gd$ is noted beside each data point. Although there is a paucity of data at any given pressure ratio, trends are discernible as indicated by the faired curves for pressure ratios of 0, 0.25, 1.0, and 2.0. Should these trends be verified by further experiments, it would indicate that atmospheric pressure does have a major effect which cannot be ignored in any comprehensive study of explosive cratering. Further exploration of this significant effect appears warranted.

To better define the effects of the dimensionless ratio of atmospheric to lithostatic pressures on crater dimensions, an experimental investigation has been carried out in a large vacuum cylinder at Langley Research Center where small spherical charges of high explosives were detonated at various depths in sand, ground limestone, and a mixture of the two. Data from these experiments and existing small-scale high-g explosive-cratering data are compared with data from large-scale field experiments. Based on the results of this comparison, equations are developed for predicting explosive-crater dimensions in cohesionless soils on the lunar and Martian surfaces.

A motion-picture supplement L-1105 has been prepared and is available on loan. A request card and a description of the film will be found at the back of this paper.

SYMBOLS

c	sonic velocity of soil, m/s
d	burial depth of explosive charge, m

g	gravitational acceleration, m/s^2
h	maximum depth of crater from original ground level, m
K	permeability coefficient of soil, cm^2
M	effective mass of explosive charge, kg of TNT
p	atmospheric pressure, N/m^2
r	radius of crater at original ground level, m
V	volume of crater below original ground level, m^3
ρ	mass density of soil, kg/m^2
ϕ	internal-friction angle of soil, deg

MECHANISMS OF CRATERING

Based upon observations of many large-scale explosive-cratering experiments, Nordyke (ref. 10) has constructed a qualitative picture of the principal mechanisms involved in cratering. These mechanisms include compaction and plastic deformation of the material in close proximity to the explosion, spalling of material from the surface above the explosion by reflection of the compression wave, and acceleration of the fractured material by the expanding high-pressure gases. The relative magnitude of the role that each mechanism plays in cratering varies not only with the burial depth of the charge but is also very much dependent on the magnitude of the event, the soil characteristics (strength, speed of sound, transmissibility, permeability, etc.), and the characteristics of the explosive itself (rate of detonation, heat of explosion, gas production, etc.). In general terms, however, it may be said that for surface explosions, a small crater is formed primarily due to compaction, plastic deformation, and the scouring action of the high-velocity gases. For shallow burial depths, spalling becomes the major process in the formation of the crater. Gas acceleration and scouring action are of only minor importance because of the high-initial velocity given to the soil by the spalling process. At the optimum burial depth (largest resulting crater) acceleration of the material by the expanding gases becomes the dominant feature of the cratering process. Spalling becomes of lesser importance due to attenuation of the shock waves in traversing the greater distance to the surface. For very large burial depths, falling of material into an underground cavity produced by plastic deformation and compaction appears to be the major cratering mechanism.

Although a range of burial depths sufficient to cover all of these mechanisms was covered in the current investigation, the primary interest was in obtaining the largest possible crater from a given mass of high explosive.

It is of interest to note that the major cratering mechanism at optimum burial depth (acceleration by expanding gases) is not present in impact cratering events. In the absence of this cratering mechanism it is unlikely that atmospheric pressure has an appreciable effect on impact crater dimensions. As noted in reference 11, for the same energy expenditure, impact crater dimensions are comparable to those resulting from the detonation of high explosives at shallow burial depths.

APPARATUS AND TEST PROCEDURE

Explosive Charges

The spherical charge used in all experiments is depicted in figure 2 and consisted of approximately 130 mg of silver azide (AgN_3) pressed to a density of 4000 kg/m^3 surrounded by approximately 704 mg of PETN pressed to a density of 1700 kg/m^3. The combined heat of explosion is 4300 joules (from ref. 12). Although cratering laws are a function of the energy expended, it is common practice to replace the energy term in cratering parameters with the mass of the charge. The charge mass M for a cratering experiment is customarily given as the equivalent mass of TNT. Three of the more common methods of comparing the TNT equivalence of various explosives are the heat of explosion, the ballistics-mortar tests, and the Trauzl lead-block tests. The PETN to TNT equivalence as measured by these three methods and tabulated in reference 12 are 128, 145, and 173 percent, respectively. It should be noted, however, that the TNT equivalence of a particular explosive is not a constant factor but rather a variable depending on the soil characteristics and the particular application. For example, an explosive such as ammonium nitrate has a much lower detonation velocity than TNT and is therefore relatively inefficient in blasting operations where it is necessary to fracture hard rock. On the other hand, ammonium nitrate is relatively efficient for the excavation of loose or easily fragmented soils.

PETN with its high rate of detonation would be very effective in fracturing hard materials but not so effective in the present application where the primary interest is in excavating the maximum amount of loose granular material. This is particularly true when it is recalled that at the optimum burial depth spalling effects have diminished appreciably especially for small-scale explosions. Since the acceleration of the ejecta by the expanding gases appears to be the major cratering mechanism at optimum burial depths, it would seem more appropriate in this instance to base the PETN to TNT and silver azide to TNT equivalences on the relative amount of gases produced by the explosives. Based on the volume of gas produced (ref. 12), 0.704 gm of PETN and 0.13 gm of AgN_3 is found to be equivalent to a charge mass of 0.82 gm of TNT (M = 0.00082 kg).

Test Media

The spherical charges were detonated in three different soils; 68 in sand, 31 in ground limestone, and 35 in a mixture of 30 percent ground limestone and 70 percent sand by weight. The particle size and density, void ratio, internal-friction angle, and permeability to gases are given in the appendix.

The soil bed was prepared for each test by first excavating (by shovel) a crater appreciably larger than that anticipated in the test. The soil was then replaced a few centimeters at a time and raked with an ordinary garden rake until the desired burial depth of the charge was reached. The charge was then planted and the filling and raking process continued until the crater was filled. The surface was leveled with a screed. In situ densities of 1520, 1240, and 1600 kg/m^3 were measured for sand, ground limestone, and the mixture, respectively, when the bed was prepared in this manner. For most of the tests in ground limestone, the bed was packed to a higher density of 1450 kg/m^3 by refilling the crater a few centimeters at a time as before and at each level applying a constant force to a circular disc placed within the crater.

Test Procedure

For these experiments the soils were placed in a container measuring 2.44 meters square by 0.61 meter deep within a 16.8-meter vacuum cylinder at the Langley Research Center. To make certain that the craters resulting from the explosions were not affected by shock waves rebounding from the bottom of the container, three charges were detonated in the container filled with sand to depths of 30.5, 46, and 61 cm. Burial depth of the charge for all three experiments was 13 cm. Differences in the resulting craters were small and within the normal scatter.

To determine the effects of the atmospheric pressure on crater dimensions, each charge was buried at a depth to produce the desired value of the charge-depth parameter $d(\rho g/M)^{1/4}$. The vacuum cylinder was then pumped down to give the wanted pressure ratio $p/\rho gd$.

Crater measurements were made with the aid of the adjustable probes depicted in figure 3. Most of the craters were symmetric and depth measurements were taken along one radius only. The area moment (about the crater center line) of the resulting profile was measured with the aid of an integrator and multiplied by 2π to obtain the crater volume.

RESULTS AND DISCUSSION

Effect of Atmospheric Pressure

The experimental results of the 134 explosions in three soils are shown graphically in figures 4 to 8, pictorially in figures 9 to 13 and in tabular form in table I. Crater profiles are given in figures 14 to 17 where repeated tests are shown by solid or half-open symbols.

In figures 4, 5, and 6 the fourth-root radius, depth, and volume parameters are plotted as a function of the charge-depth parameter for the tests in sand, ground limestone, and a mixture of the two, respectively. Curves are faired through the data points for discrete values of the dimensionless ratio $p/\rho gd$ ranging from 0.01 to 50.

Sand.- As may be observed in figure 4, the ratio of atmospheric to lithostatic pressure has a major effect on the crater dimensions. In general, as the charge depth is increased, the curve for a given pressure ratio initially follows the curve obtained for a near vacuum $\left(\frac{p}{\rho gd} = 0.1\right)$ but reaches its peak at a smaller burial depth and the higher the ratio, the smaller is this optimum burial depth. For an atmospheric to lithostatic pressure ratio of 0.1 in sand, the optimum value of the charge-depth parameter based on crater radius (see fig. 4(a)) is approximately 13 whereas for a pressure ratio of 50, it has dropped to 3.5. There is no reason to suspect that this trend will not continue for even higher values of $p/\rho gd$. It is interesting to note that the range of parameters covered in these small-scale laboratory experiments represents an extremely large range of charge size for terrestrial field tests at standard atmospheric pressure. For instance, the optimum value of the charge-depth parameter of 3.5 for a pressure ratio of 50 would correspond to the detonation 0.034 kg of TNT at a depth of 0.14 meter whereas $11.1(10)^6$ kg of TNT at a depth of 68 meters would be required for a pressure ratio of 0.1 and a value of the charge depth parameter of 13.

Comparing figure 4(a) with figure 4(b) it may be seen that the optimum charge depth in sand based on crater depth is considerably different than the optimum charge depth based on crater radius. For a pressure ratio of 0.1, the optimum charge depth based on crater depth is about 5 as opposed to 13 when based on the radius.

Nearly identical crater dimensions were obtained in sand for two surface explosions for which the atmospheric pressures were 0.133 and 101.3 kN/m^2 (see table I) which indicates that the atmospheric pressure has little effect on crater dimensions for surface explosions.

It is of interest to note that for the larger burial depths in sand a modest decrease in the pressure ratio from 0.5 to 0.1 has a large effect on crater dimensions whereas decreasing the pressure ratio another order of magnitude to 0.01 has a negligible effect. (See fig. 4.)

Data points designated by $\times$ are also included in figure 4 to show the crater dimensions for five experiments at varying charge depths for which the pressure was standard atmospheric pressure. Starting at the surface and increasing the burial depth, the ratios of atmospheric to lithostatic pressure for these tests are ∞, 320, 158, 105, and 79. These data points are included only as an indication of the inadequacy of small-scale laboratory cratering experiments in which the effects of atmospheric pressure are not considered.

A close examination of the data points in figure 4 shows that many of the faired curves should break sharply to the right at values of the charge-depth parameter appreciably greater than the optimum, thus indicating that further increase of the burial depth has only a small effect on crater dimensions. Because the optimum burial depth was of primary interest, and for the sake of clarity, this portion of the faired curve was omitted. For these deep (relative to the optimum burial depth) explosions in a cohesionless soil it is likely that the chief cratering mechanism is subsidence of the sand into an underground cavity produced by compaction.

Referring to figures 14(e), 14(g), 14(h), and 14(j) it may be observed that mounds appear at the bottom of several of the craters in sand. Although these mounds have little or no effect on the crater radii and only a small effect on crater volume, the effect on crater depth is appreciable. The concave portion of the crater-depth curve (see fig. 4(b)) for $\frac{p}{\rho gd} = 0.1$ is at least partially attributable to these mounds.

The formation of a few of these mounds is apparent in high-speed motion pictures of the explosions. For some of the smaller burial depths the explosion throws some of the ejecta upward and inward into a slender column of sand (see fig. 9) which then descends into the crater. High-speed motion pictures were taken of 27 of the 68 explosions in sand. Of these 27 experiments, a column of sand was apparent in only 5 of them while mounds appeared in 14 of the resulting craters. The experiments for which motion pictures were obtained are indicated in figure 8. There is the possibility that all of the mounds were produced by sand columns, most of which were obscured from view in the motion pictures by the outer envelope of ejecta. Mounds could also be formed by the slumping of sand from the initially steep crater walls.

Another possible means by which some of these mounds were formed is suggested by results reported in reference 13 which describes an experimental investigation of soil erosion due to jet impingement in a vacuum. For experiments in fine soils it was found that the small crater formed by jet erosion was sometimes destroyed upon shutdown of the jet by the rapid expansion to the surface of gases which had penetrated the soil in the stagnation region during the run. Further experiments and an analysis of this phenomena are reported in reference 14. It would seem plausible that mounds could be formed in the bottom of explosive craters in a similar manner, especially at the greater burial depths. As the high-pressure bubble of gas expands toward the surface, some of the gas diffuses in all directions through the permeable sand. Upon venting of the gas bubble, the gases diffused in the sand beneath the crater escape upward toward a region of lower pressure throwing sand from the sloping crater walls toward the center of the crater.

Ground limestone and mixture of sand and ground limestone.- Although the primary goal of determining the magnitude of the effect on crater dimensions of variations in the ratio of the atmospheric to lithostatic pressure was achieved by the tests in sand, further tests were undertaken to observe the effects of less permeable materials. Because of its small particle size, ready availability, and economy ground limestone was chosen as a test material. Charges were detonated in the ground limestone alone and in a mixture consisting of 30 percent ground limestone and 70 percent sand by weight. The ground limestone and the mixture of ground limestone and sand were found to be less permeable to gases than sand by factors of approximately 400 and 40, respectively (see the appendix). The internal angles of friction for the ground limestone, the mixture, and the sand were 36.5°, 34°, and 33°, respectively.

In figure 5, the fourth-root radius, depth and volume parameters for the experiments in ground limestone are plotted as a function of the charge-depth parameter. The initial tests were made at a pressure ratio of 0.1 in limestone loosely raked to a density of 1240 kg/m^3. Tests in the loosely packed limestone were discontinued when it was found that in some cases the surface subsided below its original level out to a distance well beyond the crater proper making it impossible to measure the crater radius or volume with any degree of accuracy (see figs. 15(d) to 15(h)). This problem was avoided by compacting the ground limestone to a density of 1450 kg/m^3 before each of the remaining 21 tests. As may be seen, the density of the limestone had little effect on the crater-radius and crater-volume parameters for a pressure ratio of 0.1 except at the greater burial depths.

The fourth-root radius, depth, and volume parameters for the experiments in the mixture of limestone and sand are plotted in figure 6 as a function of the charge-depth parameter. Comparing figures 4, 5, and 6, it may be seen that although the trends of the crater dimensions are the same as the charge-depth parameter or pressure ratio is varied, there are appreciable differences in the cratering data obtained in sand, ground limestone, and a mixture of the two. The largest differences are in crater depth. The optimum burial depth (based on crater depth) for a pressure ratio of 0.1 has increased from approximately 6 in sand to 17 in ground limestone and about 12 in the mixture. Contrary to the results obtained in sand, the optimum burial depths based on crater radii are nearly the same as those based on crater depth or crater volume in limestone or the mixture. Although there were no mounds at the bottom of the limestone craters (see figs. 15 and 16) as there were in sand, the crater-depth curve for a pressure ratio of 0.1 (see fig. 5(b)) is still inexplicably concave at medium burial depths.

For ease of comparison, the faired crater radius versus charge-depth curves for $\frac{p}{\rho gd} = 0.1$ of figures 4(a), 5(a), and 6(a) are reproduced in figure 7. The curves for ground limestone and the mixture both fall below the data obtained in sand at the small to medium charge depths and above at the largest burial depths. The optimum burial depth based on crater radius is approximately 13 in sand, 17 in the ground limestone, and 15 in the mixture of ground limestone and sand.

Photographs of craters in three soils.- The effect of the dimensionless ratio $p/\rho gd$ on explosive craters in sand, ground limestone, and the mixture of the two is pictorially illustrated in figures 10, 11, and 12, respectively. Each set of photographs shows the craters resulting from detonation of charges at a constant value of the charge-depth parameter and several values of the pressure ratio. As the pressure ratio is increased, the crater dimensions are seen to become smaller in each case while the crater lip generally becomes larger. The crater lips in sand are smooth and symmetric but for the greater charge depths in ground limestone or the mixture the lips are uneven and exhibit radial rays and troughs. A similar trend with particle size was noted in reference 13 for craters formed by erosion due to jet impingement.

Figure 13 is a frame taken from high-speed motion pictures of the detonation of a charge in sand at a value of the charge-depth parameter of 11.3 and a pressure ratio of 0.1. The thin veil of material preceding the primary dome of ejecta was evident only in sand at medium burial depths and low-pressure ratios. Although this phenomena was not investigated further, it was noted that the velocity of the material in the veil dropped off rapidly with increasing burial depth which suggests that this material may have been ejected from the surface by shock-induced particle motion.

Comparison With Large-Scale Field Experiments

As mentioned previously, early attempts to correlate the crater dimensions of field experiments utilized cube-root scaling which proved satisfactory over a limited range of charge size. In figure 18(a) the crater radii obtained in the Nevada-desert-alluvium cratering tests are compared with crater radii of the present small-scale tests in sand by means of cube-root scaling. Only the upper boundary $\left(\frac{p}{\rho gd} = 0.1\right)$ of the small-scale test is shown. The correspondence is poor.

In figure 18(b) the large-scale alluvium data are compared to the small-scale tests in sand by means of three-tenths power scaling. Although this empirical scaling succeeds fairly well in reducing the alluvium field tests to a common basis, it does not correlate these field results well with the current small-scale experiments.

The crater dimensions from the large-scale alluvium tests are compared with those of the small-scale experiments in sand by means of fourth-root scaling in figure 19. Considering that the effective charge masses cover a range of 11 orders of magnitude, the overall correspondence is good. For explosions on the surface the magnitude of the crater-radius parameters (see fig. 19(a)) are in excellent agreement, but as the burial depth is increased, the curves for the small-scale tests rise relatively fast and then fall off at a relatively small charge depth. In a similar manner, the crater depths and volumes (see figs. 19(b) and 19(c)) for the small-scale tests in sand drop off at a relatively small charge depth. This is particularly true of the crater depth. For values of the charge-depth parameter greater than 8, the small-scale craters are seen to be much too shallow, especially for the lower ratios of atmospheric to lithostatic pressure.

In figure 20, the faired crater-dimension curves for ground limestone (see fig. 5) are compared to the large-scale alluvium cratering data. Except for surface bursts, the upper boundary of the limestone data $\left(\frac{p}{\rho g d} = 0.1\right)$ correlates with large-scale alluvium data much better than did the sand-cratering data. This is especially true for crater depths at larger values of the charge-depth parameter. In figure 19(b) it may be observed that the explosion of a 0.00082 kg charge in sand at a value of the charge-depth parameter of 16 and pressure ratio of 0.1 produced a crater having a scaled depth only half as great as for the largest chemical explosion of 454 000 kg of TNT in alluvium at a comparable value of the charge-depth parameter and pressure ratio. The value of the crater-depth parameter obtained in ground limestone under similar conditions approached the large-scale results but is still somewhat less as are the crater-radius and crater-volume parameters. The greatest disparity between small-scale laboratory- and full-scale-test results is noted for the largest explosion ($90.8(10)^6$ kg of TNT) at a fourth-root scaled burial depth of approximately 22 at which all of the small-scale crater-dimension parameters are appreciably less than those for the largest full-scale explosion.

Although caution must be exercised in comparing nuclear and chemical-explosive cratering results, it is considered likely that much of this remaining difference can be attributed to improper scaling of the speed of sound in the test material. As noted previously, this failing also tends towards larger fourth-root scaled crater dimensions for the larger charge weights. As related in reference 10, time histories of the velocities of several surface targets were measured during the explosion of the 454 000 kg chemical charge in alluvium. These results showed that spalling due to the reflected shock wave at the surface imparted a velocity of approximately 22 m/s to the material at ground zero within a few milliseconds of detonation. After a brief period of free fall (350 ms) the target was given a second boost by the expanding gases which accelerated it to a maximum velocity of 54 m/s at the end of 1.2 seconds. Although it is apparent that in this instance gas acceleration is the major cratering mechanism, the energy given the ejecta by the spalling action is of consequence. Since the mass of the nuclear charge at a value of the charge-depth parameter of 22 is larger by a factor of 200 than the charge mass in this illustrative case, the effects of spalling would be expected to be larger. In contrast, high-speed motion pictures taken of the small-scale explosions at a value of the charge-depth parameter of 16 and pressure ratio of 0.1 show only the faintest indication of an initial velocity attributable to shock-induced particle motion.

Because of the paucity of large-scale test data, comparisons with small-scale tests at higher ratios of atmospheric to lithostatic pressure are difficult except, perhaps, at a ratio of 1.0. At this pressure ratio, scaled crater dimensions of the small-scale tests appear to fall slightly beneath the large-scale alluvium test data.

Since crater dimensions in the mixture of 30 percent ground limestone and 70 percent sand differed not greatly from those in ground limestone, comparison of crater dimensions in the mixture with large-scale data is not shown. Of the three soils in which the small-scale charges were detonated, the best correlation with large-scale crater dimensions was obtained in the test medium having the lowest permeability to gas which was ground limestone.

Effect of Gravity

In fourth-root scaling, crater dimensions vary inversely as the fourth root of the gravitational acceleration. Although there is no reason to suspect any inadequacy of this scaling, little has been done to verify it.

In reference 15, the effects of gravity on the size of explosive craters were investigated by detonating small squibs and blasting caps in a bed of sand contained in an aircraft flying a parabolic arc in such a manner as to simulate 0.17, 0.38, and 2.5 times the normal acceleration due to gravity. Although qualitative effects of gravity were deduced from these experiments, the tests were conducted at ambient pressure with the result that in all cases the atmospheric pressure exceeded the lithostatic pressure by a factor of 20 or more which is well above the range of general interest in extraterrestrial or terrestrial field experiments.

Explosive cratering experiments are reported in reference 3 in which 25, 45, and 65 times the normal gravity were simulated by detonating small TNT charges ($M = 0.0027$ to 0.008 kg) in a container of sand mounted on a linear accelerator. Using experimental data from this reference, the values of the fourth-root crater-dimension parameters have been calculated and are compared with large-scale alluvium data in figure 21. These experiments were also conducted at ambient atmospheric pressure but because of the high accelerations the range of values for the pressure ratio $p/\rho gd$ is about the same as for the 116-kg tests in alluvium. Comparison of the scaled crater dimensions at corresponding values of $p/\rho gd$ shows excellent correlation thus indicating the adequacy of the fourth-root method of scaling the effects of gravity.

For proper scaling of spalling effects it is necessary that the dimensionless ratio c^2/gd (Froude number) have the same value in cratering experiments. If it is assumed that the sonic velocity in sand is comparable to that in alluvium, the values of the ratio c^2/gd for the high-g experiments of reference 3 will correspond more closely to those of the large-scale alluvium tests than will the values of c^2/gd for the 1-g tests of the subject investigation. This improved modeling with respect to spalling effects may account for the somewhat better correlation of the high-g and alluvium data than was obtained between the small-scale 1-g data of the subject investigation and the alluvium data.

Optimum Charge Depth Based on Crater Radius

For excavating a dry cohesionless soil the energy released by the explosive must not only lift the mass of the ejecta (ρgd^3) a given distance (d) against gravity but must also push the area of the expanding dome of ejecta (d^2) a distance (d) against the atmospheric pressure (p). For explosions in a loose dry soil the energy might be partitioned as follows:

$$M = C_1 \rho g d_r^{\,4} + C_2 p d_r^{\,3} \tag{1}$$

where C_1 and C_2 are constants and d_r refers to the optimum burial depth based on the crater radius. Rearranging equation (1), the optimum charge-depth parameter is given by

$$d_r \left(\frac{\rho g}{M}\right)^{1/4} = \frac{\left(1/C_1\right)^{1/4}}{\left(1 + \frac{C_2}{C_1}\frac{p}{\rho g d_r}\right)^{1/4}} \tag{2}$$

From the ground-limestone cratering data shown in figure 5(a), it is seen that for a ratio of the atmospheric to lithostatic pressure equal to 0.1, the optimum value of the charge-depth parameter for crater radius is approximately 17, while for $\frac{p}{\rho gd} = 2$, the optimum value of $d(\rho g/M)^{1/4}$ is approximately 9. Substituting these two sets of values into equation (2) and solving the resulting simultaneous equations gives values of $C_1 = 4.54(10)^{-6}$ and $C_2 = 74(10)^{-6}$. Thus equation (1) becomes

$$M = 4.54(10)^{-6}\rho g d_r^{\,4} + 74(10)^{-6} p d_r^{\,3} \tag{3}$$

and equation (2),

$$d_r\left(\frac{\rho g}{M}\right)^{1/4} = \frac{21.6}{\left(1 + 16.3\,\frac{p}{\rho g d_r}\right)^{1/4}} \tag{4}$$

Equation (4) is shown in graphical form by the solid curve of figure 22. Comparison of the optimum charge depth, as given by this curve, with the results in figures 5(a) and 21(a) shows excellent agreement. For example, for a pressure ratio of 65 an optimum value of 4 is indicated for the charge-depth parameter which correlates very well with the data of reference 3 shown in figure 21(a). Similarly, the value of $d_r\left(\frac{\rho g}{M}\right)^{1/4} = 10.4$ for $\frac{p}{\rho g d} = 1$ is in very good agreement with both the large-scale alluvium data and the high-g data. An optimum value of 15.8 is indicated for the charge-depth parameter for a pressure ratio of 0.16 which would imply that the largest chemical explosion in desert alluvium 454 000 kg of TNT was detonated very near the optimum burial depth.

It is of significance to note that for ratios of the atmospheric to lithostatic pressure in excess of 0.2, a nearly identical curve is obtained when the gravity term is omitted from equation (3) (dashed curve of fig. 22) thus indicating the optimum burial depth for a given charge depends only on the atmospheric pressure and is independent of the soil density and the gravitational acceleration. This indication is borne out by the experiments of reference 15 in which the same optimum burial depth (based on crater radius) is reported for simulated gravitational accelerations 0.16, 0.38, 1, and 2.5 times the acceleration at the surface of the earth. For cratering experiments conducted in a loose particulate soil and at standard atmospheric pressure conditions the optimum burial depth for charges smaller than approximately 250 000 kg of TNT is then given by

$$d_r = 0.5M^{1/3} \tag{5}$$

It should be noted that only the optimum burial depth appears to vary with the cube root of the charge weight; as pointed out previously, the crater dimensions do not.

For explosive cratering at low atmospheric pressure $\left(\frac{p}{\rho g d} \approx 0\right)$ such as found on the lunar and Martian surfaces, equation (4) would indicate $d_r\left(\frac{\rho g}{M}\right)^{1/4} = 21.6$. Until more large-scale explosive cratering data at very low ratios of the atmospheric to lithostatic pressure become available, however, a more conservative value of 18 might be in order which is more in line with the small-scale results in limestone. Due to the flatness of the crater-dimension curves versus charge-depth curves in the vicinity of the optimum charge depth, this reduced burial depth should have only a minor effect on the resulting crater dimensions. Burial of the charge at reduced depth has the advantage of being easier to implement.

From the results of this investigation, the optimum value of the fourth-root burial-depth parameter and corresponding crater-dimension parameters for small-scale charges detonated in a fine particulate material under high vacuum, or for very large charges at atmospheric pressure, would appear to be approximately as follows:

$$d_r\left(\frac{\rho g}{M}\right)^{1/4} = 18 \tag{6}$$

$$r\left(\frac{\rho g}{M}\right)^{1/4} = 18 \tag{7}$$

$$h\left(\frac{\rho g}{M}\right)^{1/4} = 9 \tag{8}$$

$$V\left(\frac{\rho g}{M}\right)^{3/4} = 4000 \tag{9}$$

Assuming a soil density of 1500 kg/m^3, crater dimensions on the earth, Mars, and the moon are given by

	Earth (vacuum)	Mars	Moon
d_r	$1.6M^{1/4}$	$2.1M^{1/4}$	$2.6M^{1/4}$
r	$1.6M^{1/4}$	$2.1M^{1/4}$	$2.6M^{1/4}$
h	$0.8M^{1/4}$	$1.0M^{1/4}$	$1.3M^{1/4}$
V	$3.0M^{3/4}$	$6.1M^{3/4}$	$11.4M^{3/4}$

As noted, these dimensions are for a loose, particulate soil. For accurate small-scale simulation of the explosion of a charge in bedrock or soil of appreciable strength, it would be necessary to scale the strength and sonic velocity. A more direct approach would be through the use of direct dimensional scaling (cube-root scaling) of identical materials and simulating gravity forces by keeping the product of g and d constant (refs. 2 and 3). Thus, the detonation of a 1-kg charge buried on the moon or Mars would be simulated in a vacuum chamber on the earth's surface by the detonation of 0.00463 kg and 0.055 kg buried 0.167 and 0.38 times as deep, respectively. Greater reduction in scale could be realized through the use of a linear accelerator (ref. 3) or centrifuge although Coriolis forces may rule out the use of the latter.

CONCLUSIONS

In view of the results of small-scale explosive-cratering experiments conducted in a vacuum and the correlation of these and other laboratory test results with large-scale field experiments, the following conclusions are deemed justified for explosive-cratering operations in a loose, dry, particulate soil:

1. For surface explosions, atmospheric pressure has little effect on crater dimensions.

2. At finite burial depths, the ratio of atmospheric to lithostatic pressure can be of major importance in determining crater dimensions.

3. For cratering experiments conducted under standard atmospheric pressure and gravity conditions, the atmosphere had a relatively greater effect on the small explosions than on the large ones at a given value of the charge-depth parameter.

4. The optimum value of the burial-depth parameter varies widely depending on the ratio of the atmospheric to lithostatic pressure.

5. For ratios of the atmospheric to lithostatic pressure in excess of 0.2, the optimum burial depth for a given charge was found to be dependent only on the atmospheric pressure and independent of the soil density and gravitational acceleration.

6. At corresponding values of the dimensionless ratio $p/\rho gd$, fourth-root scaling correlated crater dimensions reasonably well over a range of charge masses of nearly 11 orders of magnitude.

7. The effects on crater dimensions of varying the effective gravitational acceleration over a range of 65 to 1 were adequately accounted for by the use of fourth-root scaling.

8. Permeability of the three soils (sand, ground limestone, and a mixture of the two) had an appreciable effect on crater dimensions.

Langley Research Center,
National Aeronautics and Space Administration,
Hampton, Va., June 23, 1971.

APPENDIX

PROPERTIES OF TESTING MEDIA

As noted in the text, the cratering experiments were conducted in three media: sand, ground limestone, and a mixture of the two (30 percent ground limestone by weight). A summary of the properties of these media is given in the table below. Details of these and other measurements are discussed in the following paragraphs. The moisture content of the media was negligible due to a vacuum presoak of each of the soils before initial testing.

	Sand	Ground limestone	Mixture (30% limestone)
Particle density, G, kg/m^3	2550	2710	2660
Apparent density, G_A, kg/m^3 (dense) . . .	1650	1600	1680
Apparent density, G_A, kg/m^3 (loose) . . .	1300	1020	1200
Apparent density, G_A, kg/m^3 (in situ) . . .	1520	[a]1450	1600
Void ratio $= \frac{G}{G_A} - 1$, (dense)	0.55	0.69	0.58
Void ratio $= \frac{G}{G_A} - 1$, (loose)	0.96	1.65	1.22
Void ratio $= \frac{G}{G_A} - 1$, (in situ)	0.68	0.87	0.66
Internal friction angle, ϕ, deg	33.0	36.5	34.0
Permeability to liquid, K_{liq}, cm^2	$196(10)^{-9}$	$0.20(10)^{-9}$	$4.2(10)^{-9}$

[a]Density for the 10 initial tests was 1240.

Particle Size

A sieve analysis was made of the sand used in the cratering experiments. In this method of measuring particle size (refs. 16 and 17), the soil is sifted through successively final square-mesh screens and the percentage of the total sample weight retained by each screen is measured accurately. The percentage coarser or finer is then plotted as a function of particle size which is taken to be the size of the sieve opening. The results for the sand are plotted in figure 23. The range of particle sizes measured would indicate this to be a medium-fine sand. The uniformity of the particle size may be expressed by the uniformity coefficient, Cu, which is the ratio of D_{60} to D_{10} where D_{60} is the particle diameter at which 60 percent of the soil weight is finer and D_{10} is the corresponding value at 10 percent finer as noted in figure 23. A soil is considered uniform if the uniformity coefficient is less than 2. For the sand used in these experiments,

$$Cu = \frac{D_{60}}{D_{10}} = \frac{0.26}{0.17} = 1.53$$

Sieve testing of the ground limestone used in the cratering experiments was not practicable due to the extremely small particle size. Examination under a microscope indicated individual particles ranging in size from 1 to 4 microns, most of which were a part of loose clusters ranging in size up to about 200 microns.

Ultimate Friction Angle

The simplest method of obtaining a measure of a cohesionless soil's resistance to shear is to measure its angle of repose. The maximum slope obtainable in a tilt box with loose sand of these experiments was 33.5°. There was appreciable cohesion between the small particles of ground limestone making it impossible to measure its angle of repose. Instead, direct shear tests (refs. 16 and 17) were performed on the ground limestone as well as the sand and the mixture of the two. In the direct shear test a normal force is applied to a sample of the test soil by means of dead weights. The horizontal force required to shear the sample is then recorded. For small strains the shearing stress is very much dependent on the initial compaction of the soil but at larger strains the shearing stress levels off to a constant value or ultimate shearing stress. In these tests only the ultimate shearing stress was recorded. The ultimate shearing stress of each of the three test media is plotted in figure 24 as a function of the normal stress. The resulting fairings are linear and the ultimate friction angles are the angles bounded by these straight lines and the horizontal. The friction angles for ground limestone and the mixture are 36.5° and 34°, respectively. The friction angle of 33° for the sand compares well with its 33.5° angle of repose.

Permeability

As noted in reference 18, the standard unit of permeability of a porous medium to fluids is the "darcy," which is defined as the rate of flow in milliliters per second of a fluid of 1 centipoise viscosity through a cross section of 1 square centimeter of a porous medium under a pressure gradient of 1 atmosphere per centimeter and conditions of viscous flow. In keeping with the SI system of units used in this paper, the permeability constant K is given in units of cm^2. The conversion factor to darcys is given by

$$\text{Darcys} = \frac{(10)^9}{9.86} K$$

The technique used to measure the permeability of the three test media to air is illustrated in figure 25. Air from a pressure vessel flows through the test media into a vessel at a lower initial pressure. By making the volumes of the two vessels equal, the mean pressure across the specimen will remain constant as the differential pressure declines. The permeability coefficient may be determined from the following equation.

$$K = \frac{\mu L V_p \ln \frac{p_1}{p_2}}{2Ap_m \, \Delta t} \tag{A1}$$

where

K	permeability coefficient, cm^2
μ	viscosity of fluid (air), $N\text{-}s/cm^2$
L	length of porous media specimen, cm
V_p	volume of each pressure vessel, cm^3
A	cross-sectional area of test specimen, cm^2
p_m	arithmetic mean pressure across test specimen, N/cm^2
Δt	time between differential pressure readings, s
p_1	pressure differential across test specimen at time t_1, N/cm^2
p_2	pressure differential across test specimen at time t_2, N/cm^2

In figure 26, the pressure differential across samples of each of the three cratering media is plotted as a function of time for five values of the mean pressure p_m. For these tests the test specimens were packed as densely as possible to simulate the conditions in close proximity to an explosion. For the ground limestone, the test specimen was 13.7 cm in length by 20.25 cm^2 in cross-sectional area. As may be observed in figure 26(a), 10 minutes were required to obtain only a modest decline in differential pressure. When the same specimen container was used for the sand-permeability measurements, the flow through the specimen was so rapid that it was not possible to read the manometer. For these tests, the specimen length was therefore increased to 142 cm and the cross-sectional area reduced to 1.98 cm^2. As may be seen in figure 26(d), this modification results in a reasonable pressure decline rate. As a check on possible wall effects, pressure declines for the mixture of limestone and sand were measured using both specimen containers. The container of 1.98 cm^2 cross-sectional area was loaded to only 2.54 cm of its 142-cm length in order to keep the pressure decline time at a reasonable value.

The permeability coefficient was determined by use of equation (A1) for each of the three cratering media for five values of the mean pressure. The results are given in figure 27 where the permeability coefficient is plotted as a function of the reciprocal of the mean pressure. When plotted in this manner, the data should fall along a straight line which, when extrapolated to infinite mean pressure, indicates the permeability of the test media to a liquid. It may be observed that the sand is three orders of magnitude more permeable to a liquid than is the ground limestone.

As may be seen in figure 27(b), the permeability coefficients for the mixture of limestone and sand in the two different containers are in very good agreement.

REFERENCES

1. Chabai, Albert J.: On Scaling Dimensions of Craters Produced by Buried Explosives. J. Geophys. Res., vol. 70, no. 20, Oct. 15, 1965, pp. 5075-5098.
2. Sedov, Leonid Ivanovich (Morris Friedman, transl.): Similarity and Dimensional Methods in Mechanics. Academic Press, Inc., 1959.
3. Viktorov, V. V.; and Stepenov, R. D. (Marcel I. Weinreich, transl.): Modeling of the Action of an Explosion With Concentrated Charges in Uniform (Homogeneous) Ground. SCL-T-392, Sandia Corp., 1961.
4. Chabai, A. J.: Crater Scaling Laws for Desert Alluvium. SC-4391(RR), Sandia Corp., Dec. 1959.
5. Murphey, B. F.; and Vortman, L. J.: High-Explosive Craters in Desert Alluvium, Tuff, and Basalt. J. Geophys. Res., vol. 66, no. 10, Oct. 1961, pp. 3389-3404.
6. Nordyke, M. D.: An Analysis of Cratering Data From Desert Alluvium. J. Geophys. Res., vol. 67, no. 5, May 1962, pp. 1965-1974.
7. Nordyke, M. D.; and Wray, W.: Cratering and Radioactivity Results From a Nuclear Cratering Detonation in Basalt. J. Geophys. Res., vol. 69, no. 4, Feb. 15, 1964, pp. 675-689.
8. Vaile, R. B., Jr.: Pacific Craters and Scaling Laws. J. Geophys. Res., vol. 66, no. 10, Oct. 1961, pp. 3413-3438.
9. Violet, Charles E.: A Generalized Empirical Analysis of Cratering. J. Geophys. Res., vol. 66, no. 10, Oct. 1961, pp. 3461-3470.
10. Nordyke, M. D.: Nuclear Craters and Preliminary Theory of the Mechanics of Explosive Crater Formation. J. Geophys. Res., vol. 66, no. 10, Oct. 1961, pp. 3439-3459.
11. Moore, H. J.: Craters Produced by Missile Impacts. Astrogeologic Studies – Annual Progress Report, Pt. B, U.S. Dep. Interior, Nov. 1966, pp. 79-105. (Available as NASA CR-82745.)
12. Anon.: Engineering Design Handbook – Properties of Explosives of Military Interest. AMCP 706-177, U.S. Army, Mar. 1967. (Available from DDC as AD 814 964.)
13. Land, Norman S.; and Clark, Leonard V.: Experimental Investigation of Jet Impingement on Surfaces of Fine Particles in a Vacuum Environment. NASA TN D-2633, 1965.
14. Scott, Ronald F.; and Ko, Hon-Yim: Transient Rocket-Engine Gas Flow in Soil. AIAA J., vol. 6, no. 2, Feb. 1968, pp. 258-264.

15. Johnson, S. W.; Smith, J. A.; Franklin, E. G.; Moraski, L. K.; and Teal, D. J.: Gravity and Atmospheric Pressure Effects on Crater Formation in Sand. J. Geophys. Res., vol. 74, no. 20, Sept. 15, 1969, pp. 4838-4850.

16. Lambe, T. William; and Whitman, Robert V.: Soil Mechanics. John Wiley & Sons, Inc., 1969.

17. Lambe, T. William: Soil Testing for Engineers. John Wiley & Sons, Inc., c.1951.

18. Biles, Martin B.; and Putnam, John A.: Use of a Consolidated Porous Medium for Measurement of Flow Rate and Viscosity of Gases at Elevated Pressures and Temperatures. NACA TN 2783, 1952.

TABLE I.- TABULATION OF CRATER DIMENSIONS

Charge depth, d, cm	Atmospheric pressure, p, kN/m^2	Crater radius, r, cm	Crater depth, h, cm	Crater volume, V, cm^3	Charge-depth parameter, $d(\rho g/M)^{1/4}$	Pressure ratio, $p/\rho g d$	Crater-radius parameter, $r(\rho g/M)^{1/4}$	Crater-depth parameter, $h(\rho g/M)^{1/4}$	Crater-volume parameter, $V(\rho g/M)^{3/4}$
					Sand (ρ = 1520 kg/m^3)				
0	0.133	11.4	4.3	737	0	∞	7.5	2.8	209
0	.133	10.9	4.4	765	0	∞	7.2	2.9	216
0	101.3	11.7	4.8	795	0	∞	7.7	3.2	225
2.0	.033	16.8	8.0	2 940	1.4	0.10	11.0	5.3	832
2.1	16.65	15.5	7.7	1 960	1.4	53.2	10.2	5.1	555
2.1	101.3	15.0	6.6	1 960	1.4	320.0	9.8	4.3	555
4.3	.067	21.3	9.1	5 830	2.8	.10	14.0	6.0	1650
4.3	.067	21.0	8.0	------	2.8	.10	13.8	5.3	----
4.3	6.600	20.3	9.5	4 250	2.8	10.4	13.3	6.2	1205
4.3	16.66	19.4	9.3	4 250	2.8	26.0	12.7	6.1	1205
4.3	33.30	19.1	9.8	3 880	2.8	52.0	12.5	6.4	1100
4.3	101.3	17.3	7.6	2 970	2.8	158.0	11.4	5.0	842
6.5	4.000	21.8	10.1	6 000	4.3	4.1	14.3	6.6	1700
6.5	10.00	23.7	9.9	7 020	4.3	10.3	15.6	6.5	1990
6.5	10.00	21.1	9.6	5 580	4.3	10.3	13.9	6.3	1580
6.5	25.00	20.9	8.9	5 180	4.3	25.8	13.7	5.8	1470
6.5	46.00	18.1	7.5	3 880	4.3	47.5	11.9	4.9	1100
6.5	101.3	13.0	3.8	1 020	4.3	105.0	8.5	2.5	290
8.6	.133	25.4	9.1	9 340	5.7	.10	16.7	6.0	2650
8.6	1.330	25.4	10.9	8 460	5.7	1.04	16.7	7.2	2400
8.6	2.660	23.5	9.4	6 880	5.7	2.10	15.4	6.2	1950
8.6	2.660	23.5	9.7	7 000	5.7	2.10	15.4	6.4	1980
8.6	5.320	23.6	9.9	7 220	5.7	4.20	15.5	6.5	2050
8.6	13.30	20.8	7.4	5 010	5.7	10.4	13.7	4.9	1420
8.6	33.30	17.5	3.1	1 790	5.7	26.0	11.5	2.0	506
8.6	66.60	15.0	.5	0	5.7	50.0	9.8	.3	0
8.6	101.3	0	0	0	5.7	79.0	0	0	0
10.8	3.330	25.1	11.9	8 500	7.1	2.10	16.5	7.8	2410
10.8	6.660	22.6	8.9	6 360	7.1	4.10	14.8	5.8	1800
10.8	16.60	16.5	2.4	1 350	7.1	10.3	10.8	1.6	381
12.9	.200	28.6	7.6	9 450	8.5	.10	18.8	5.0	2680
12.9	1.000	26.9	9.7	10 500	8.5	.52	17.7	6.4	2980
12.9	2.000	25.4	9.1	8 160	8.5	1.04	16.7	6.0	2310
12.9	4.000	24.1	7.4	7 100	8.5	2.08	15.8	4.9	2010
12.9	8.000	17.8	3.8	1 980	8.5	4.16	11.7	2.5	562
12.9	20.00	12.7	1.3	282	8.5	10.4	8.3	.9	81
17.2	.266	29.0	8.4	11 950	11.3	.10	19.1	5.5	3250
17.2	.266	29.5	7.5	11 080	11.3	.10	19.4	4.9	3140
17.2	.266	29.8	8.1	12 170	11.3	.10	19.6	5.3	3450
17.2	1.330	27.9	9.5	10 360	11.3	.52	18.3	6.2	2940
17.2	1.330	26.9	9.1	9 880	11.3	.52	17.7	6.0	2800
17.2	2.660	23.1	6.9	5 700	11.3	1.04	15.2	4.5	1610
17.2	2.660	23.1	6.1	6 270	11.3	1.05	15.2	4.0	1780
17.2	5.320	17.1	2.5	1 360	11.3	2.10	11.2	1.6	385
17.2	5.320	17.1	2.9	1 760	11.3	2.10	11.2	1.9	500
17.2	10.64	13.3	2.5	2 350	11.3	4.20	8.7	1.6	666
21.5	.333	29.5	8.5	11 200	14.1	.10	19.4	5.6	3170
21.5	.333	30.4	8.9	13 040	14.1	.10	20.0	5.8	3700
21.5	.333	29.8	8.5	11 200	14.1	.10	19.6	5.6	3170
21.5	1.667	26.6	7.5	8 650	14.1	.52	17.5	4.9	2450
21.5	1.667	25.6	7.1	7 480	14.1	.52	16.8	4.7	2120
21.5	1.667	24.6	7.0	6 230	14.1	.52	16.2	4.6	1780
21.5	3.330	17.5	5.6	2 410	14.1	1.04	11.5	3.7	684
21.5	3.330	17.8	3.3	2 150	14.1	1.04	11.7	2.2	611
21.5	3.330	16.6	4.9	2 260	14.1	1.04	10.9	3.2	641
21.5	6.670	15.3	5.6	2 040	14.1	2.10	10.1	3.7	579
21.5	6.670	15.3	5.6	2 240	14.1	2.10	10.1	3.7	635
21.5	13.30	14.0	4.9	1 640	14.1	4.2	9.2	3.2	465
21.5	33.30	12.7	3.6	1 130	14.1	10.4	8.3	2.4	322
21.5	101.3	8.9	4.2	------	14.1	31.6	5.9	2.8	----
25.9	.040	29.2	7.3	10 630	17.0	.010	19.2	4.8	3010
25.9	.400	28.6	6.3	9 350	17.0	.10	18.8	4.1	2650
25.9	.400	28.2	7.2	9 480	17.0	.10	18.5	4.7	2680
25.9	2.000	20.6	5.1	3 400	17.0	.52	13.5	3.4	965
25.9	4.000	16.5	4.8	2 240	17.0	1.04	10.8	3.2	645
34.5	.053	22.1	4.2	3 670	22.7	.010	14.5	2.8	1040
34.5	.530	21.1	3.3	2 410	22.7	.10	13.9	2.2	684
38.8	.060	15.2	4.1	1 870	25.5	.010	10.0	2.7	531

TABLE I.- TABULATION OF CRATER DIMENSIONS – Concluded

Charge depth, d, cm	Atmospheric pressure, p, kN/m^2	Crater radius, r, cm	Crater depth, h, cm	Crater volume, V, cm^3	Charge-depth parameter, $d(\rho g/M)^{1/4}$	Pressure ratio, $p/\rho g d$	Crater-radius parameter, $r(\rho g/M)^{1/4}$	Crater-depth parameter, $h(\rho g/M)^{1/4}$	Crater-volume parameter, $V(\rho g/M)^{3/4}$
Loose ground limestone (ρ = 1240 kg/m^3)									
0	0.133	10.8	6.6	1 160	0	∞	6.7	4.1	282
4.6	.053	19.0	9.0	4 530	2.9	0.10	11.9	5.6	1101
9.2	.107	23.2	12.5	9 370	5.7	.10	14.5	7.8	2277
18.5	.227	28.6	13.9	16 100	11.5	.10	17.8	8.7	3912
18.5	2.270	----	11.7	------	11.5	1.00	----	7.3	----
23.1	2.800	27.9	8.1	8 900	14.4	1.00	17.4	5.1	2162
27.7	.333	29.9	14.8	17 200	17.3	.10	18.7	9.2	4179
27.7	3.330	----	6.1	------	17.3	1.00	----	3.8	----
34.4	.533	31.1	13.7	17 000	21.5	.13	19.4	8.5	4130
46.4	.560	----	8.1	------	29.0	.10	----	5.1	----
Packed ground limestone (ρ = 1450 kg/m^3)									
0	0.133	8.6	6.1	820	0	∞	5.6	4.0	225
8.9	.125	22.2	10.7	7 420	5.8	0.10	14.4	7.0	2038
8.9	2.500	16.8	11.4	3 290	5.8	2.00	10.9	7.4	903
8.9	2.500	18.8	9.6	4 810	5.8	2.00	12.2	6.2	1321
17.8	.253	26.7	10.9	11 000	11.6	.10	17.4	7.1	3021
17.8	1.265	23.5	11.2	8 600	11.6	.50	15.3	7.3	2362
17.8	2.530	22.2	8.9	6 650	11.6	1.00	14.4	5.8	1826
17.8	5.060	19.5	8.1	4 470	11.6	2.00	12.7	5.3	1228
22.2	.306	26.4	11.7	11 050	14.4	.10	17.2	7.6	3035
22.2	.786	24.4	12.7	9 420	14.4	.25	15.9	8.3	2587
22.2	1.560	20.8	10.2	4 910	14.4	.50	13.5	6.6	1348
22.2	1.560	24.8	11.0	8 800	14.4	.50	16.1	7.2	2417
22.2	3.130	21.8	9.1	6 680	14.4	1.00	14.2	5.9	1834
22.2	6.260	14.0	3.5	1 220	14.4	2.00	9.1	2.3	335
27.6	.373	28.7	13.0	13 600	17.9	.10	18.7	8.5	3735
27.6	.972	21.8	12.0	7 240	17.9	.25	14.2	7.8	1988
27.6	1.860	16.1	7.5	3 200	17.9	.50	10.5	4.9	879
27.6	3.730	3.4	2.5	------	17.9	1.00	2.2	1.6	----
35.6	.050	25.4	8.9	8 200	23.1	.01	16.5	5.8	2252
35.6	.50	23.5	8.6	7 240	23.1	.10	15.3	5.6	1988
35.6	1.250	20.3	5.7	2 940	23.1	.25	13.2	3.7	807
Mixture of 30% ground limestone and 70% sand (ρ = 1600 kg/m^3)									
0	0.133	10.0	5.3	764	0	∞	6.7	3.5	226
0	.133	10.0	4.5	650	0	∞	6.7	3.0	192
4.3	.067	18.4	8.9	3 900	2.9	0.10	12.2	5.9	1152
4.3	2.660	16.7	9.3	3 600	2.9	3.9	11.1	6.2	1063
8.6	.133	22.9	11.7	7 520	5.7	.10	15.3	7.8	2221
8.6	2.660	19.9	11.7	6 340	5.7	2.0	13.3	7.8	1873
8.6	5.320	18.4	10.4	4 810	5.7	3.9	12.3	6.9	1421
12.9	.200	24.4	10.8	10 210	8.6	.10	16.3	7.2	3016
12.9	1.000	22.3	11.9	8 580	8.6	.50	14.8	7.9	2535
12.9	2.000	21.3	13.0	8 000	8.6	1.00	14.2	8.7	2363
12.9	4.000	19.0	10.0	6 620	8.6	2.00	12.7	6.7	1956
12.9	8.000	16.5	4.3	2 630	8.6	4.00	11.0	2.9	777
17.1	.266	26.0	12.2	12 100	11.4	.10	17.3	8.1	3574
17.1	1.330	21.8	13.1	9 600	11.4	.50	14.5	8.7	2836
17.1	1.330	21.8	12.2	8 360	11.4	.50	14.5	8.1	2470
17.1	2.660	19.7	11.8	6 560	11.4	1.00	13.1	7.9	1938
17.1	5.320	15.7	6.0	2 550	11.4	2.00	10.5	4.0	753
21.6	.330	27.5	10.7	12 000	14.4	.10	18.3	7.1	3550
21.6	.330	26.0	10.9	11 320	14.4	.10	17.3	7.3	3344
21.6	1.667	23.7	11.3	9 690	14.4	.50	15.8	7.5	2860
21.6	3.330	19.0	6.9	3 960	14.4	1.00	12.7	4.6	1170
21.6	6.660	11.9	3.3	820	14.4	2.00	7.9	2.2	242
25.7	.400	26.3	11.2	10 500	17.1	.10	17.5	7.5	3102
25.7	1.000	24.3	10.5	8 300	17.1	.25	16.2	7.0	2452
25.7	2.000	23.9	9.0	7 070	17.1	.50	15.9	6.0	2088
25.7	2.00	24.1	9.5	7 420	17.1	.50	16.1	6.3	2192
25.7	3.000	22.7	7.2	5 800	17.1	.75	15.1	4.8	1713
25.7	4.000	14.1	4.0	1 320	17.1	1.00	9.4	2.7	390
30.2	.467	24.1	10.7	8 430	20.1	.10	16.1	7.1	2490
30.2	1.165	20.1	7.5	5 070	20.1	.25	13.4	5.0	1498
30.2	2.330	20.9	6.4	4 020	20.1	.50	13.9	4.3	1188
30.2	2.330	19.1	5.6	2 630	20.1	.50	12.7	3.7	777
30.2	3.500	16.8	3.9	1 480	20.1	.75	11.2	2.6	437
34.4	.533	23.5	2.8	------	22.9	.10	15.7	1.9	----
34.4	1.330	18.8	5.2	1 980	22.9	.25	12.5	3.5	585

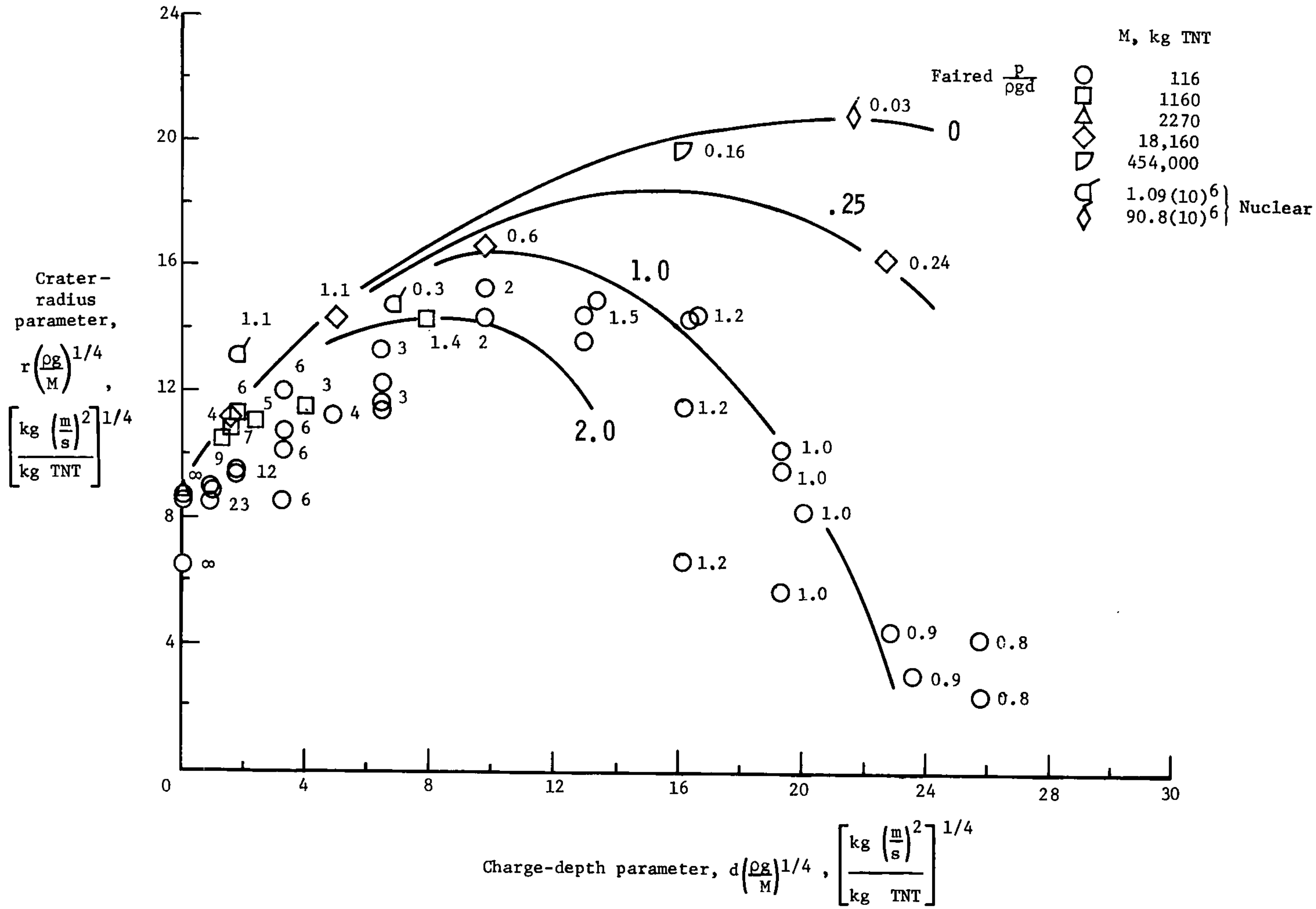

Figure 1.- Apparent effect of the given ratios of the atmospheric to lithostatic pressure on crater radii in alluvium.

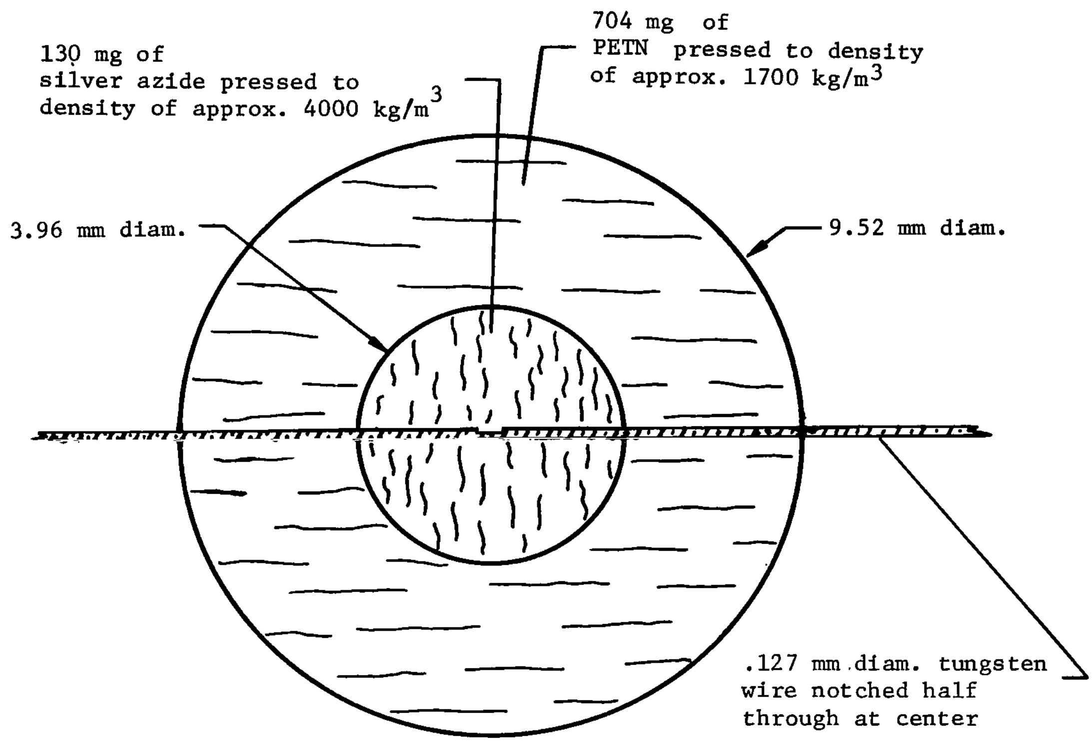

Figure 2.- Centrally initiated spherical charge.

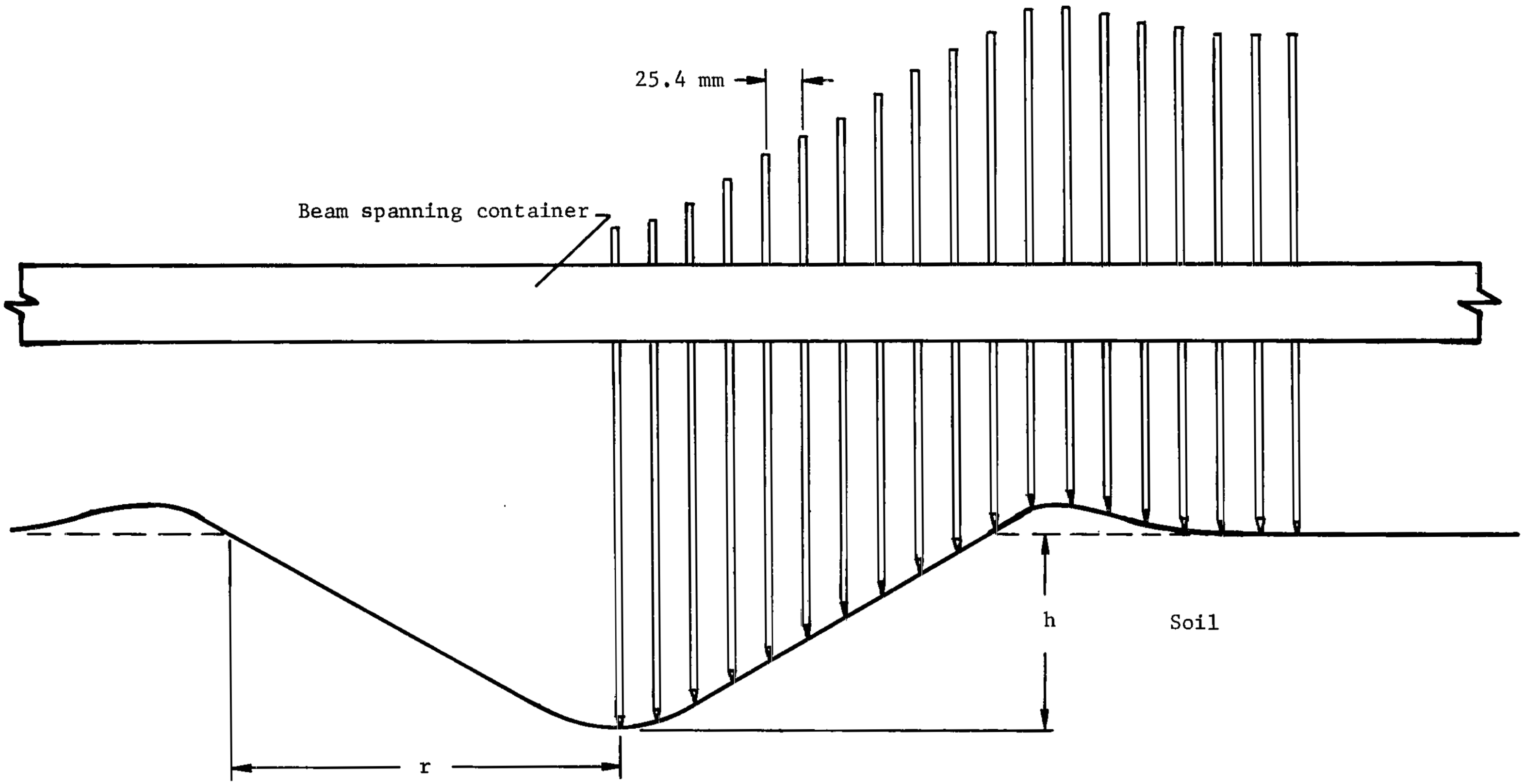

Figure 3.- Device with movable probes for measuring craters.

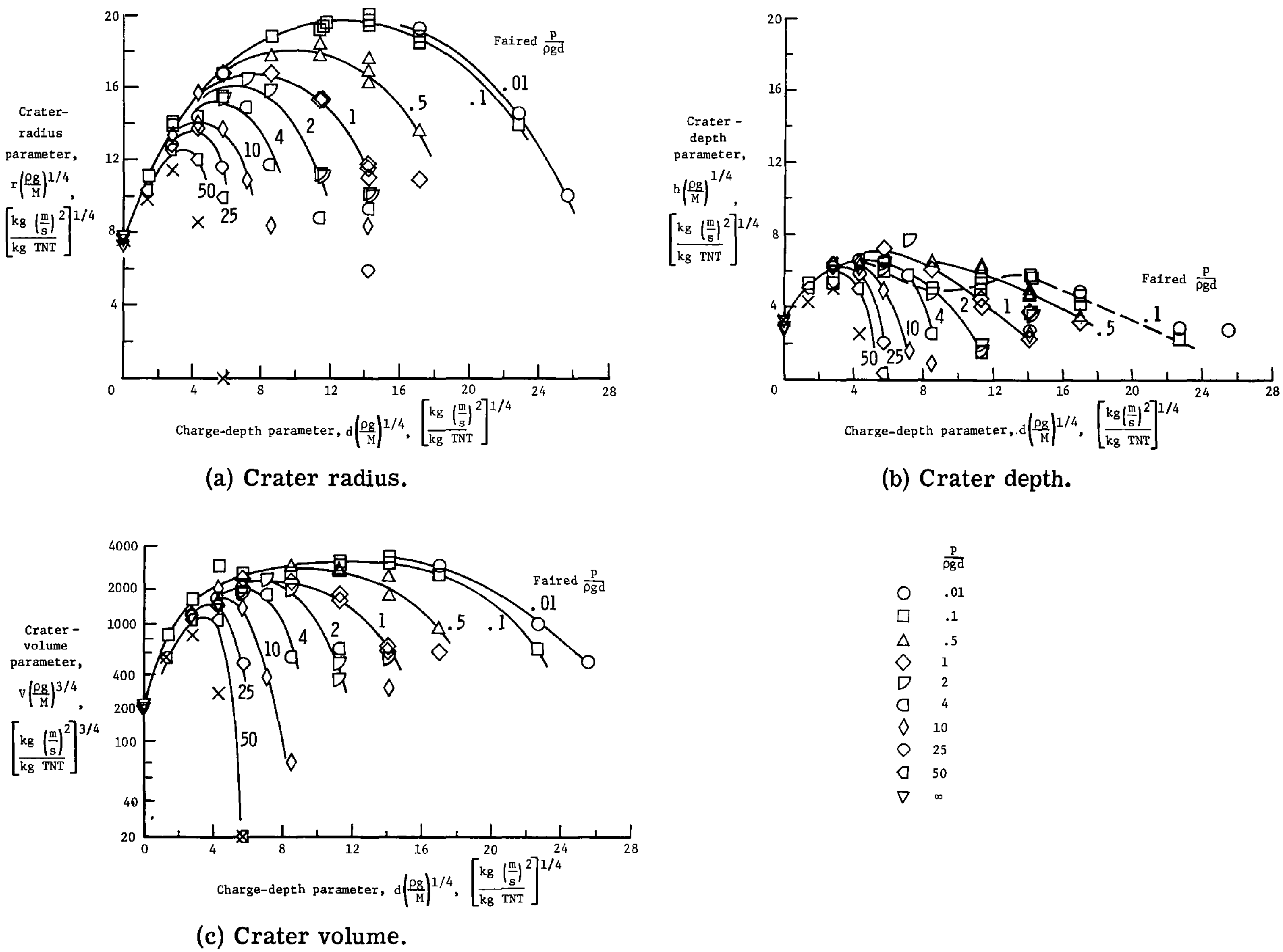

(a) Crater radius.

(b) Crater depth.

(c) Crater volume.

Figure 4.- Effect of the ratio of the atmospheric to lithostatic pressures on crater dimensions in sand. Points designated by × are for tests at standard atmospheric pressure ($p = 101.3\ kN/m^2$). $\rho = 1520\ kg/m^3$; $M = 0.00082$ kg TNT.

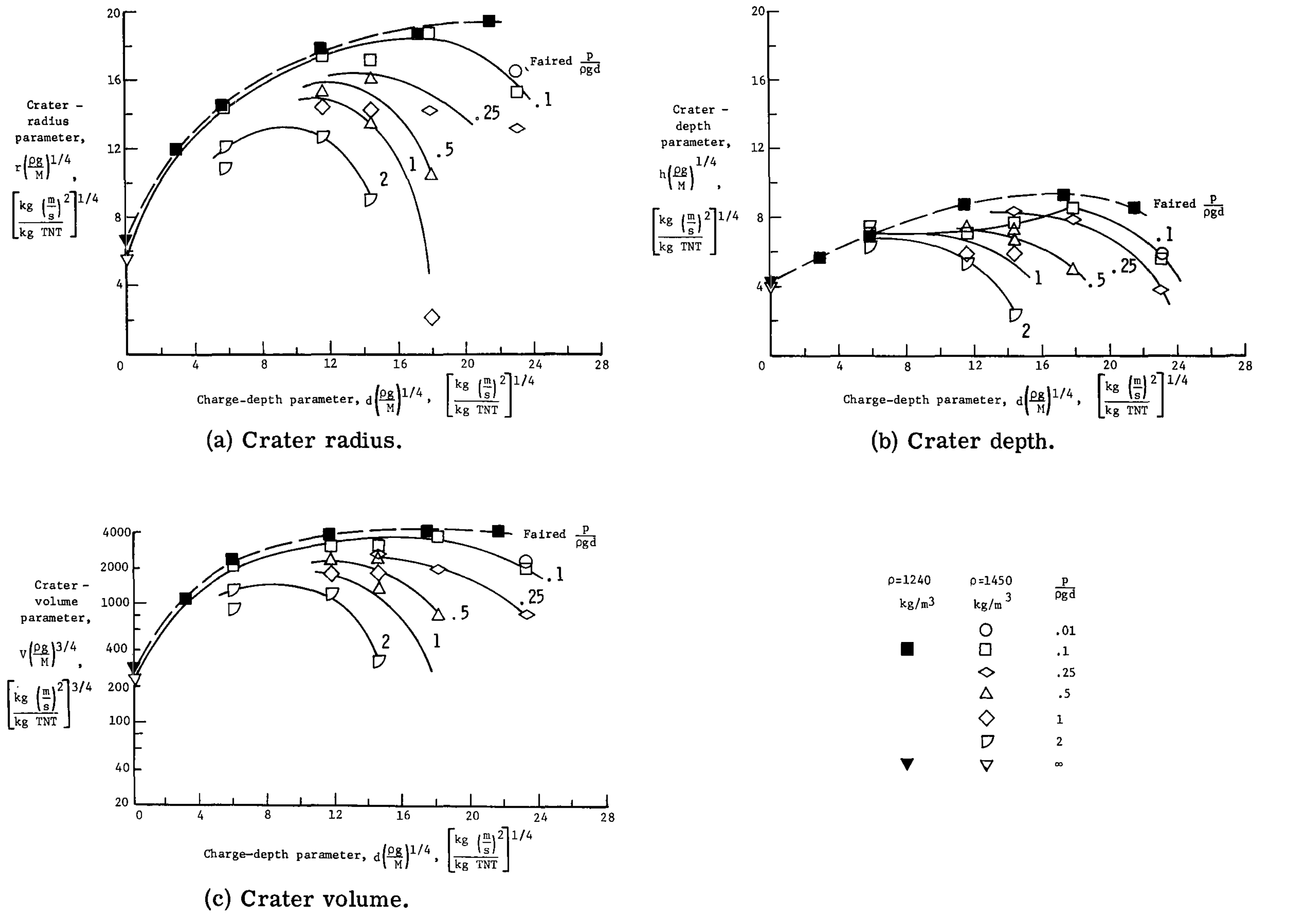

Figure 5.- Effect of the ratio of the atmospheric to lithostatic pressure on crater dimensions in ground limestone. M = 0.00082 kg TNT.

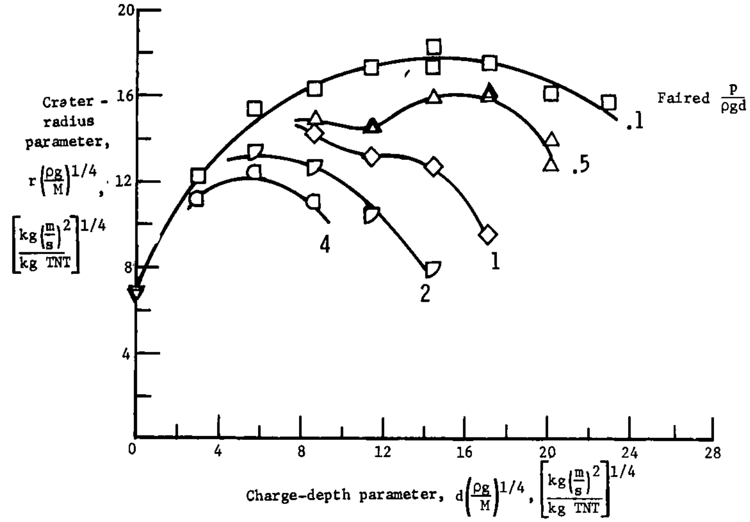

(a) Crater radius.

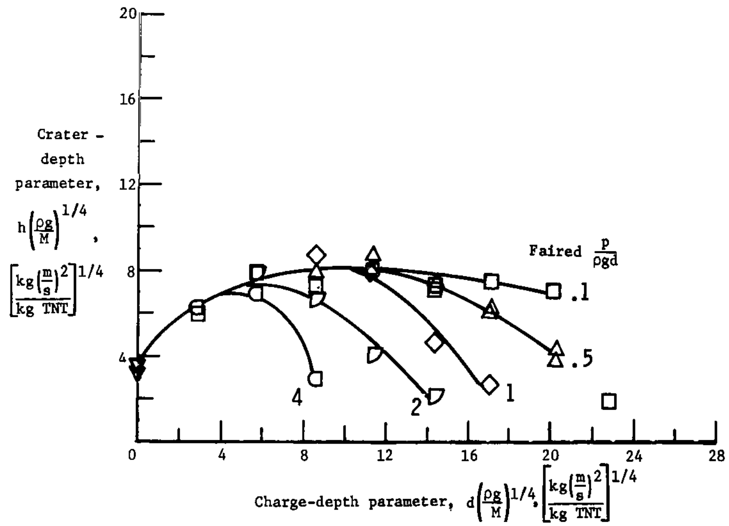

(b) Crater depth.

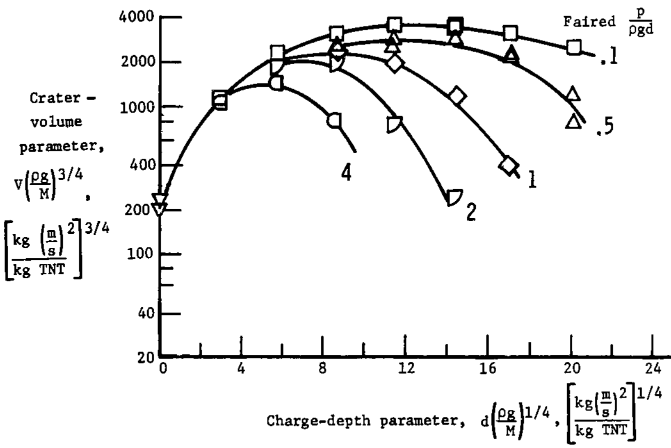

(c) Crater volume.

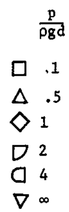

Figure 6.- Effect of the ratio of the atmospheric to lithostatic pressure on crater dimensions in a mixture of 30% ground limestone and 70% sand. ρ = 1600 kg/m^3; M = 0.00082 kg TNT.

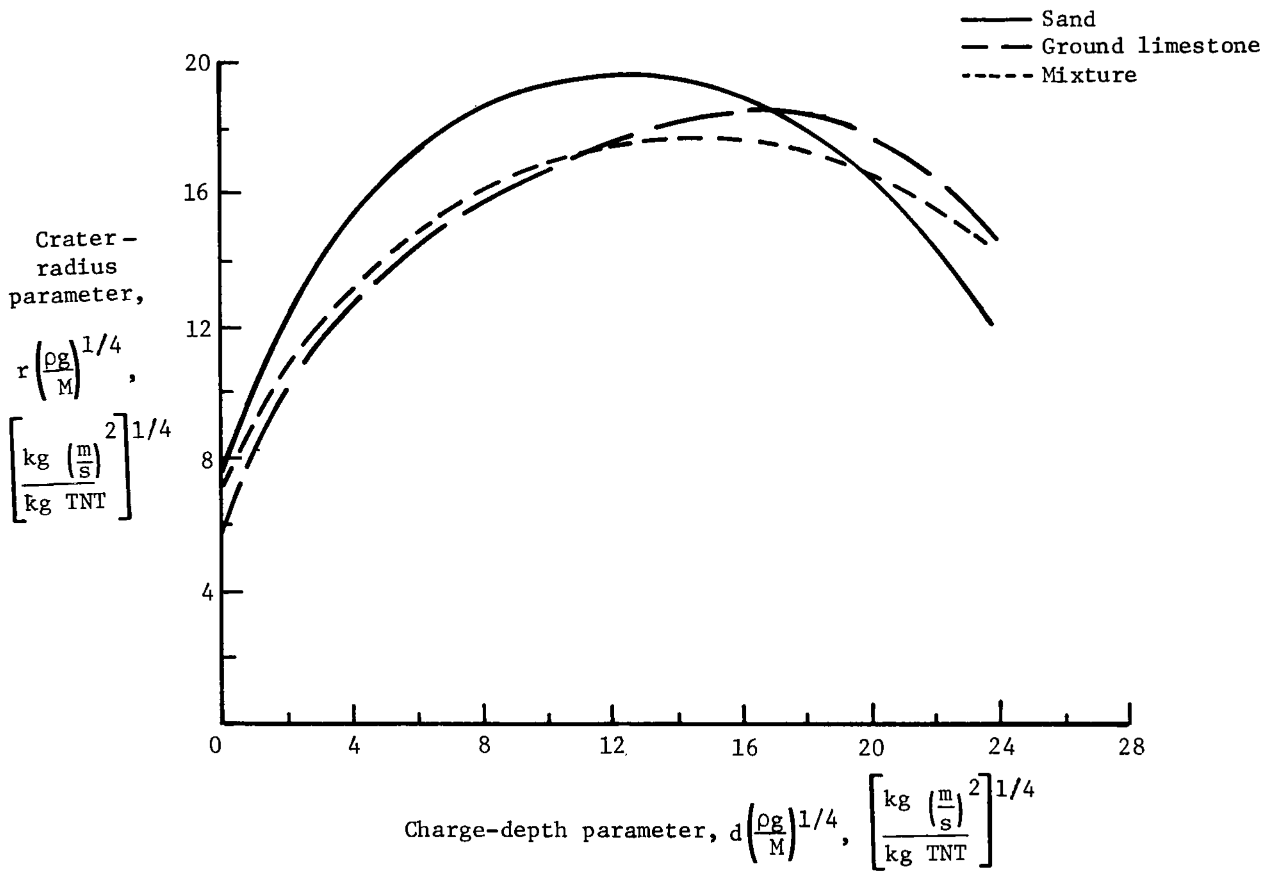

Figure 7.- Comparison of crater radii in sand, ground limestone, and a mixture of 30% ground limestone and 70% sand. $\frac{p}{\rho g d} = 0.1$.

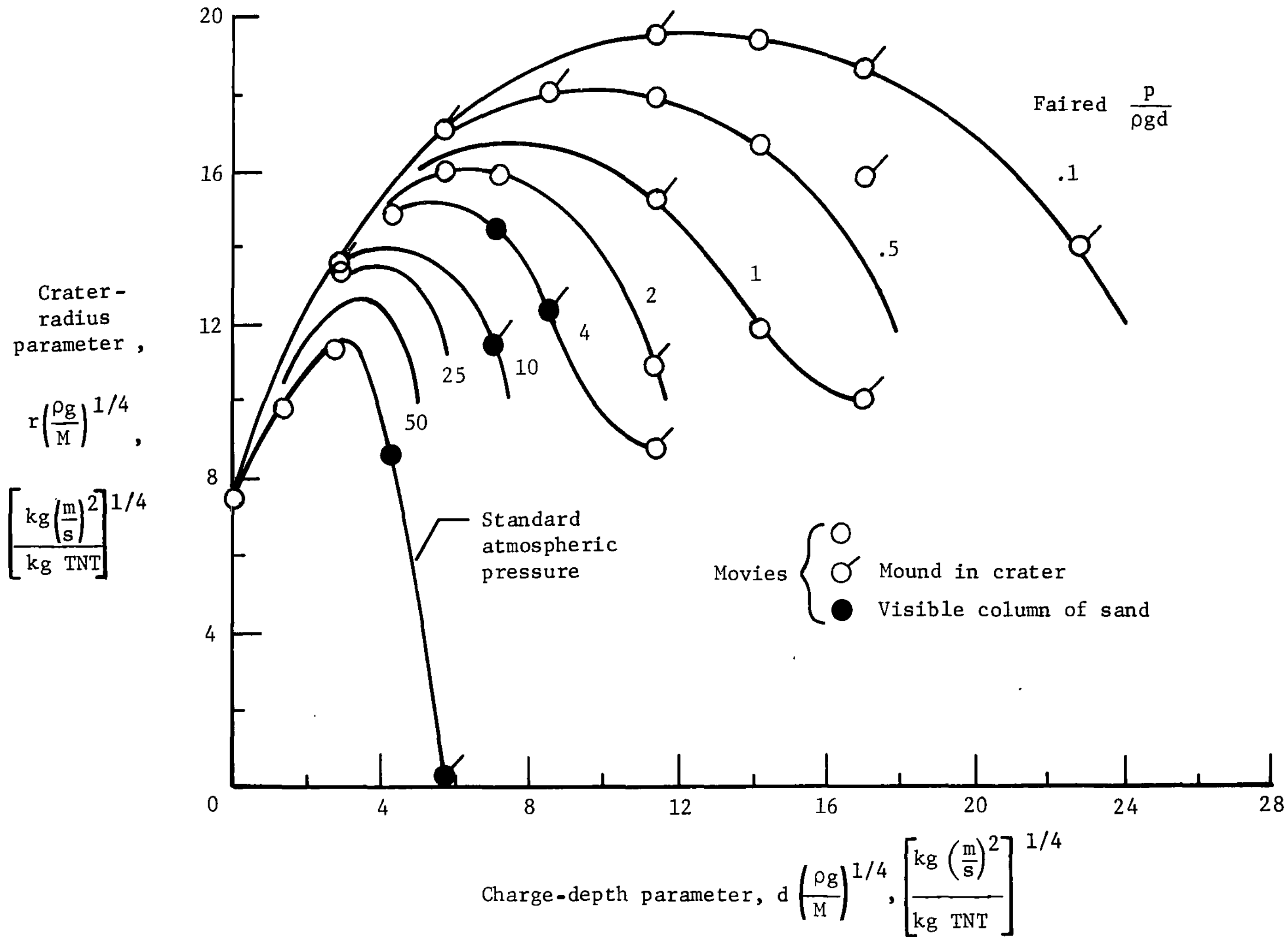

Figure 8.- Data points from figure 4(a) for which movies were taken with an indication of whether or not columns of sand were visible and if mounds were formed.

L-71-635

Figure 9.- Movie still showing column of sand.

$$d\left(\frac{\rho g}{M}\right)^{1/4} = 7.1; \quad \frac{p}{\rho g d} = 10.$$

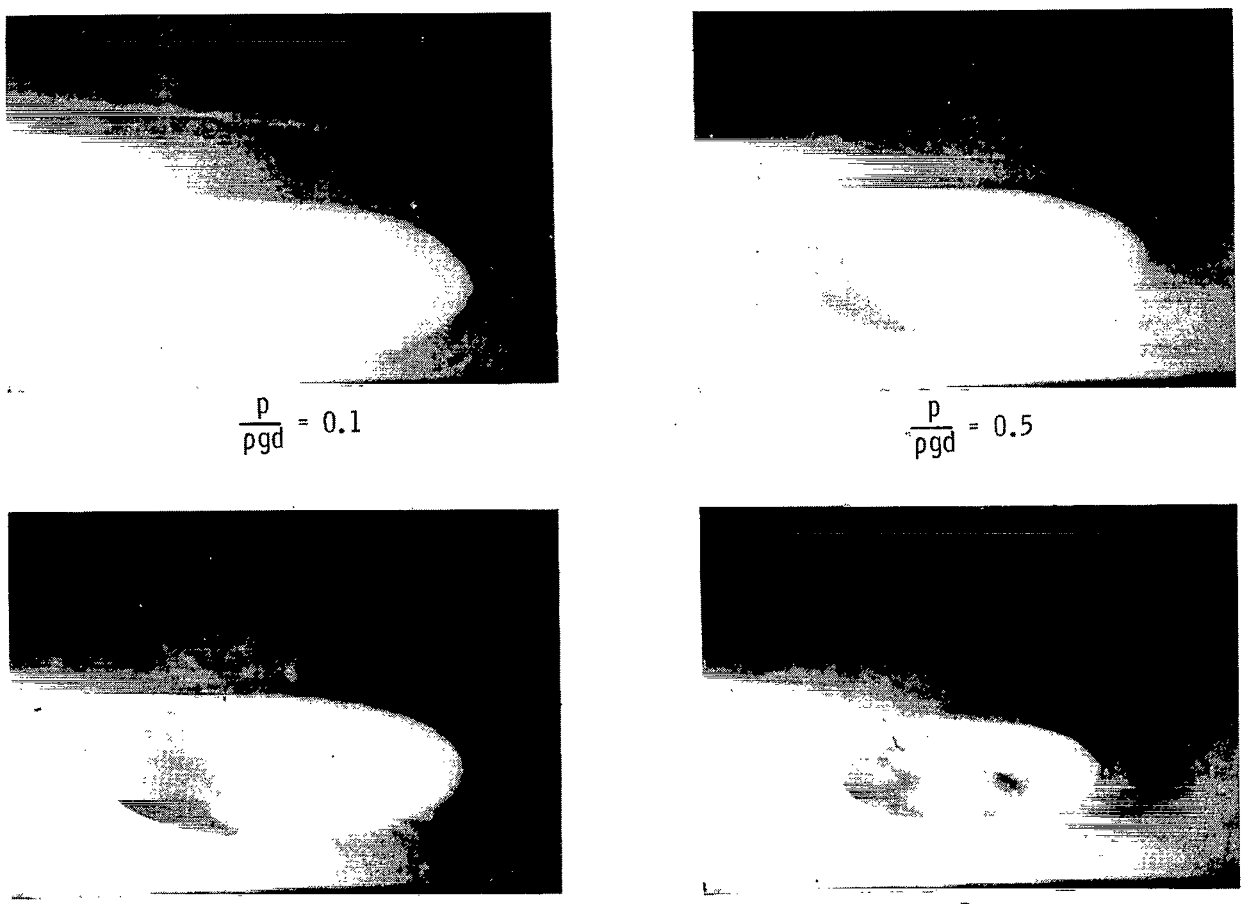

$\frac{p}{\rho g d} = 0.1$ $\quad$ $\frac{p}{\rho g d} = 0.5$

$\frac{p}{\rho g d} = 1$ $\quad$ $\frac{p}{\rho g d} = 2$

L-71-636

(a) $d\left(\frac{\rho g}{M}\right)^{1/4} = 11.3.$

Figure 10.- Craters in sand illustrating the effect of the dimensionless ratio $p/\rho gd$.

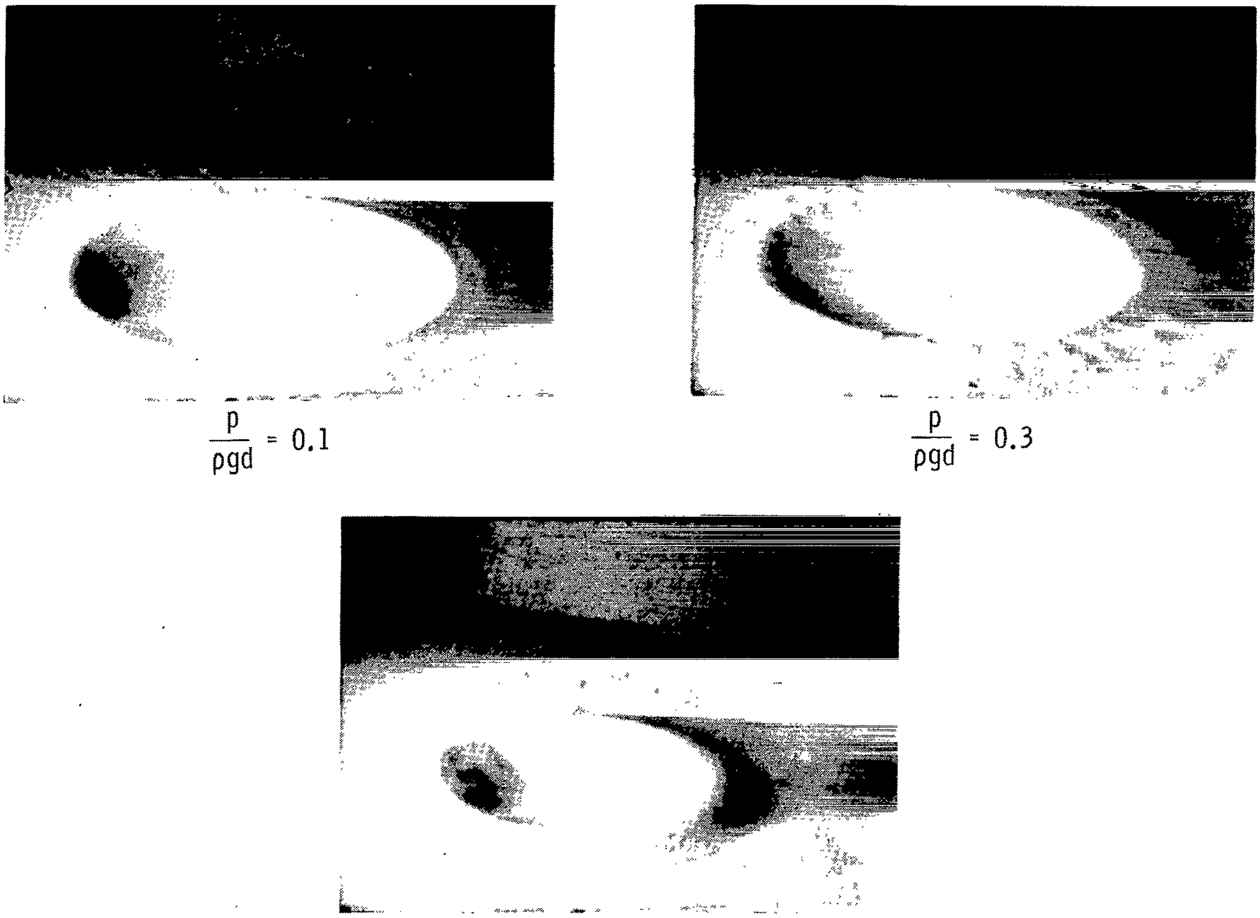

$\frac{p}{\rho g d} = 0.1$

$\frac{p}{\rho g d} = 0.3$

$\frac{p}{\rho g d} = 1$

L-71-637

(b) $d\left(\frac{\rho g}{M}\right)^{1/4} = 17.0.$

Figure 10.- Concluded.

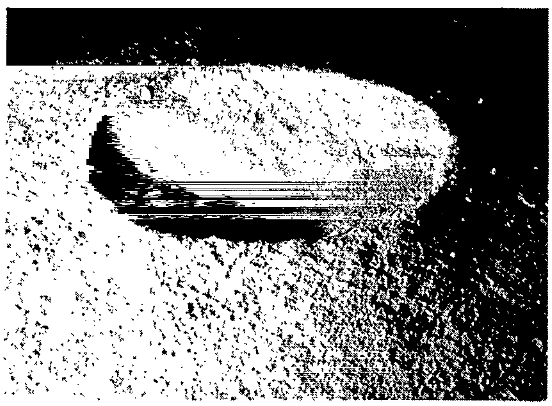

$\frac{p}{\rho g d} = 0.1$

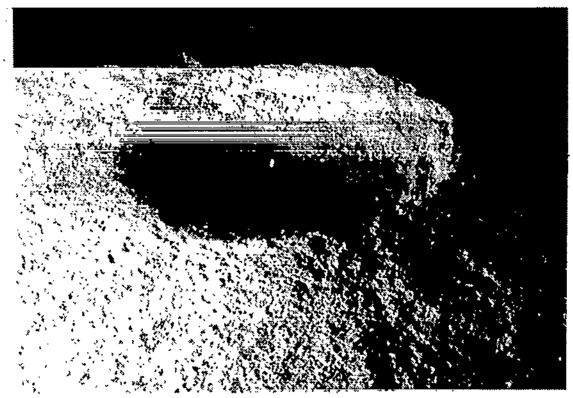

$\frac{p}{\rho g d} = 0.5$

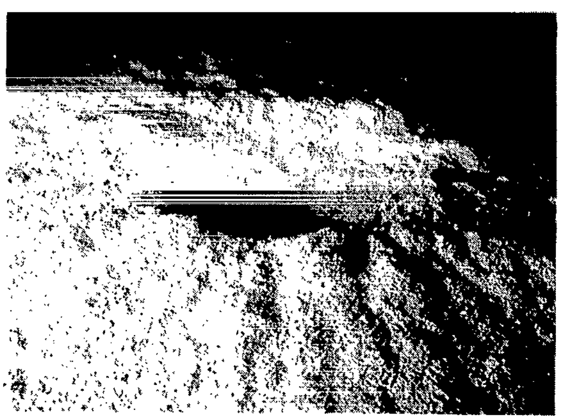

$\frac{p}{\rho g d} = 1$

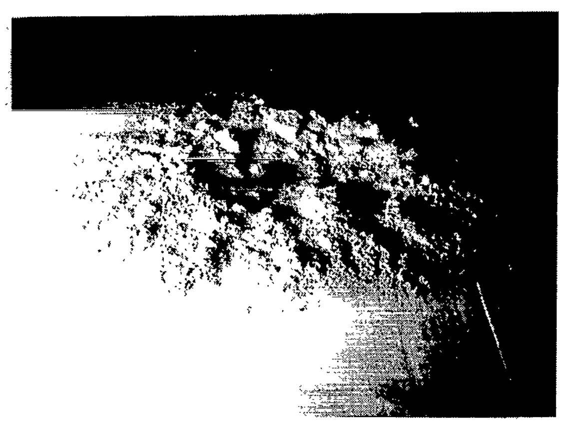

$\frac{p}{\rho g d} = 2$

L-71-638

(a) $d\left(\frac{\rho g}{M}\right)^{1/4} = 11.6.$

Figure 11.- Craters in packed ground limestone illustrating the effect of the dimensionless ratio $p/\rho g d$.

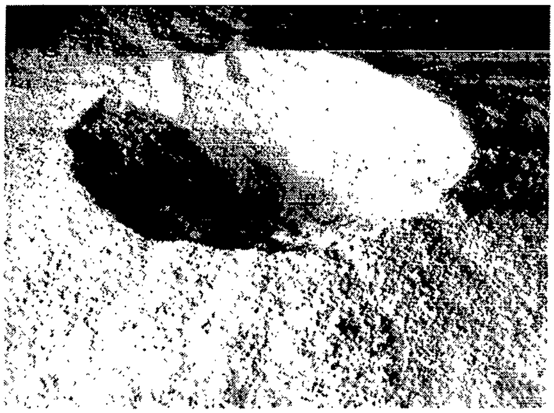

$\frac{p}{\rho g d} = 0.1$

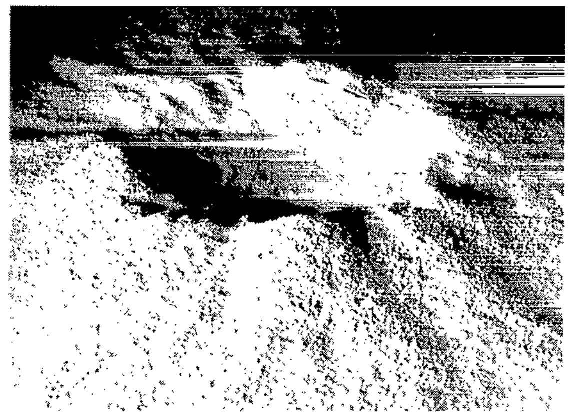

$\frac{p}{\rho g d} = 0.25$

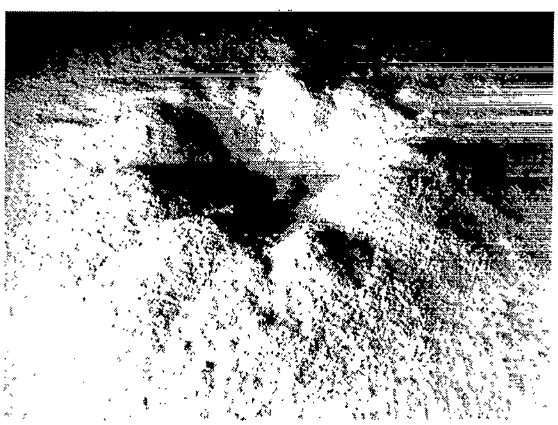

$\frac{p}{\rho g d} = 0.5$

$\frac{p}{\rho g d} = 1$

L-71-639

(b) $d\left(\frac{\rho g}{M}\right)^{1/4} = 17.9.$

Figure 11.- Concluded.

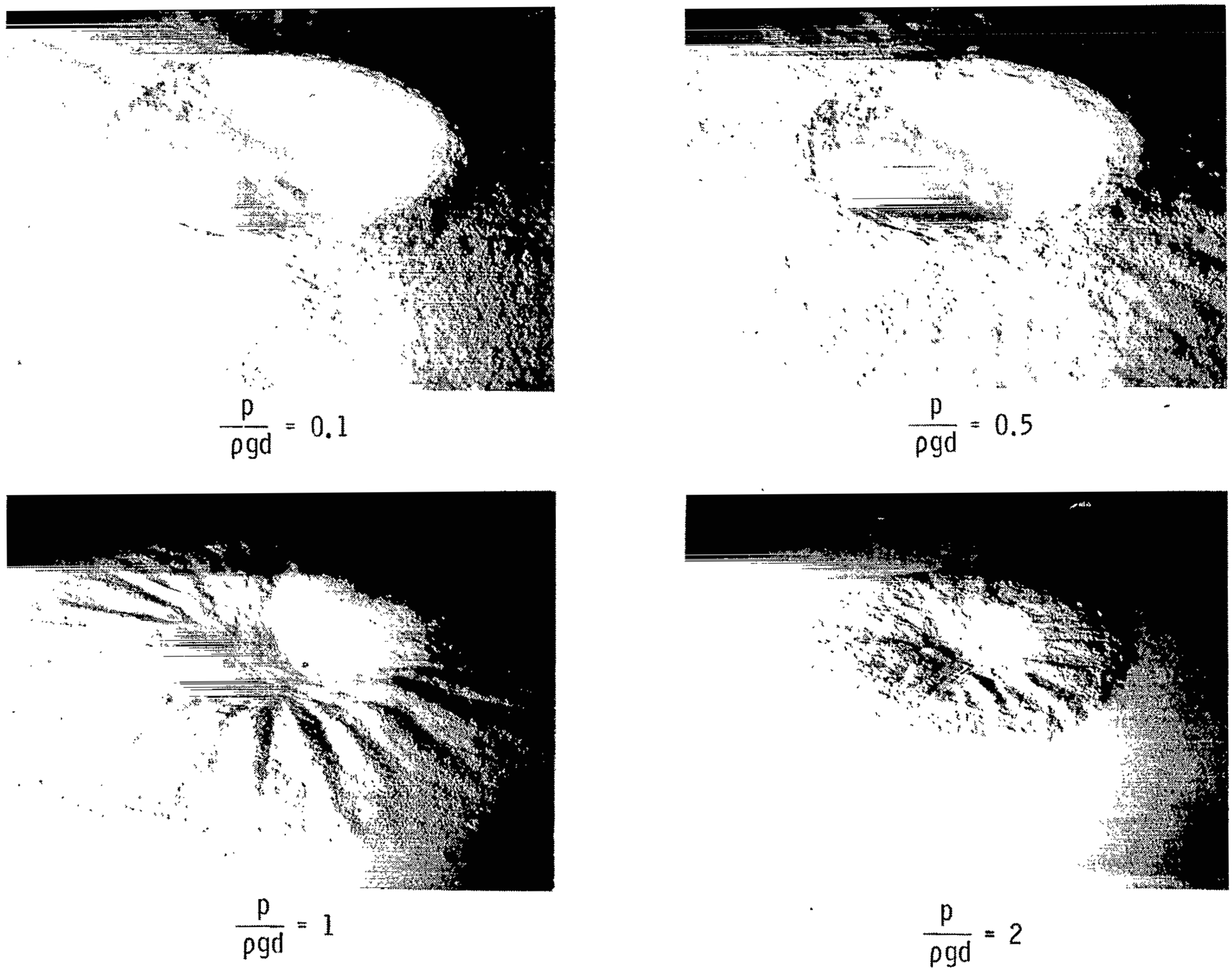

L-71-640

Figure 12.- Craters in a mixture of 30% ground limestone and 70% sand illustrating the effect of the dimensionless ratio $p/\rho gd$. $d\left(\frac{\rho g}{M}\right)^{1/4} = 14.4$.

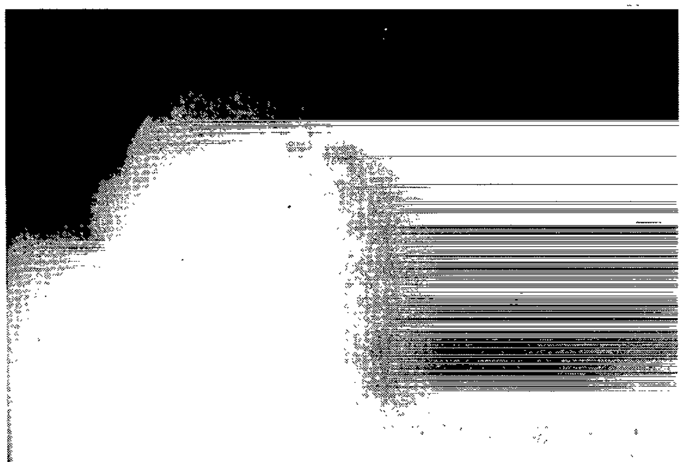

L-71-641

Figure 13.- Movie still showing thin veil of sand preceding primary dome.

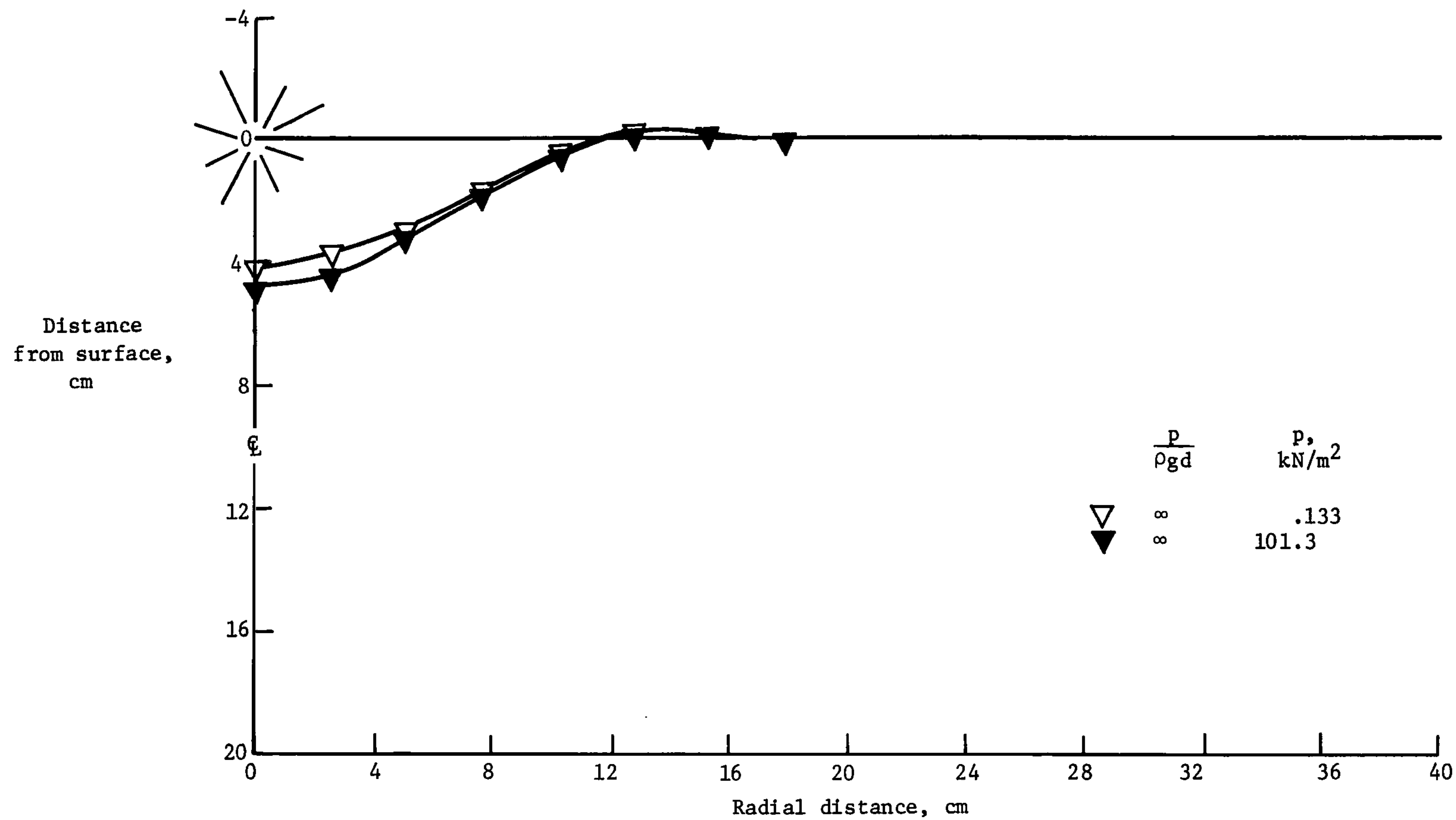

(a) Charge depth = 0 cm; $d\left(\frac{\rho g}{M}\right)^{1/4} = 0$.

Figure 14.- Crater profiles in sand. $\rho = 1520$ kg/m^3. Repeated tests are shown by solid and half-open symbols.

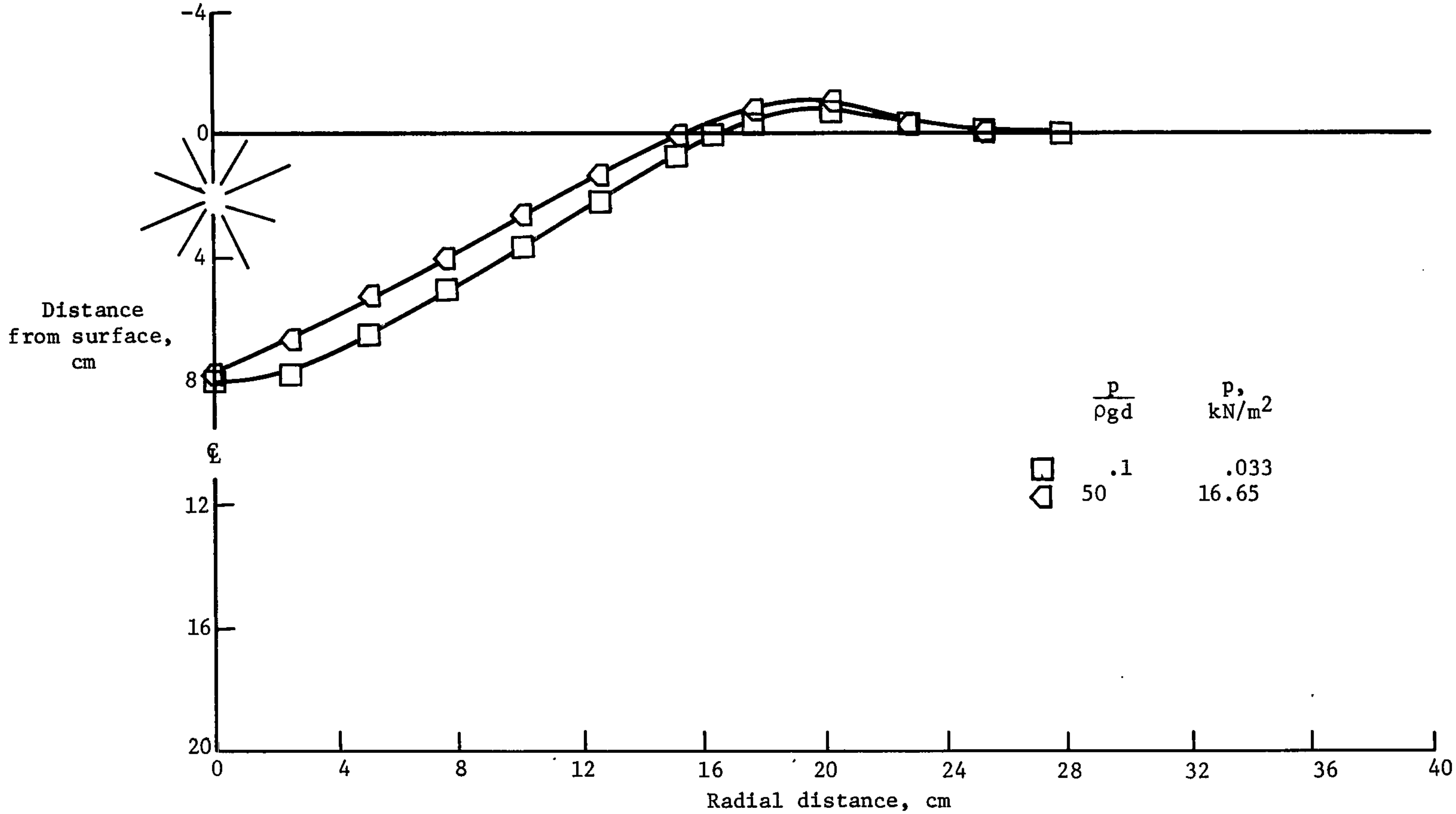

(b) Charge depth = 2.1 cm; $d\left(\frac{\rho g}{M}\right)^{1/4} = 1.4$.

Figure 14.- Continued.

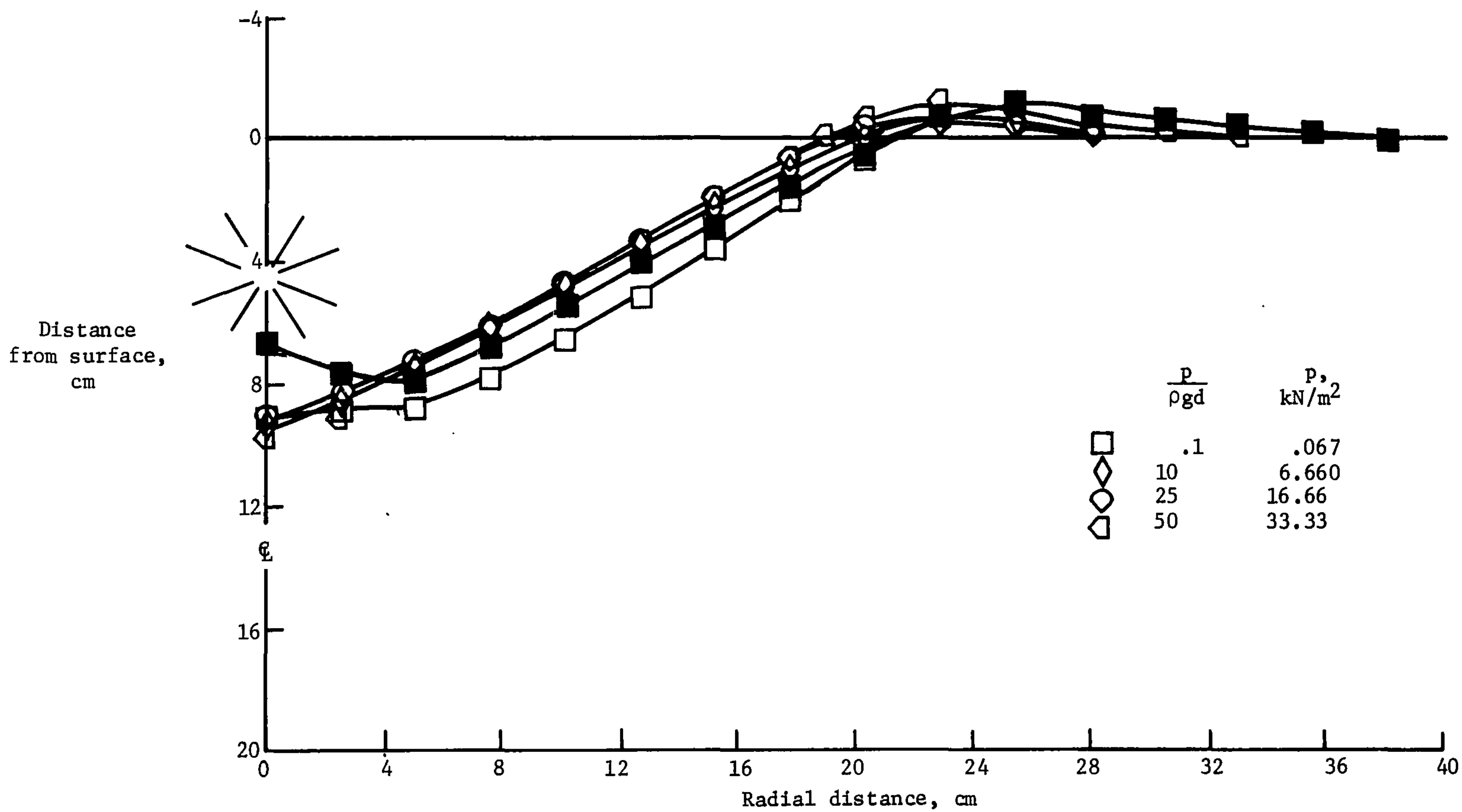

(c) Charge depth = 4.3 cm; $d\left(\frac{\rho g}{M}\right)^{1/4} = 2.8$.

Figure 14.- Continued.

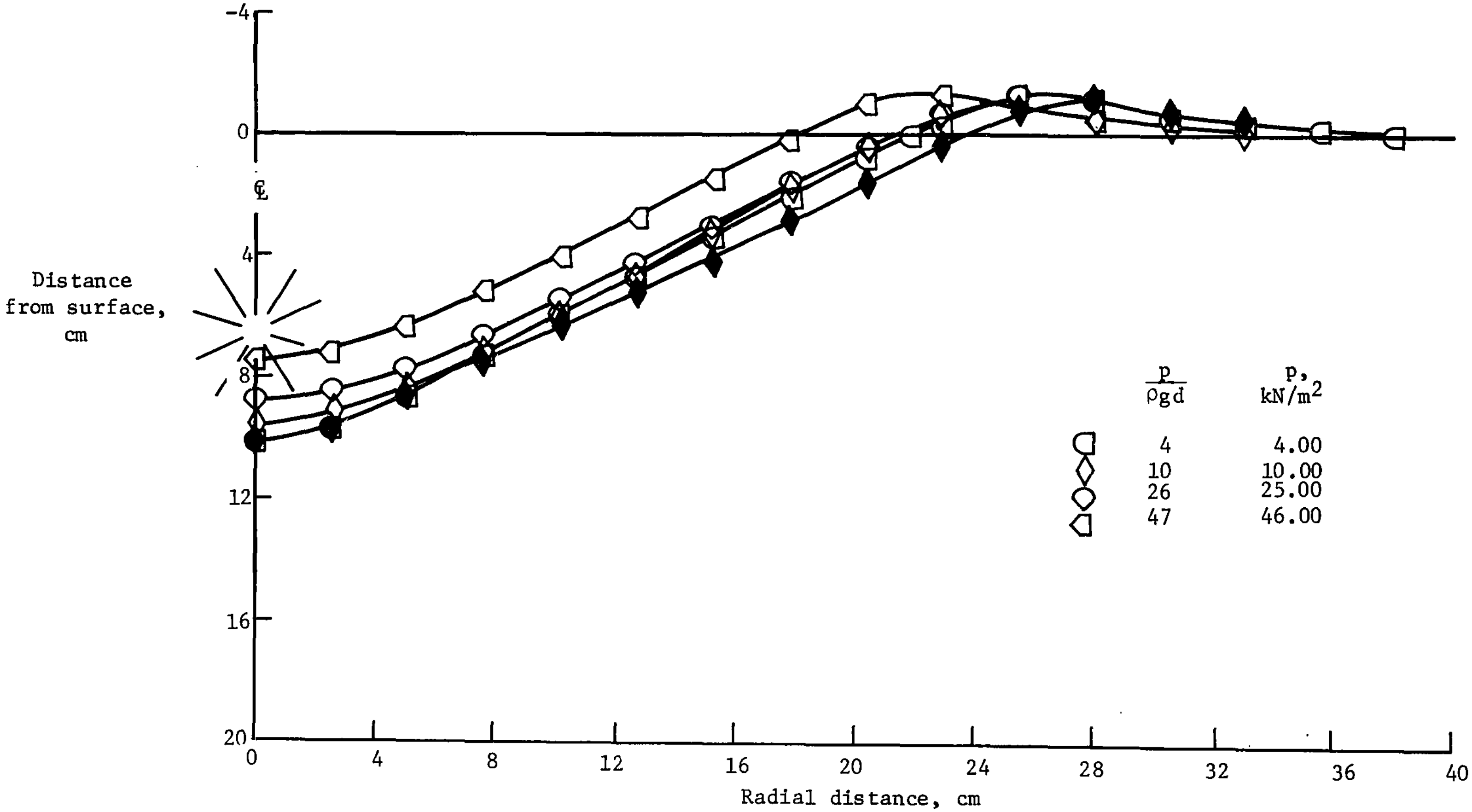

(d) Charge depth = 6.5 cm; $d\left(\frac{\rho g}{M}\right)^{1/4} = 4.3$.

Figure 14.- Continued.

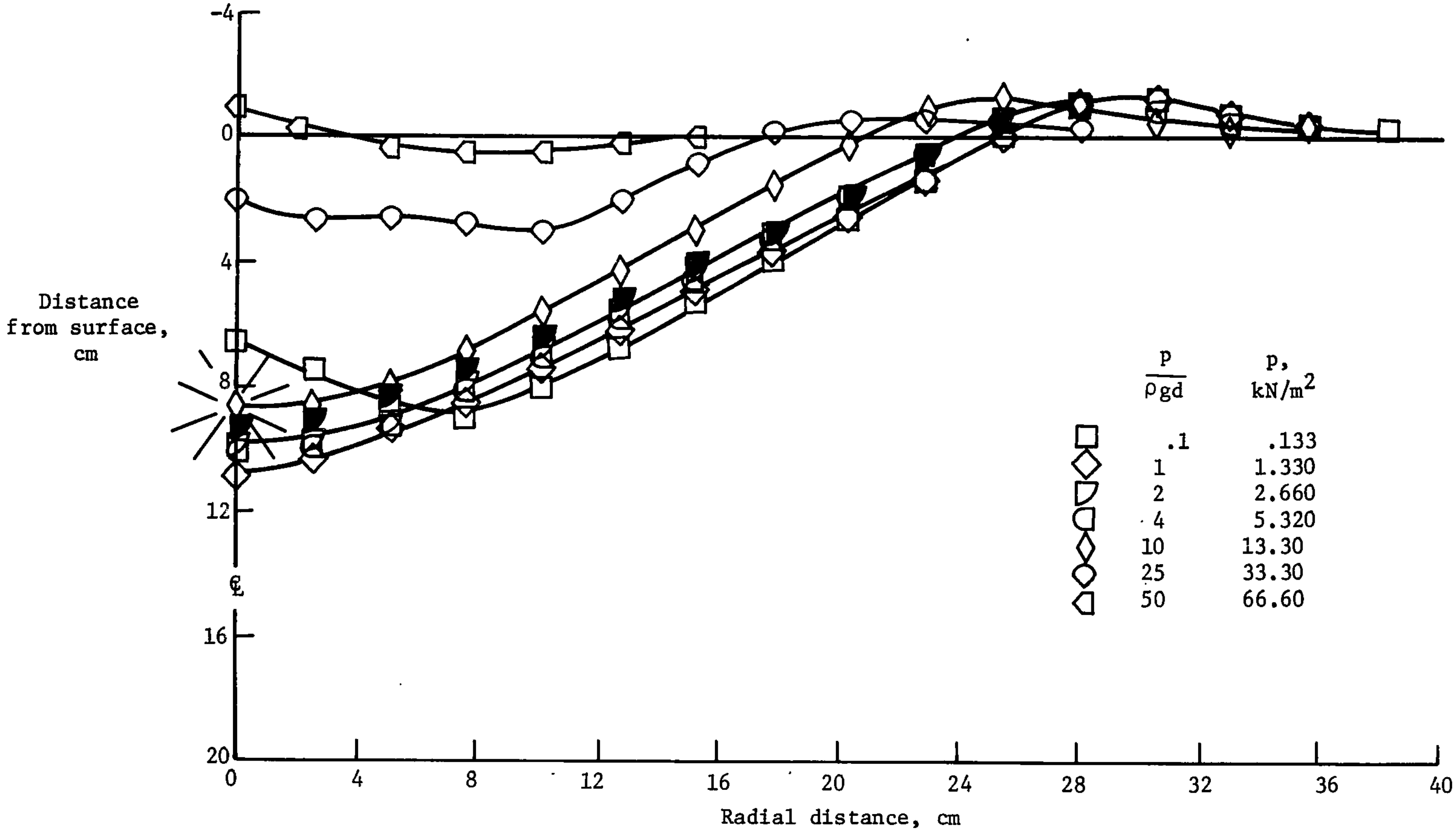

(e) Charge depth = 8.6 cm; $d\left(\frac{\rho g}{M}\right)^{1/4} = 5.7$.

Figure 14.- Continued.

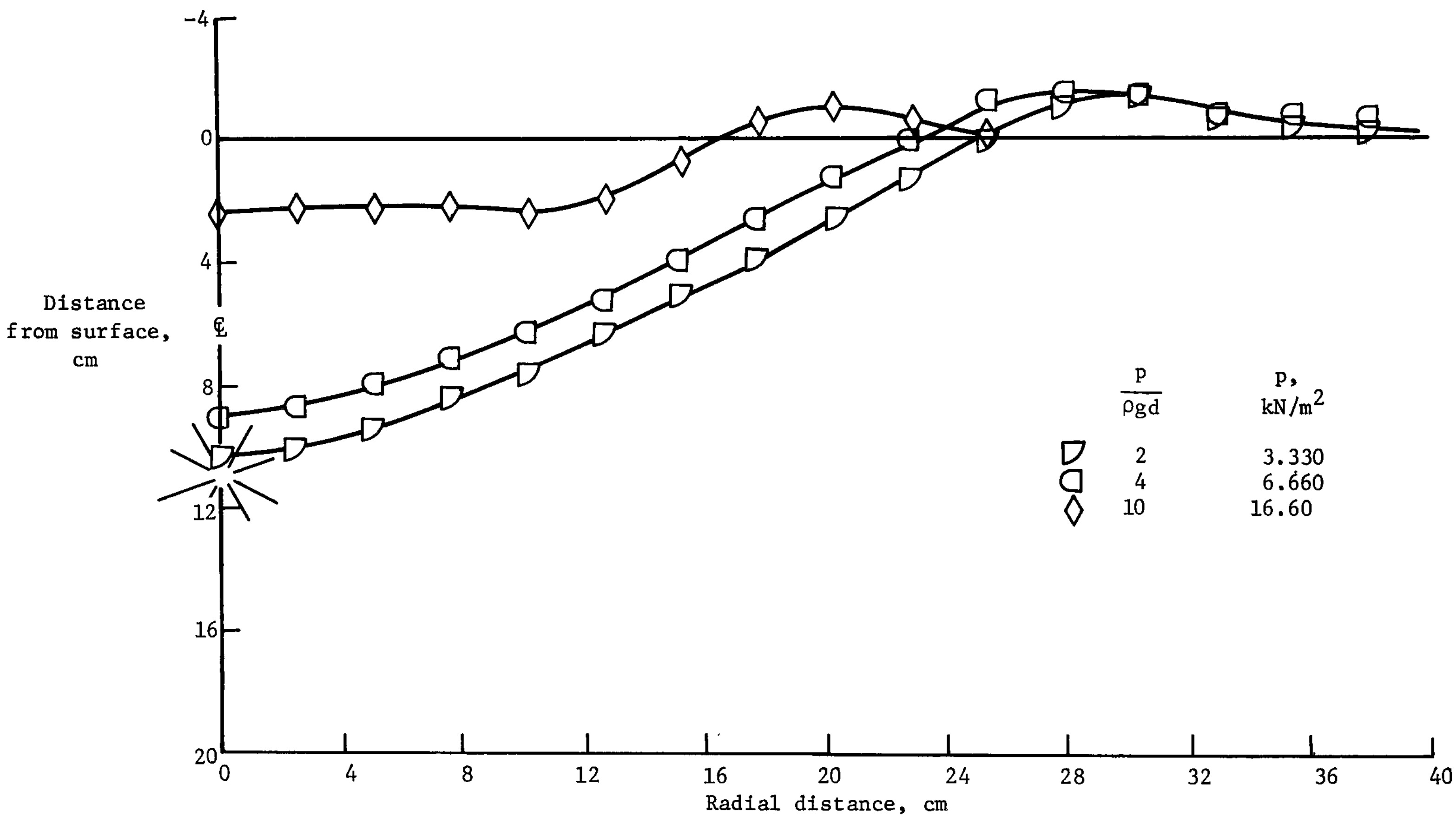

(f) Charge depth = 10.8 cm; $d\left(\frac{\rho g}{M}\right)^{1/4} = 7.1.$

Figure 14.- Continued.

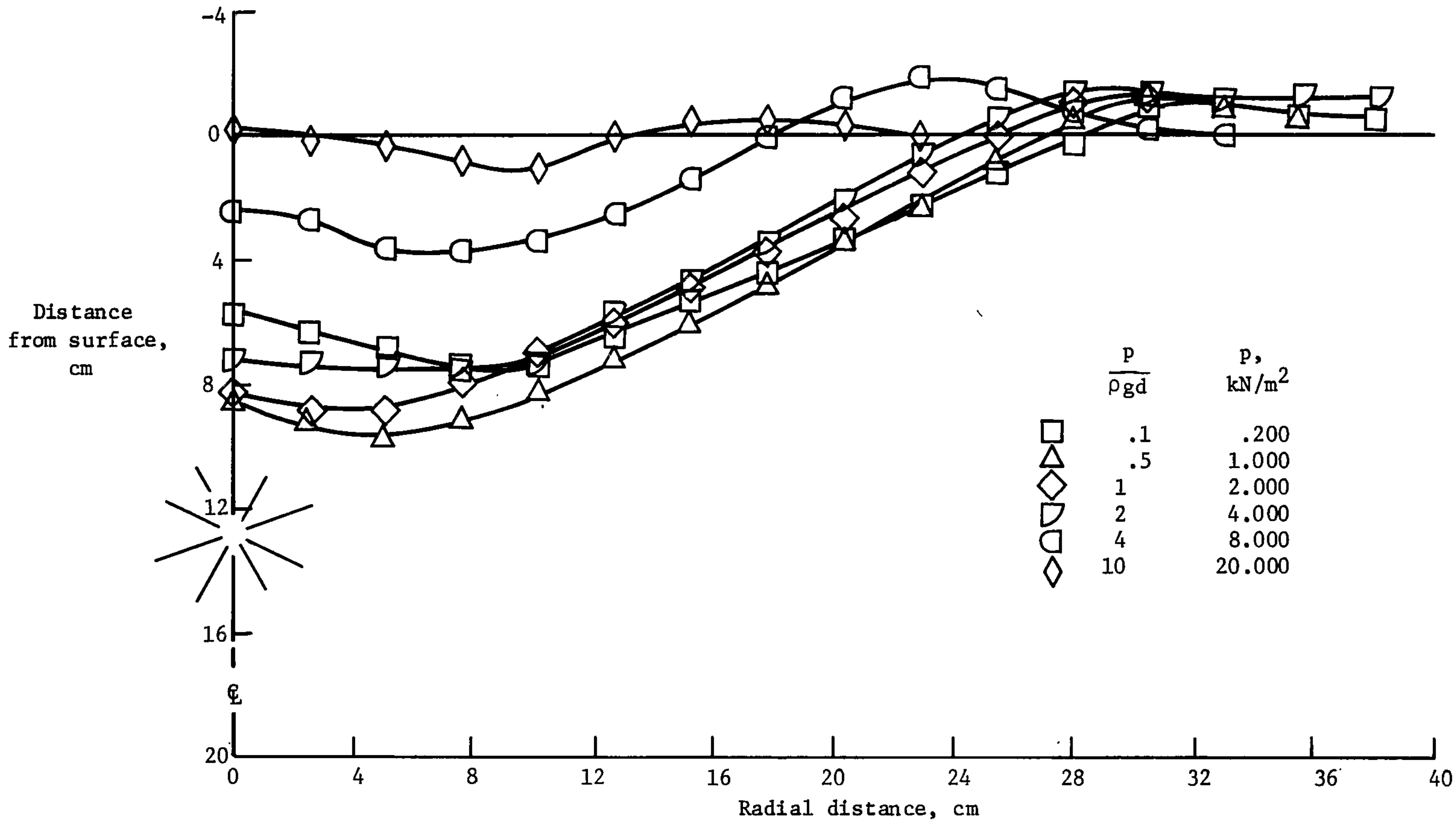

(g) Charge depth = 12.9 cm; $d\left(\frac{\rho g}{M}\right)^{1/4} = 8.5$.

Figure 14.- Continued.

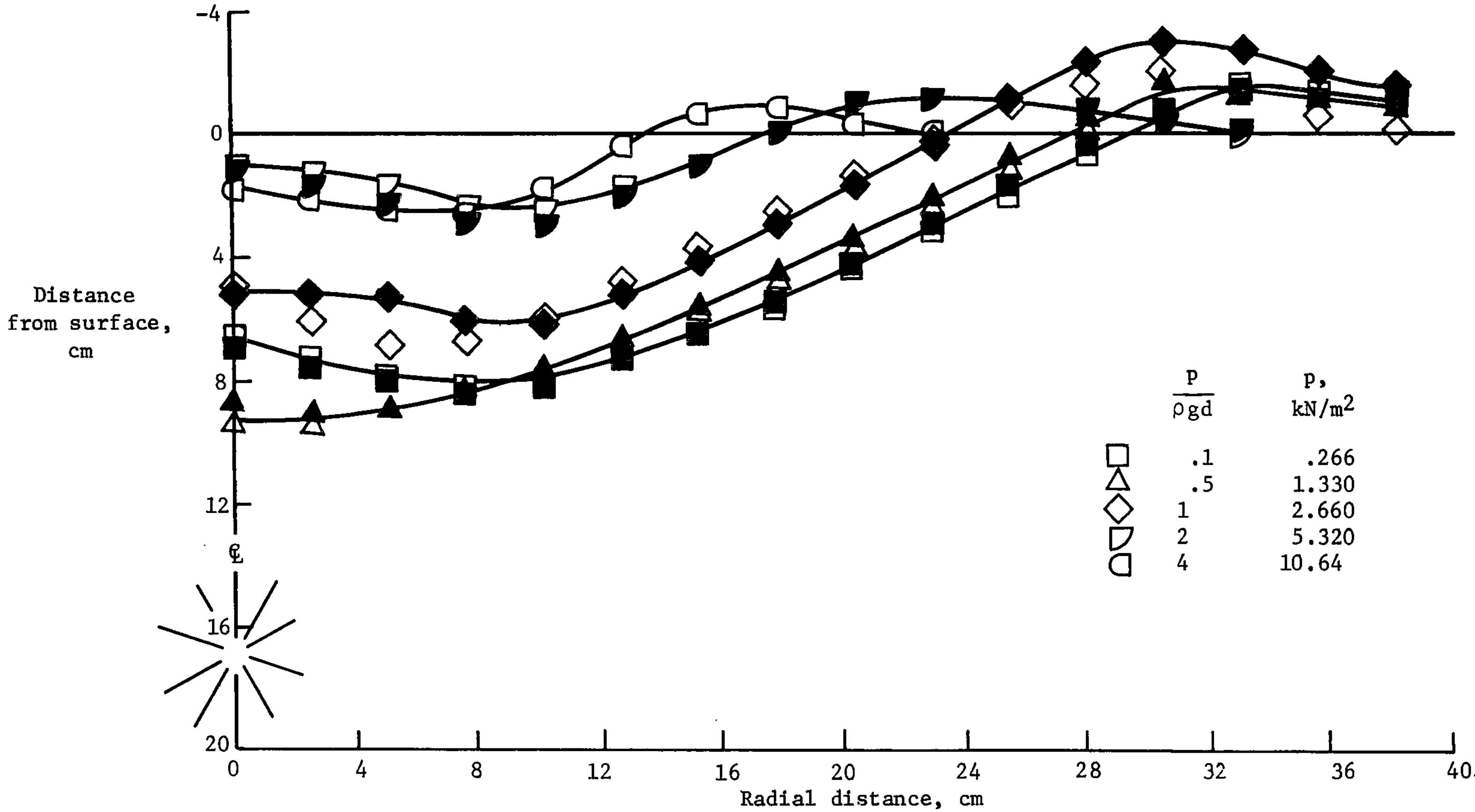

(h) Charge depth = 17.2 cm; $d\left(\frac{\rho g}{M}\right)^{1/4} = 11.3$.

Figure 14.- Continued.

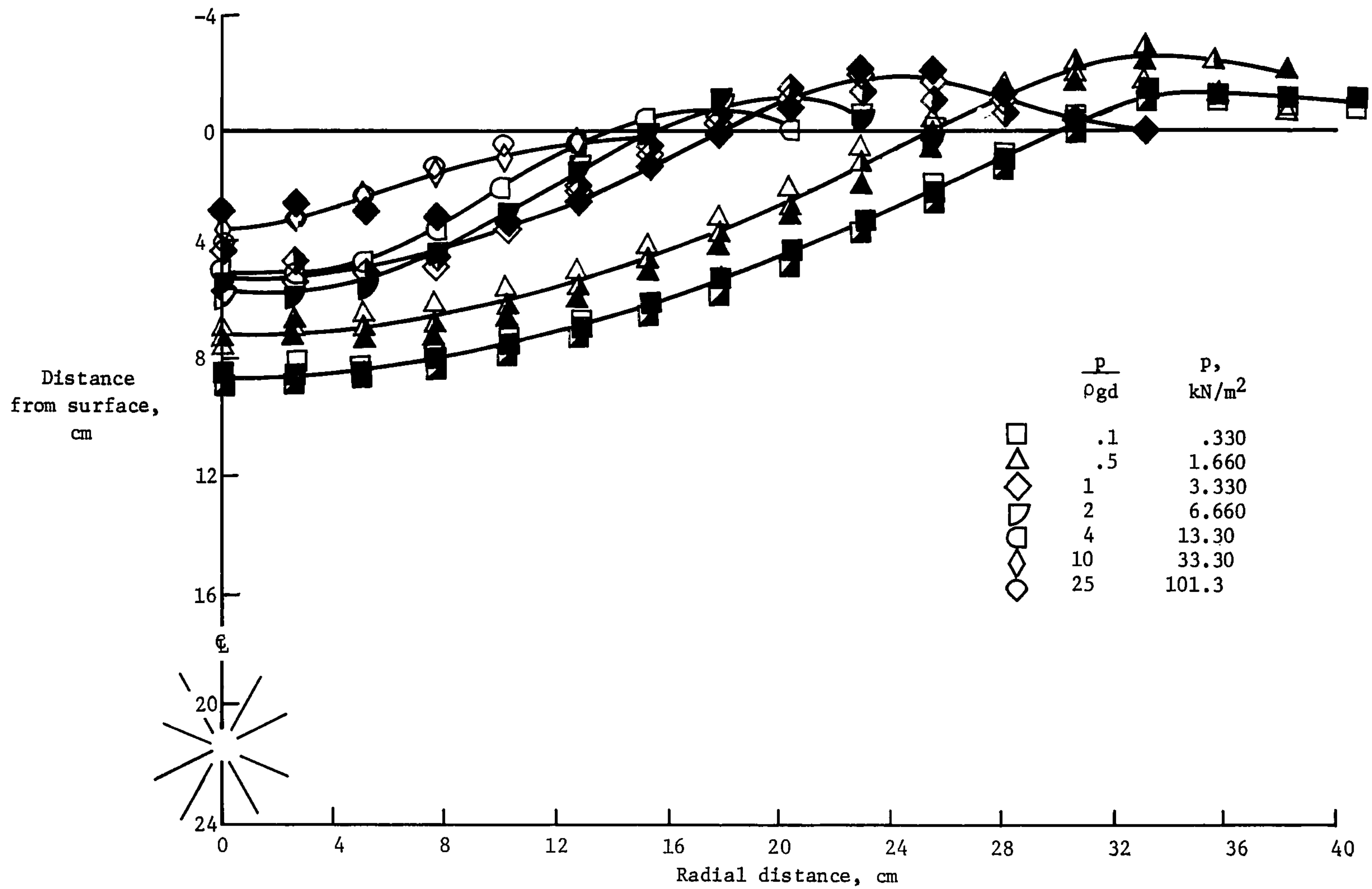

(i) Charge depth = 21.5 cm; $d\left(\frac{\rho g}{M}\right)^{1/4} = 14.1.$

Figure 14.- Continued.

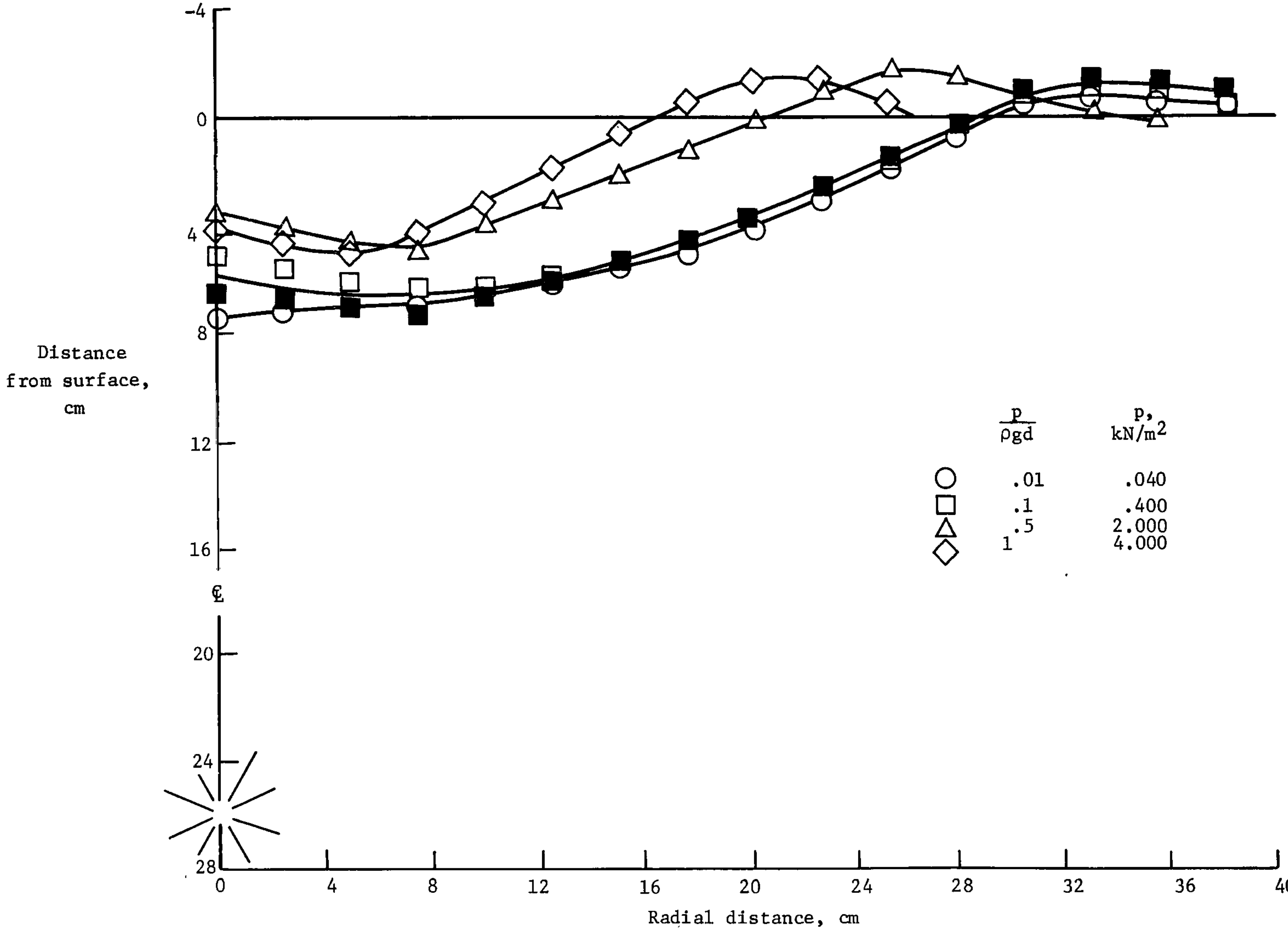

(j) Charge depth = 25.9 cm; $d\left(\frac{\rho g}{M}\right)^{1/4} = 17.0$.

Figure 14.- Continued.

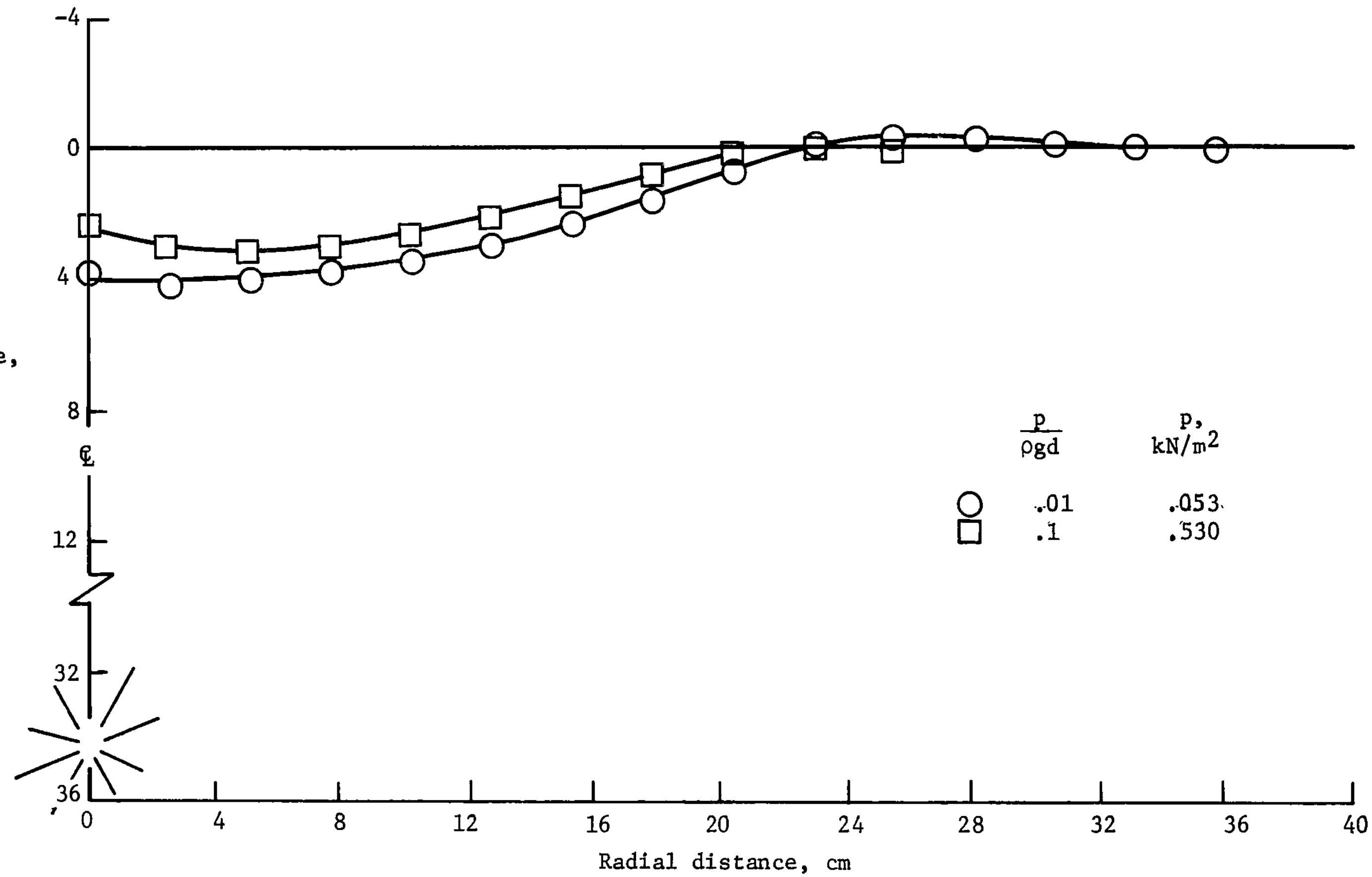

(k) Charge depth = 34.5 cm; $d\left(\frac{\rho g}{M}\right)^{1/4} = 22.7$.

Figure 14.- Continued.

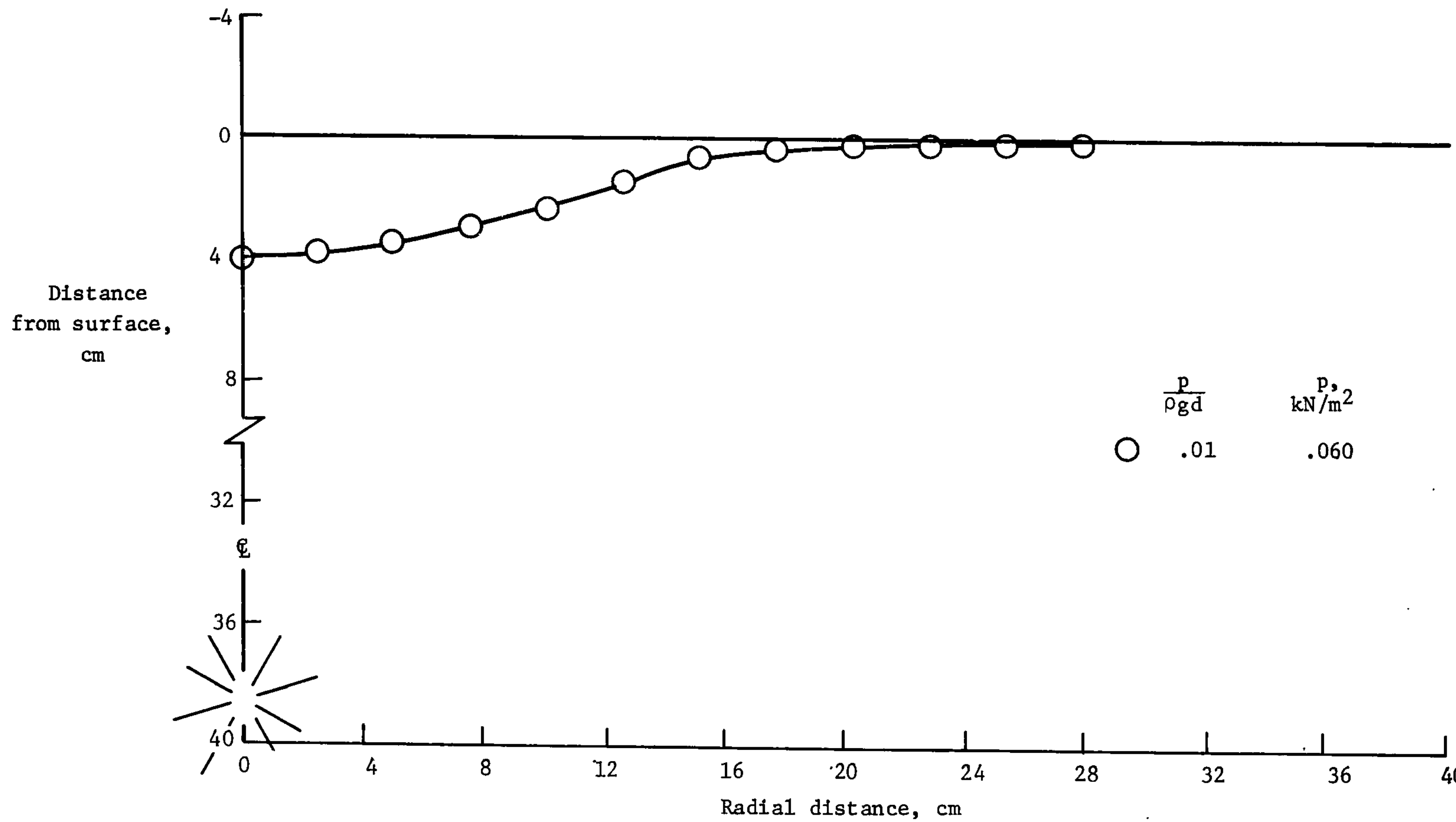

(l) Charge depth = 38.8 cm; $d\left(\frac{\rho g}{M}\right)^{1/4} = 25.5.$

Figure 14.- Concluded.

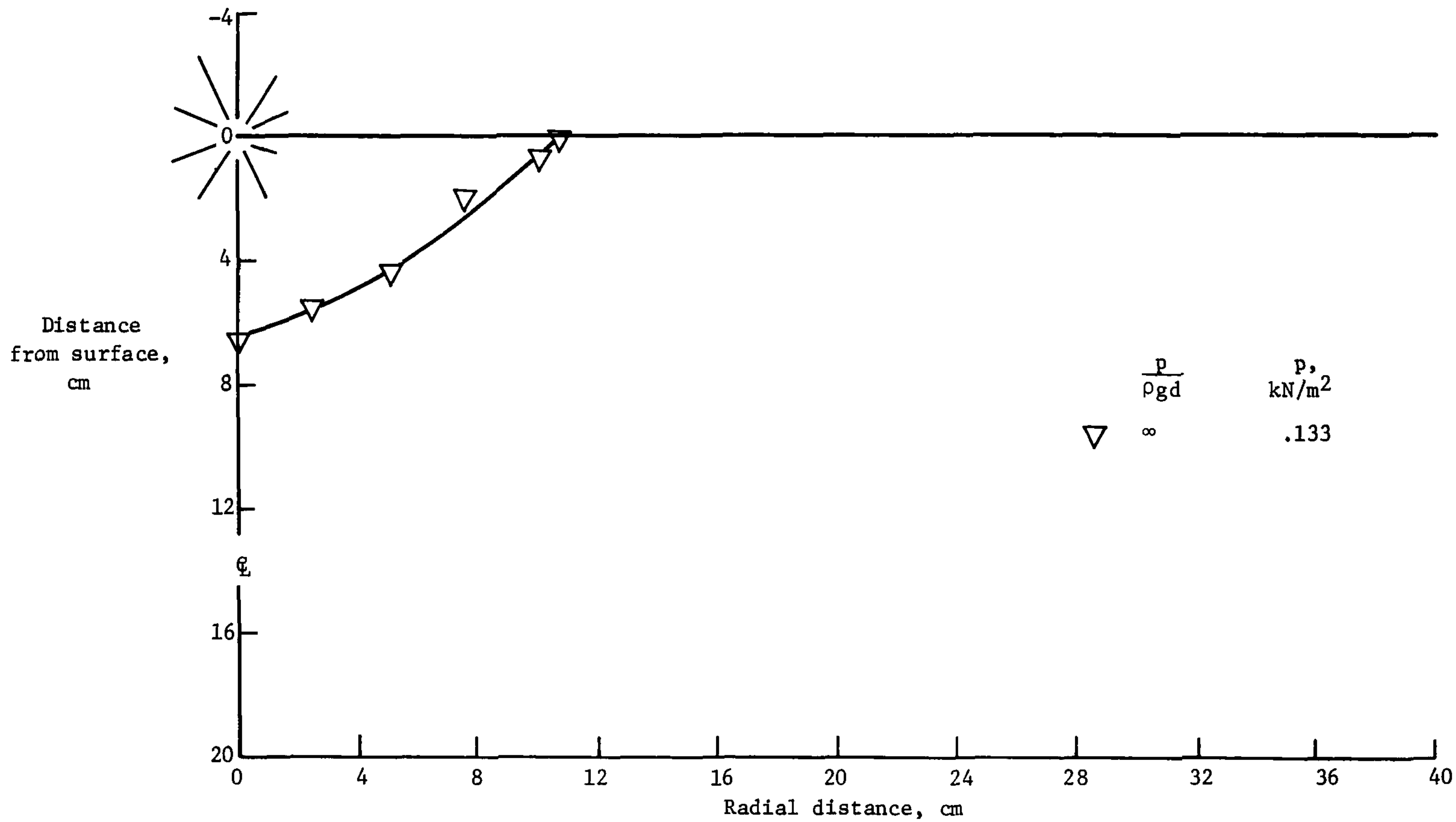

(a) Charge depth = 0 cm; $d\left(\frac{\rho g}{M}\right)^{1/4} = 0.$

Figure 15.- Crater profiles in loose ground limestone. $\rho = 1240\ kg/m^3$.

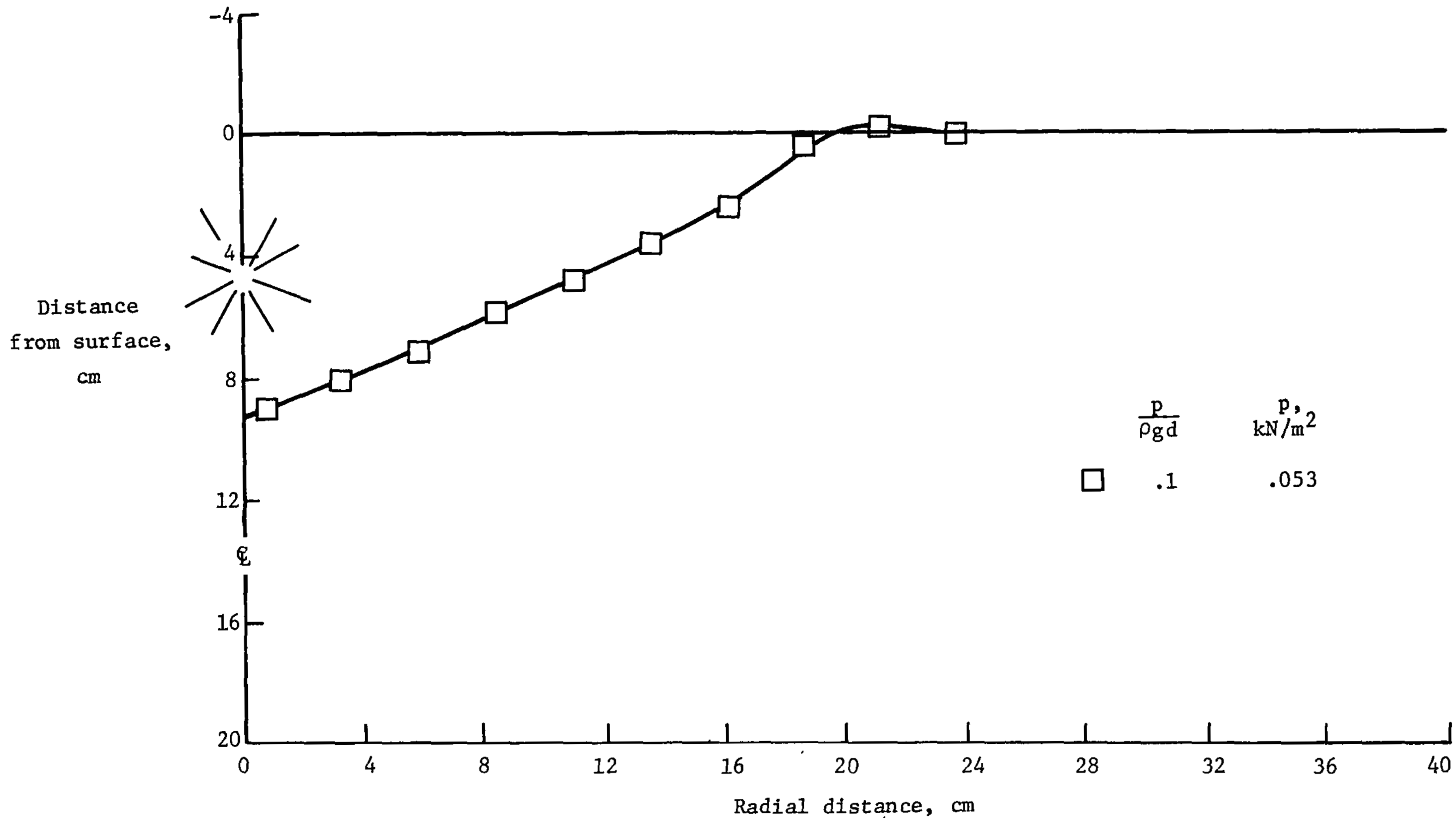

(b) Charge depth = 4.6 cm; $d\left(\frac{\rho g}{M}\right)^{1/4} = 2.9$.

Figure 15.- Continued.

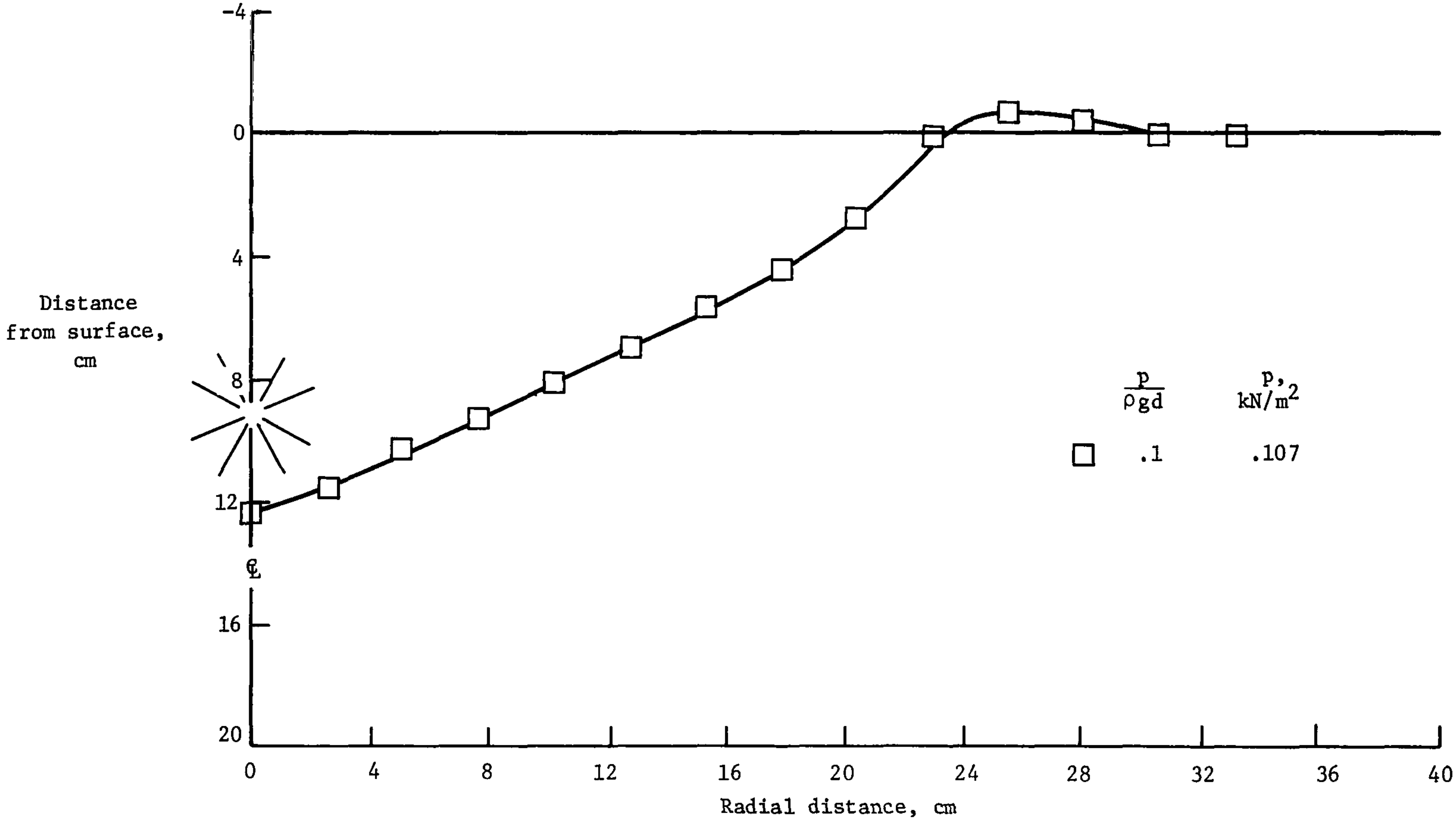

(c) Charge depth = 9.2 cm; $d\left(\frac{\rho g}{M}\right)^{1/4} = 5.7$.

Figure 15.- Continued.

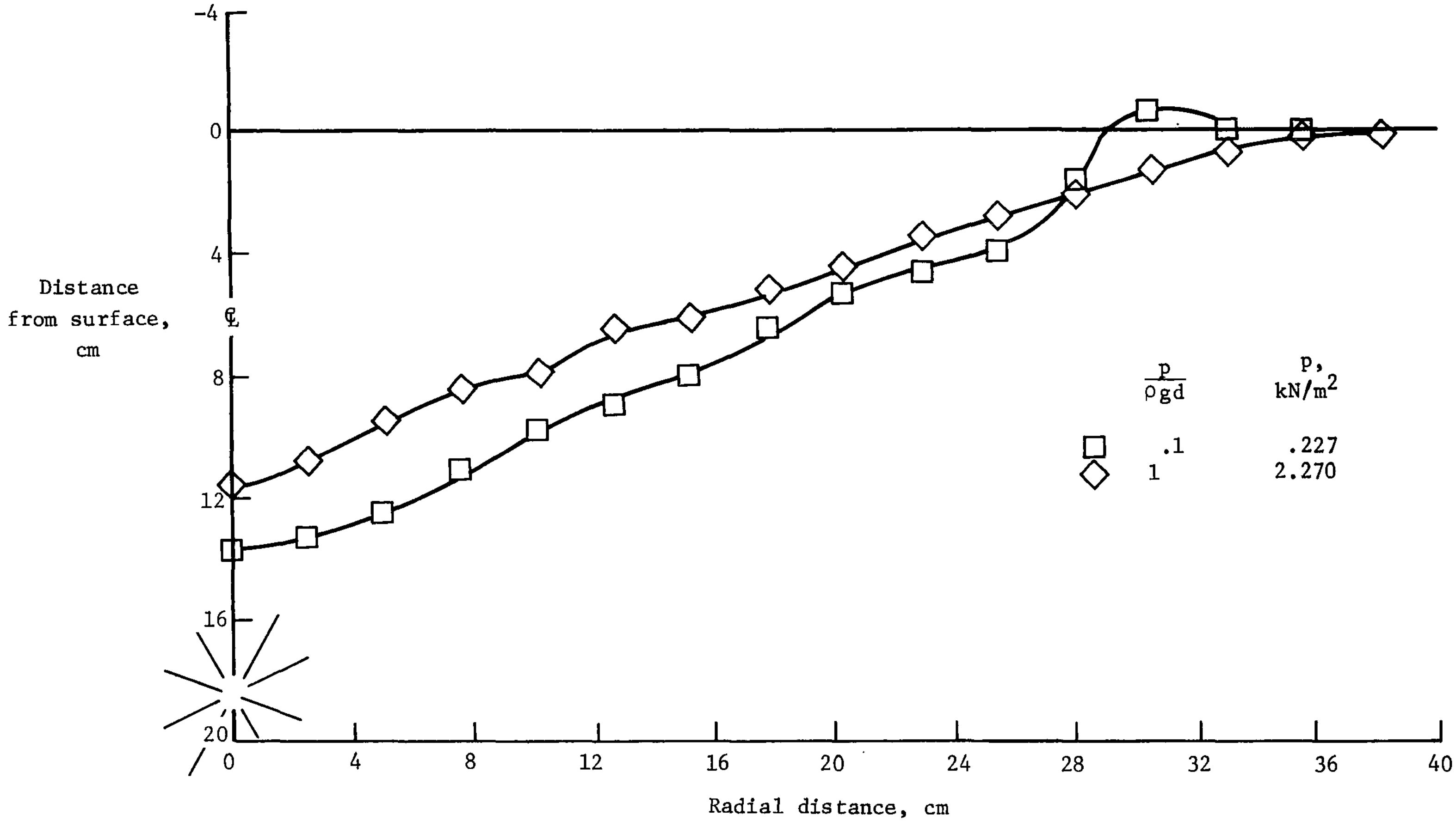

(d) Charge depth = 18.5 cm; $d\left(\frac{\rho g}{M}\right)^{1/4} = 11.5$.

Figure 15.- Continued.

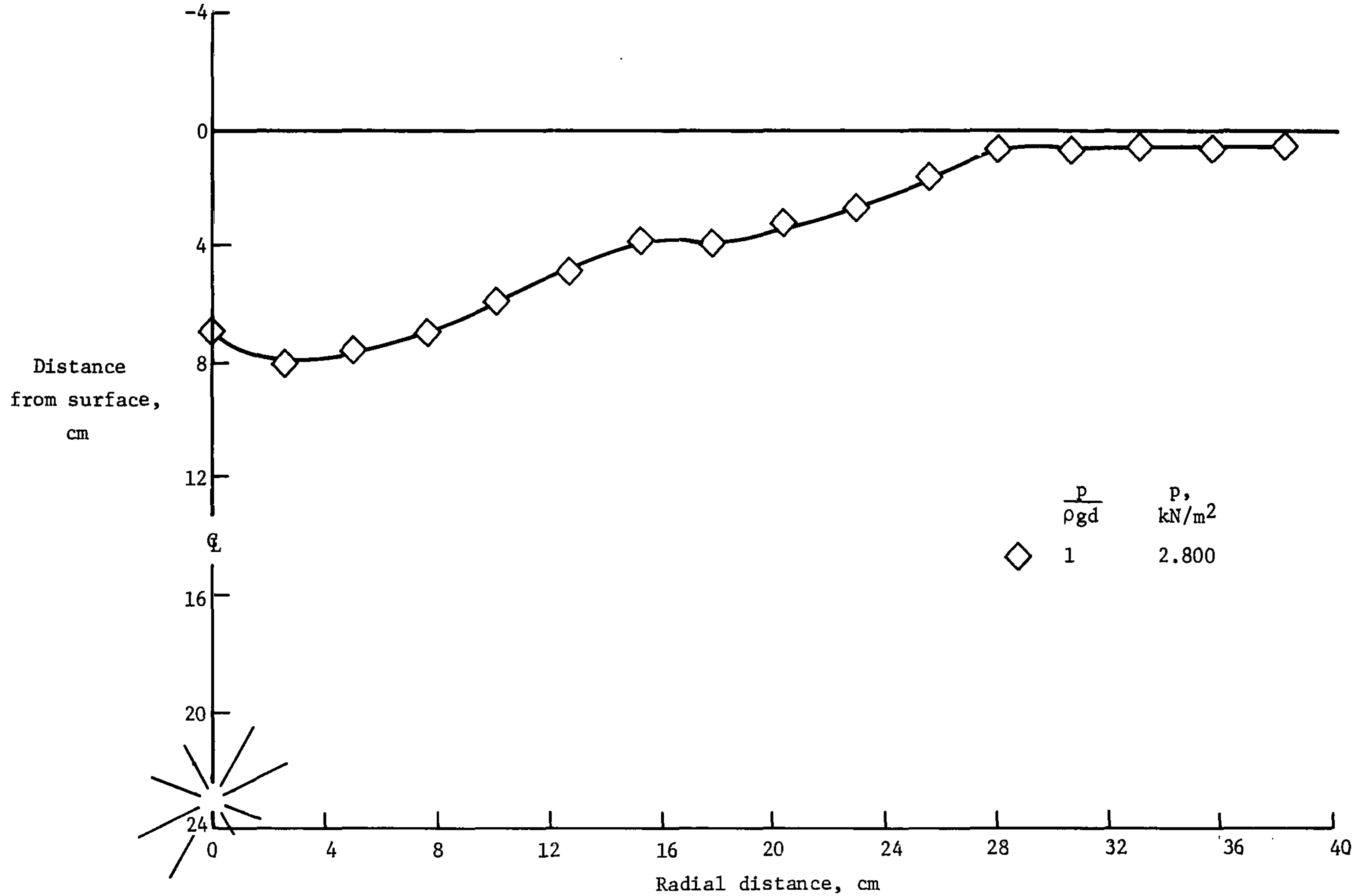

(e) Charge depth = 23.1 cm; $d\left(\frac{\rho g}{M}\right)^{1/4} = 14.4$.

Figure 15.- Continued.

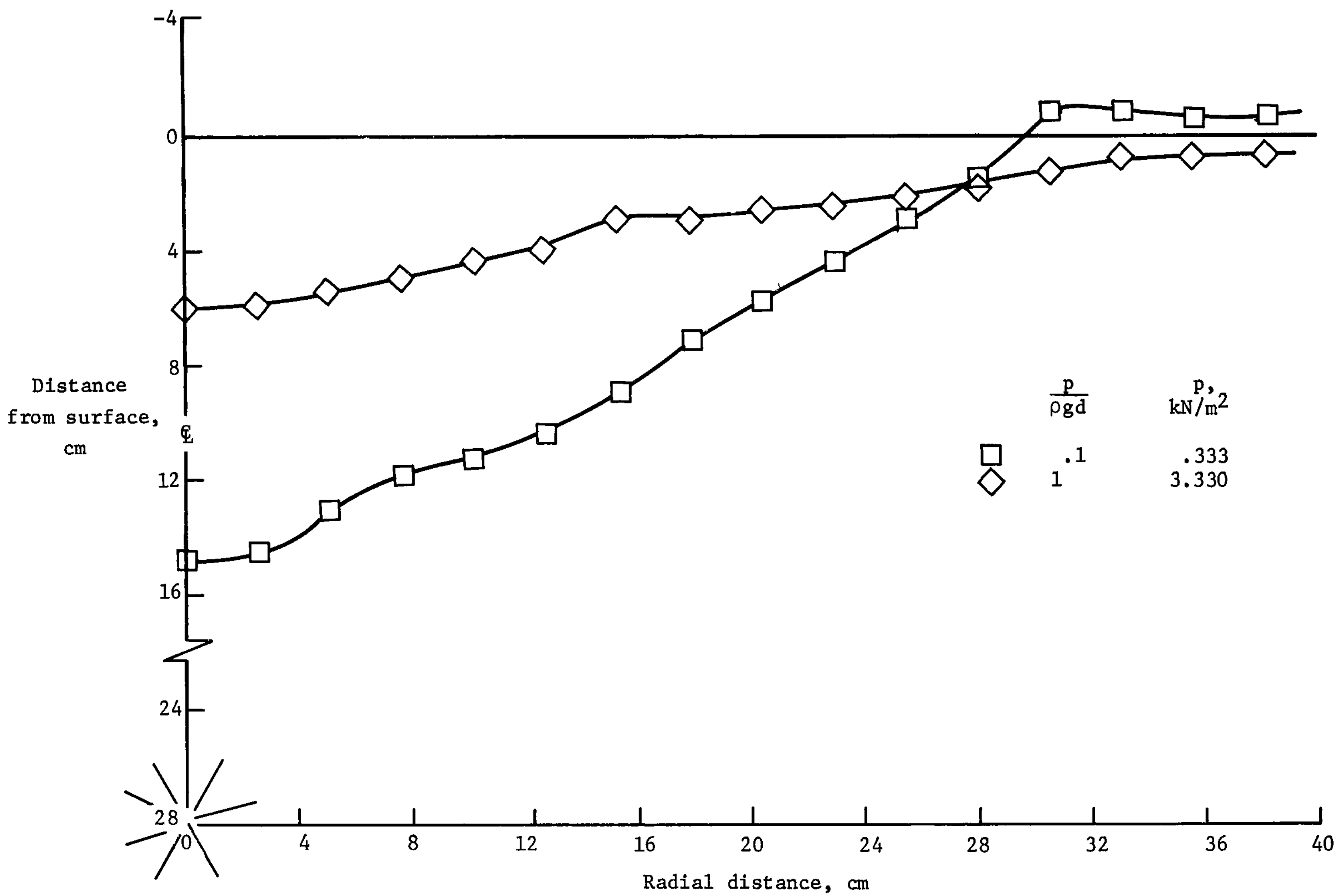

(f) Charge depth = 27.7 cm; $d\left(\frac{\rho g}{M}\right)^{1/4} = 17.3$.

Figure 15.- Continued.

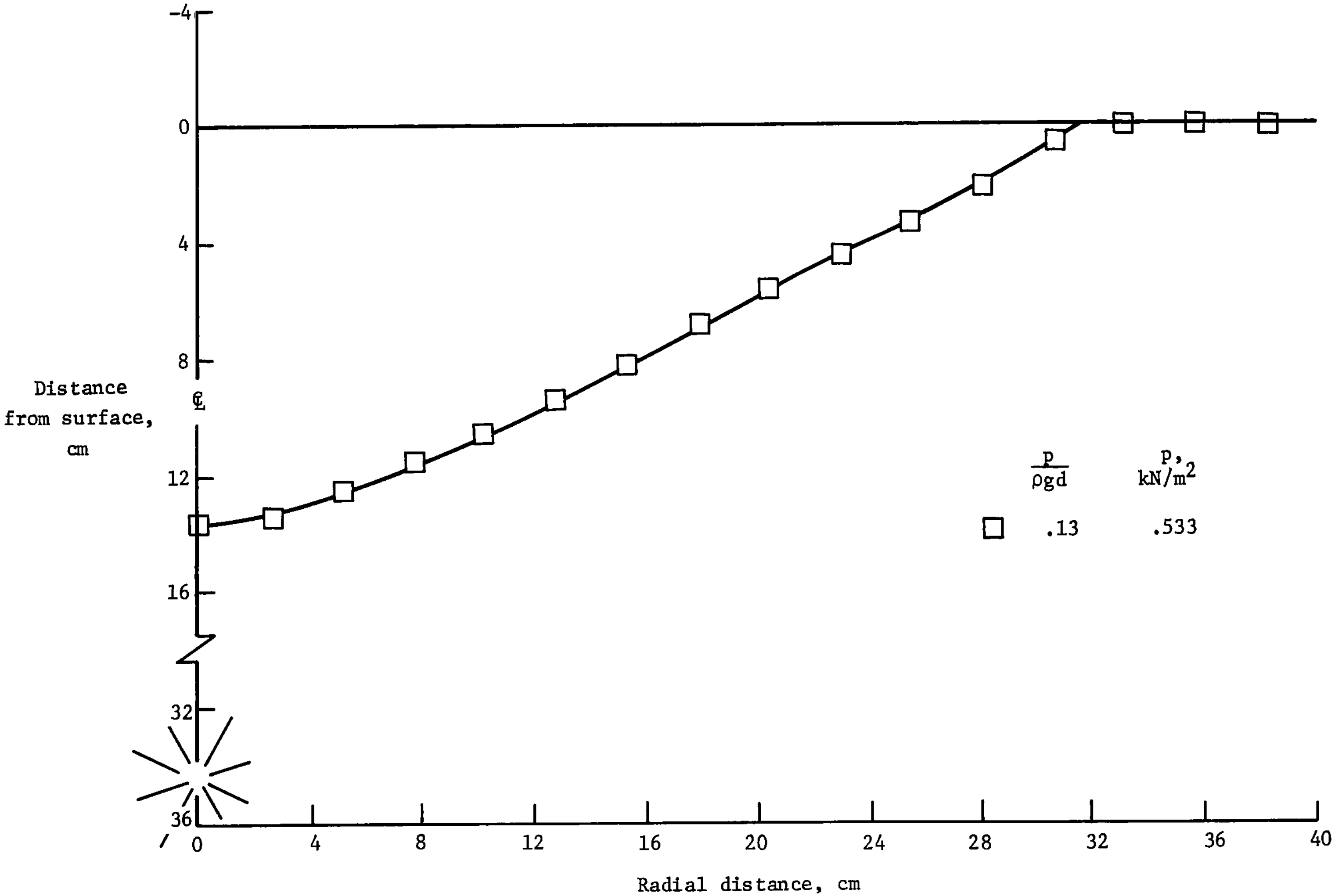

(g) Charge depth = 34.4 cm; $d\left(\frac{\rho g}{M}\right)^{1/4} = 21.5$.

Figure 15.- Continued.

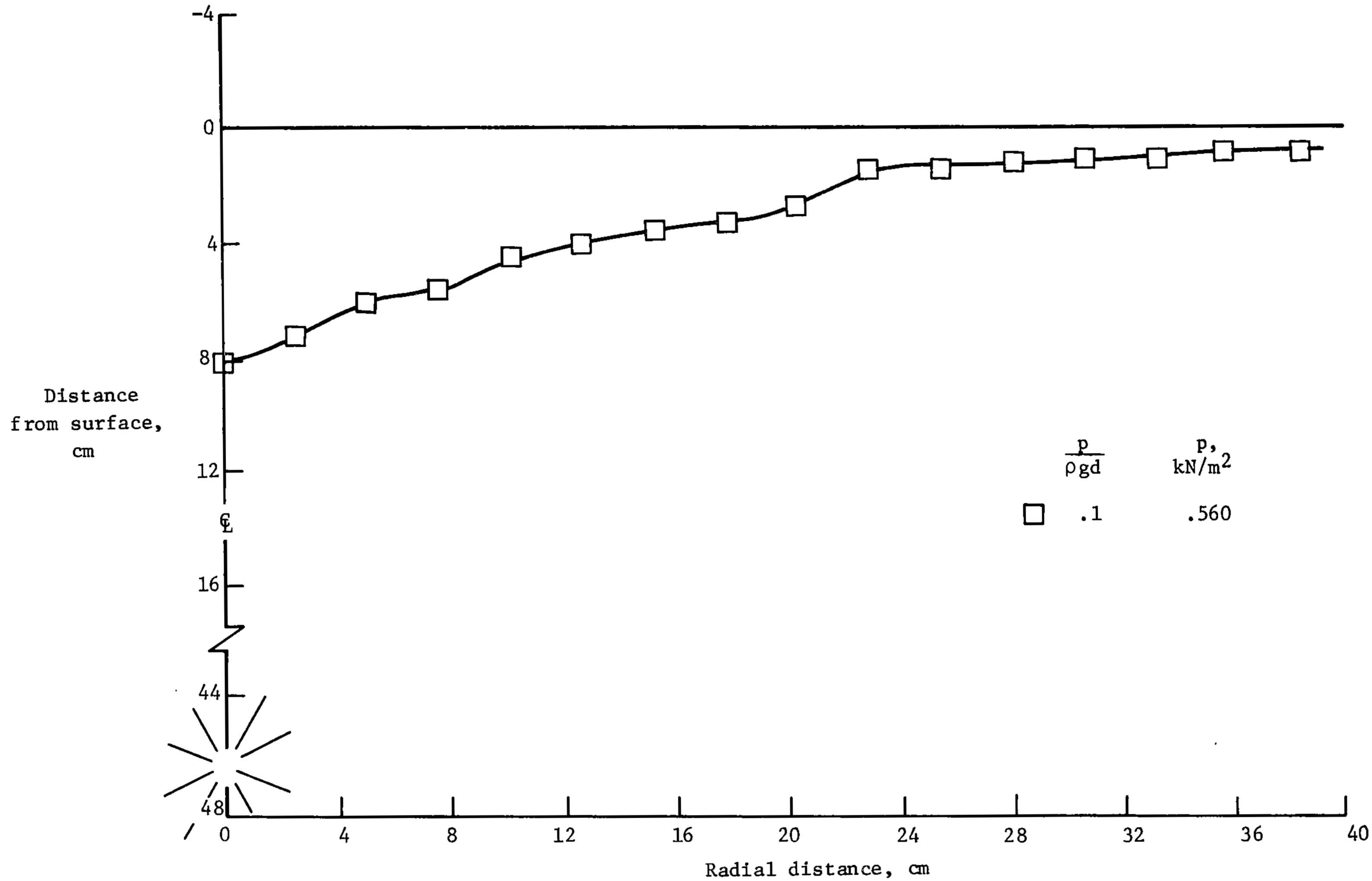

(h) Charge depth = 46.4 cm; $d\left(\frac{\rho g}{M}\right)^{1/4} = 29.0$.

Figure 15.- Concluded.

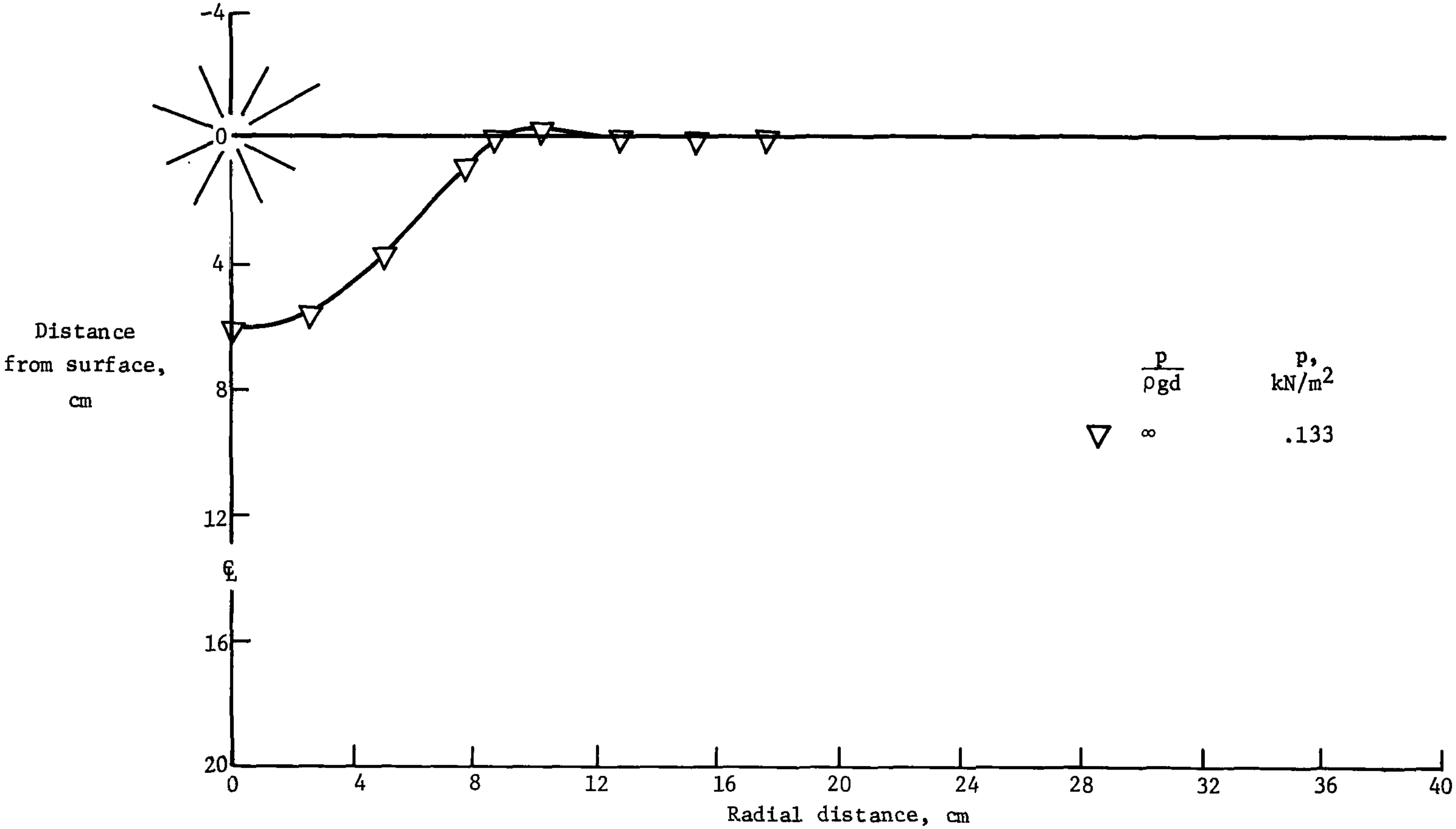

(a) Charge depth = 0 cm; $d\left(\frac{\rho g}{M}\right)^{1/4} = 0$.

Figure 16.- Crater profiles in packed ground limestone. $\rho = 1450$ kg/m^3.
Repeated tests are shown by solid symbols.

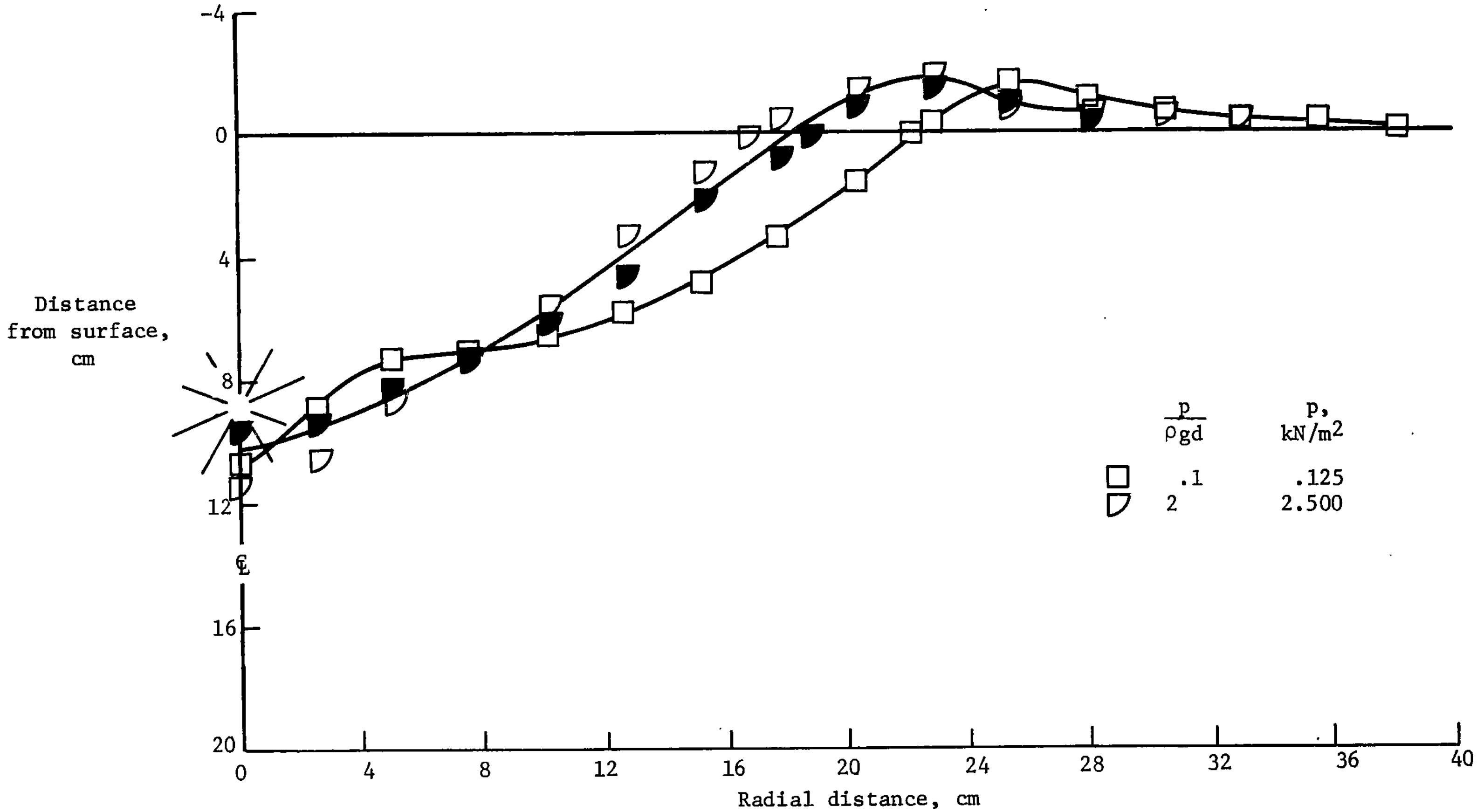

(b) Charge depth = 8.9 cm; $d\left(\frac{\rho g}{M}\right)^{1/4} = 5.8$.

Figure 16.- Continued.

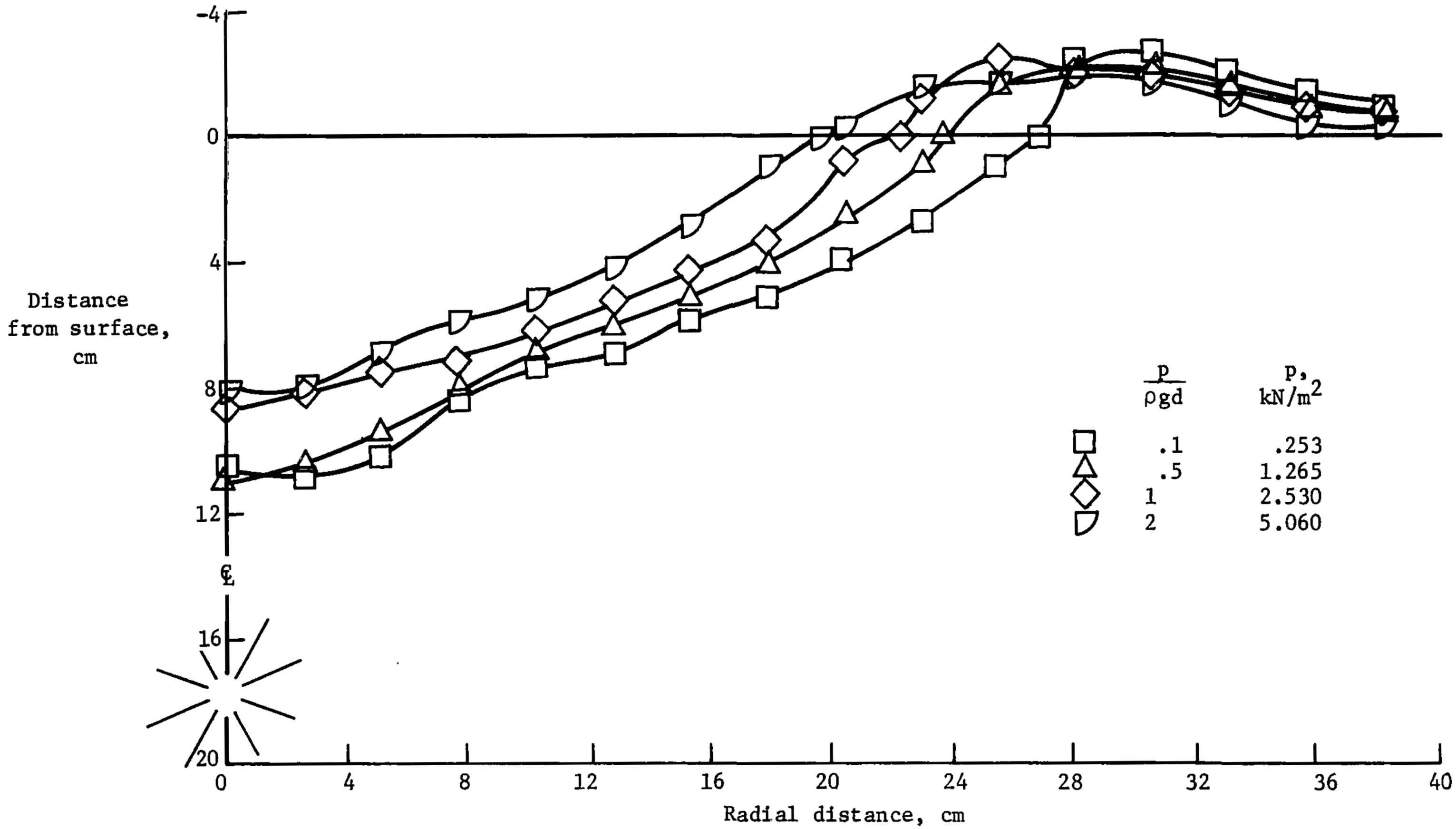

(c) Charge depth = 17.8 cm; $d\left(\frac{\rho g}{M}\right)^{1/4} = 11.6$.

Figure 16.- Continued.

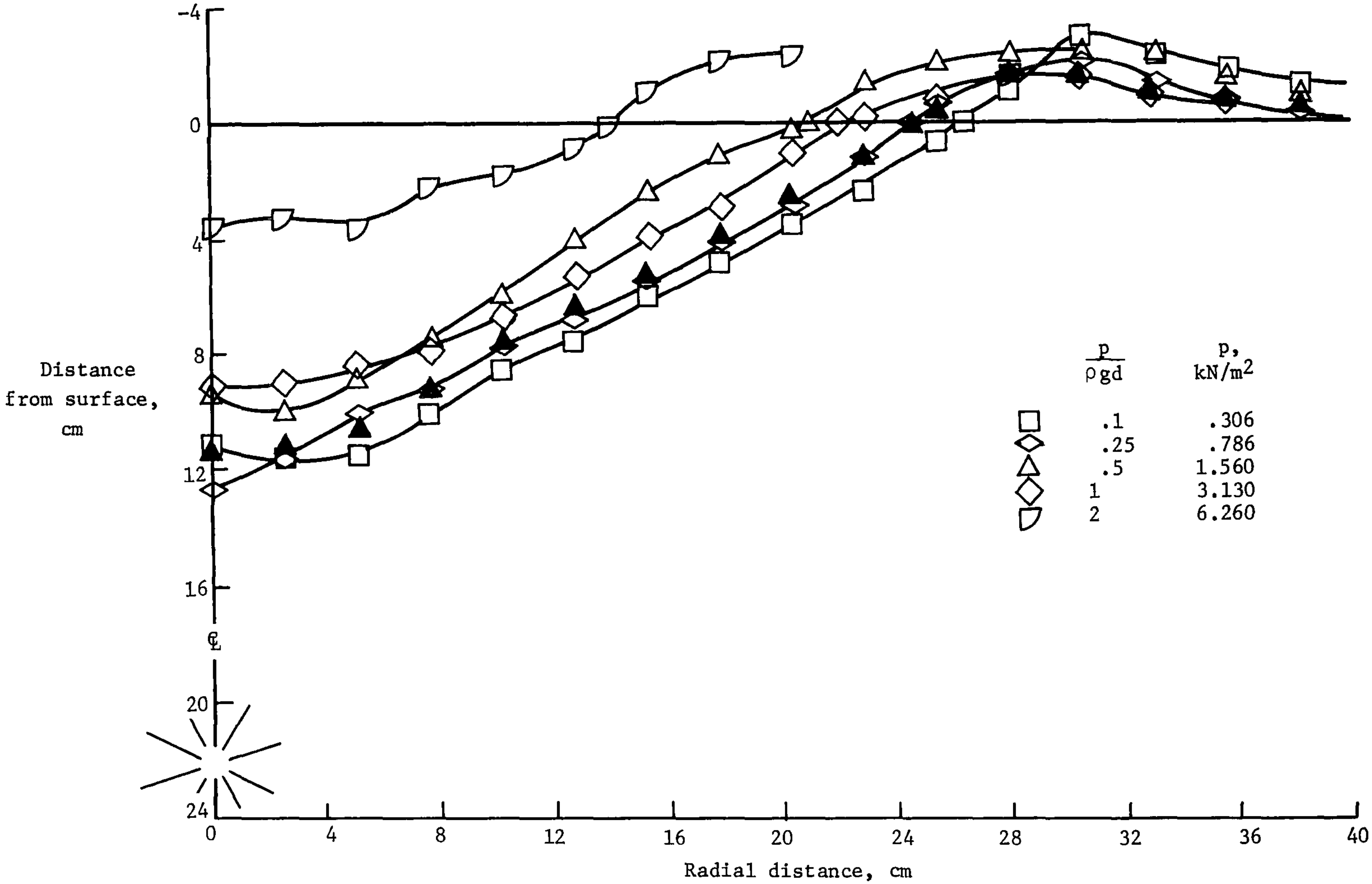

(d) Charge depth = 22.2 cm; $d\left(\frac{\rho g}{M}\right)^{1/4} = 14.4$.

Figure 16.- Continued.

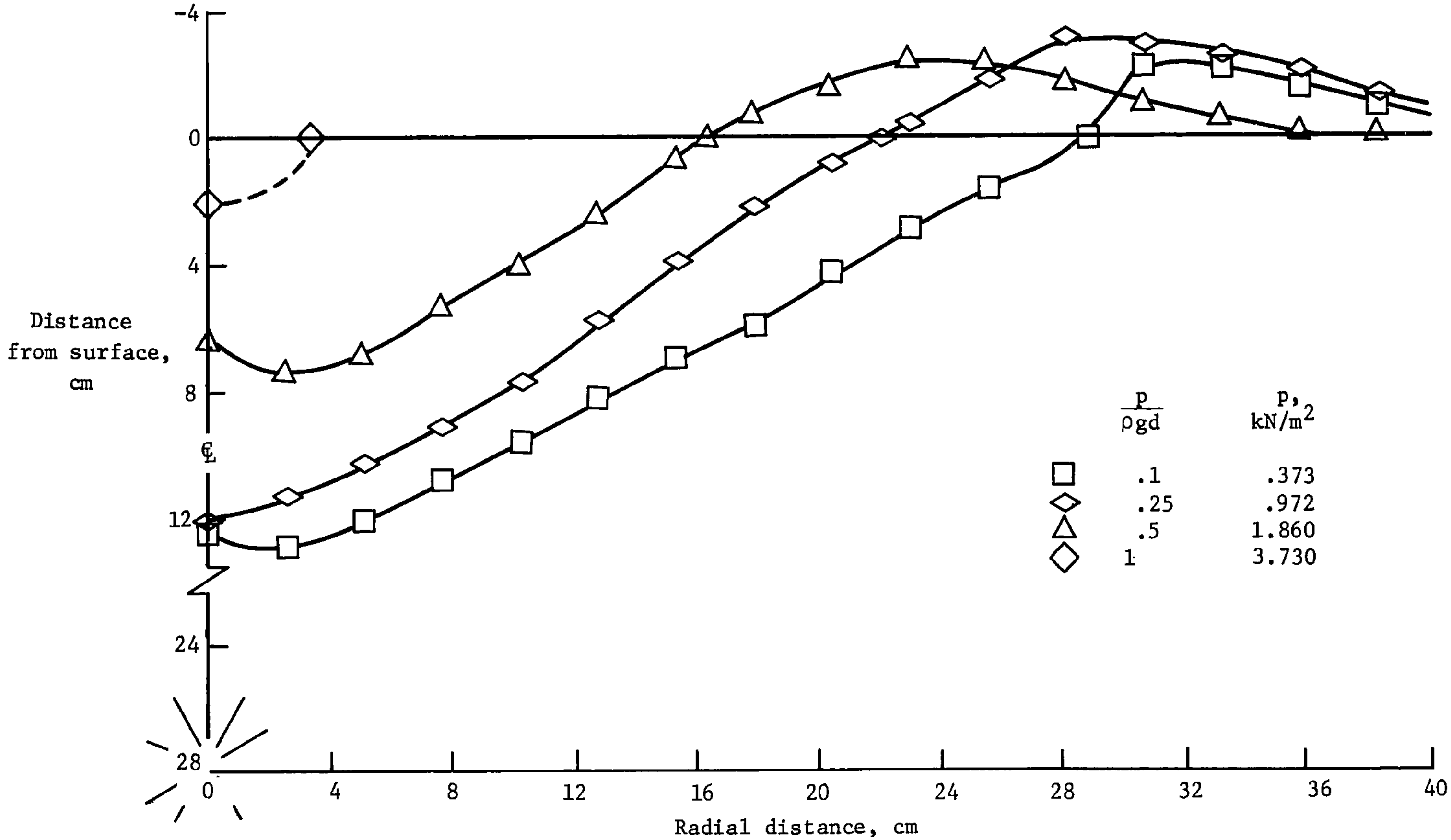

(e) Charge depth = 27.6 cm; $d\left(\frac{\rho g}{M}\right)^{1/4} = 17.9$.

Figure 16.- Continued.

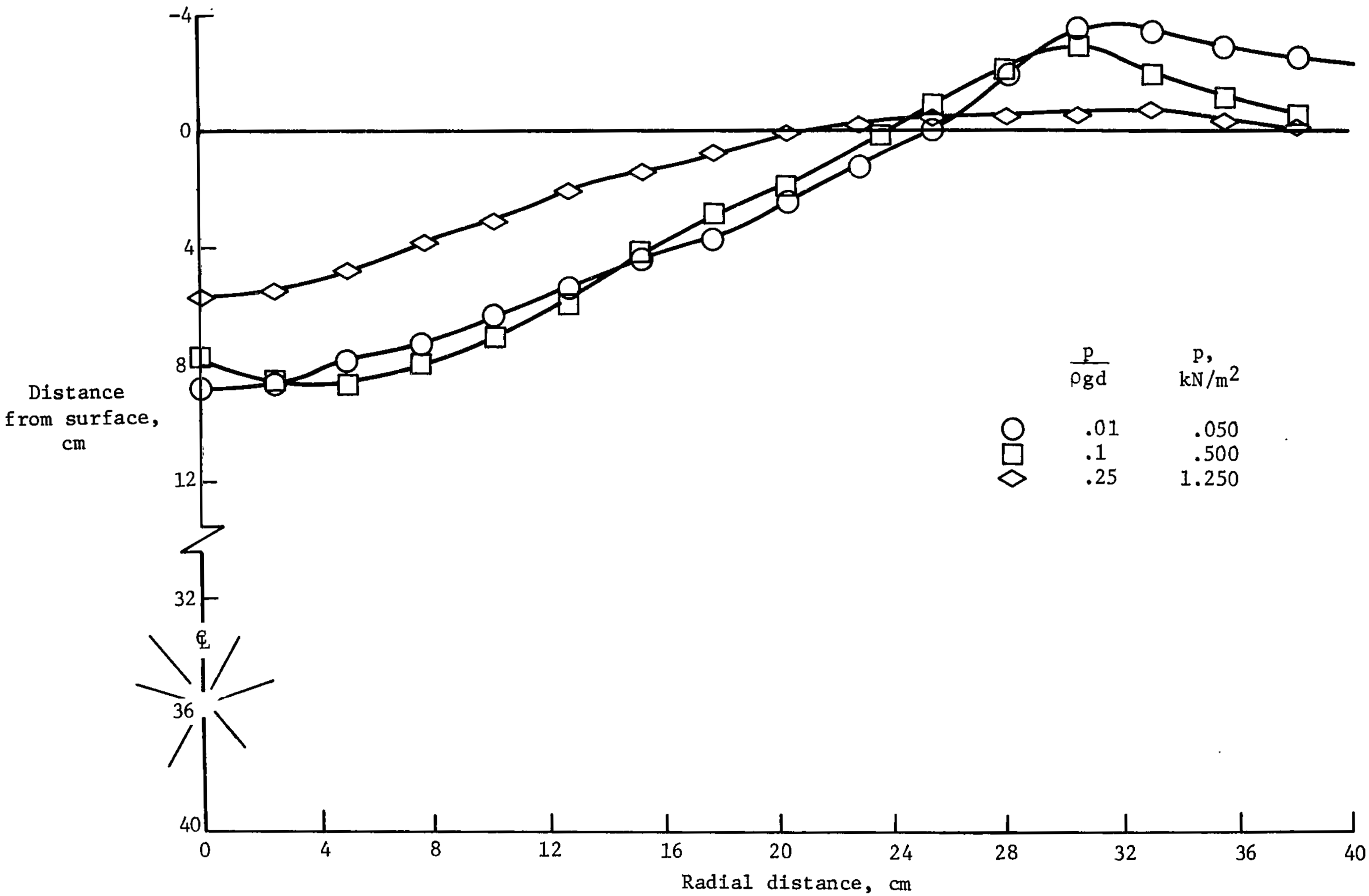

(f) Charge depth = 35.6 cm; $d\left(\frac{\rho g}{M}\right)^{1/4} = 23.1$.

Figure 16.- Concluded.

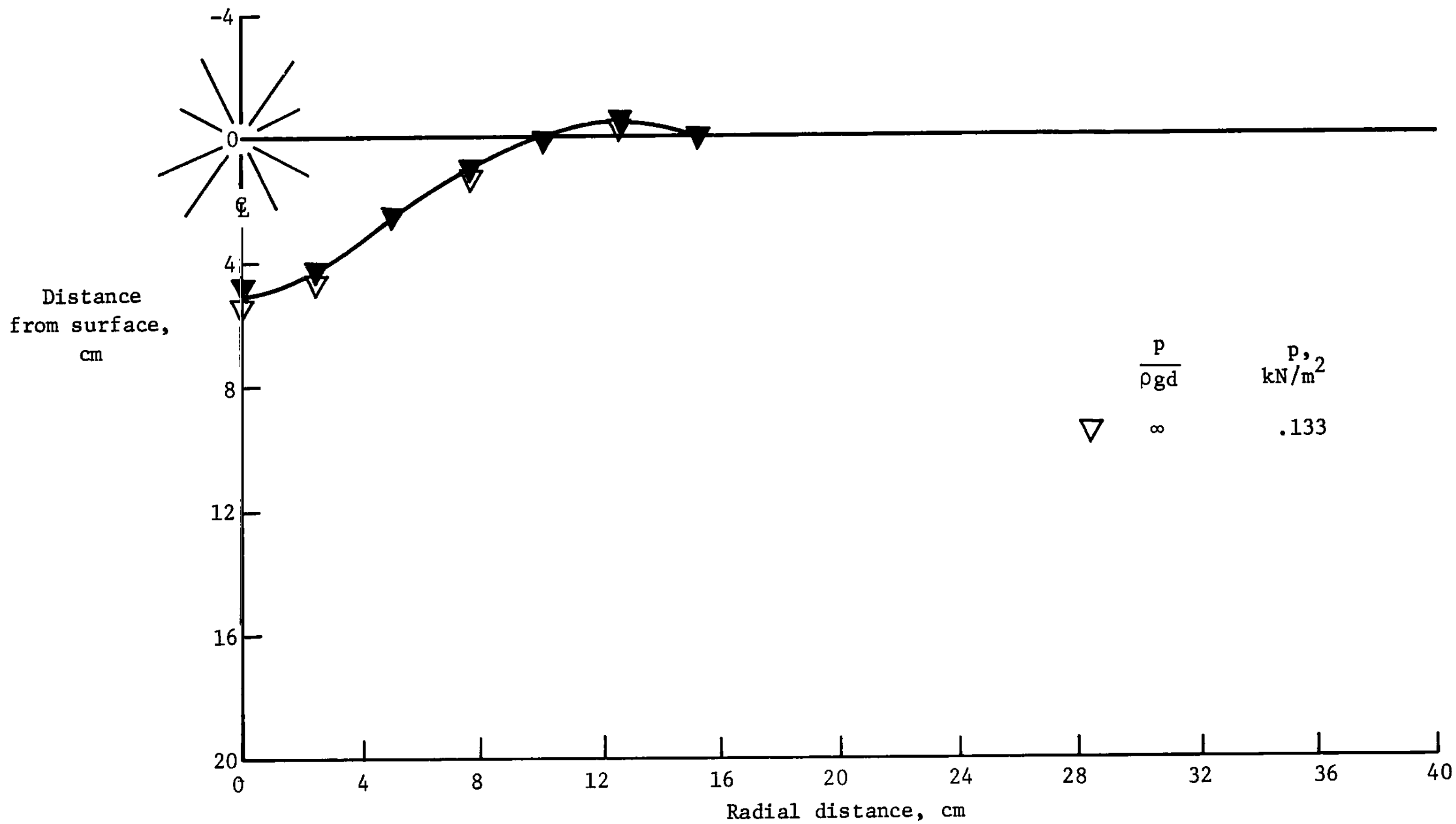

(a) Charge depth = 0 cm; $d\left(\frac{\rho g}{M}\right)^{1/4} = 0.$

Figure 17.- Crater profiles in mixture of 30% ground limestone and 70% sand. $\rho = 1600\ kg/m^3$. Repeated tests are shown by solid symbols.

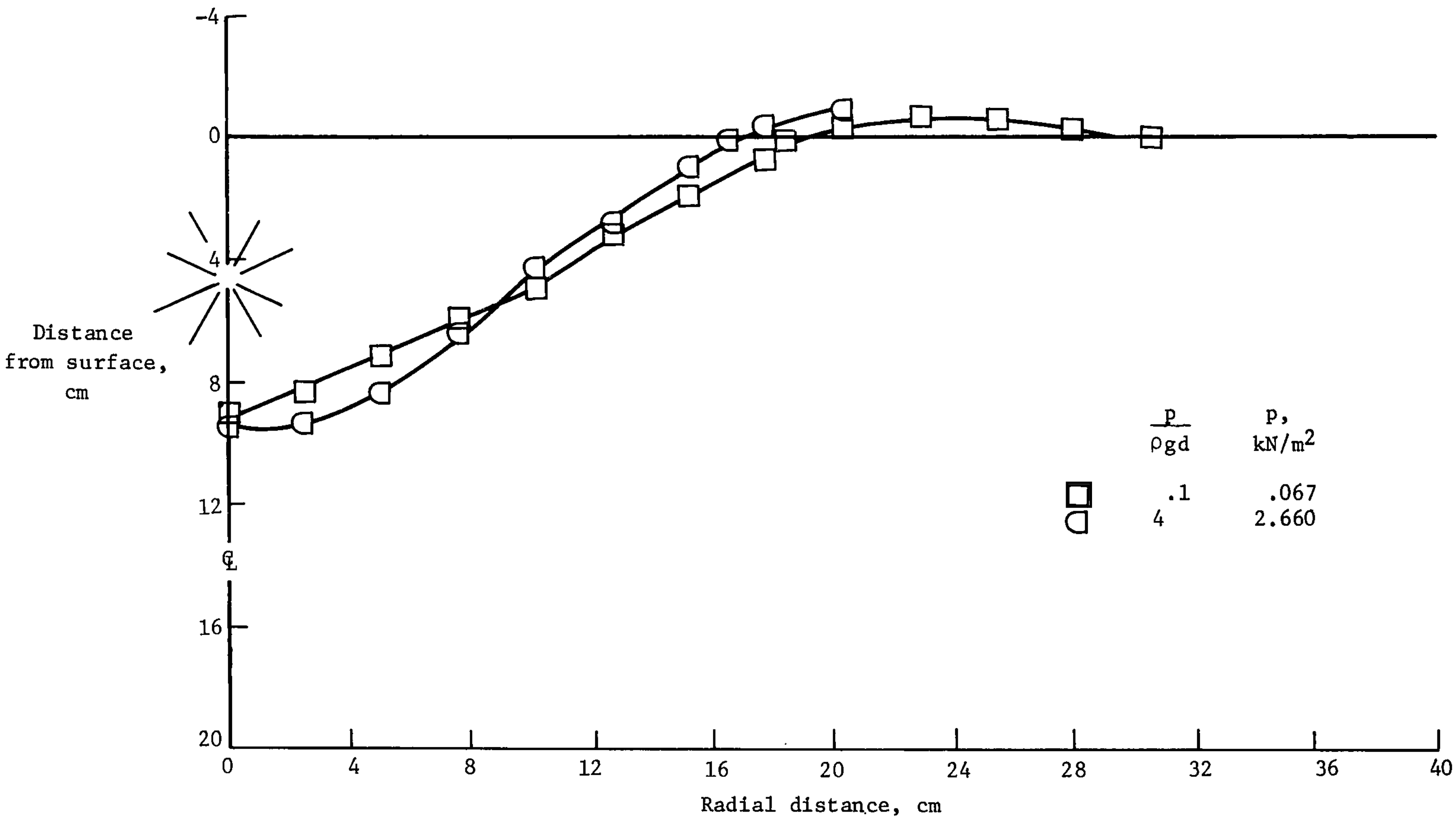

(b) Charge depth = 4.3 cm; $d\left(\frac{\rho g}{M}\right)^{1/4} = 2.9$.

Figure 17.- Continued.

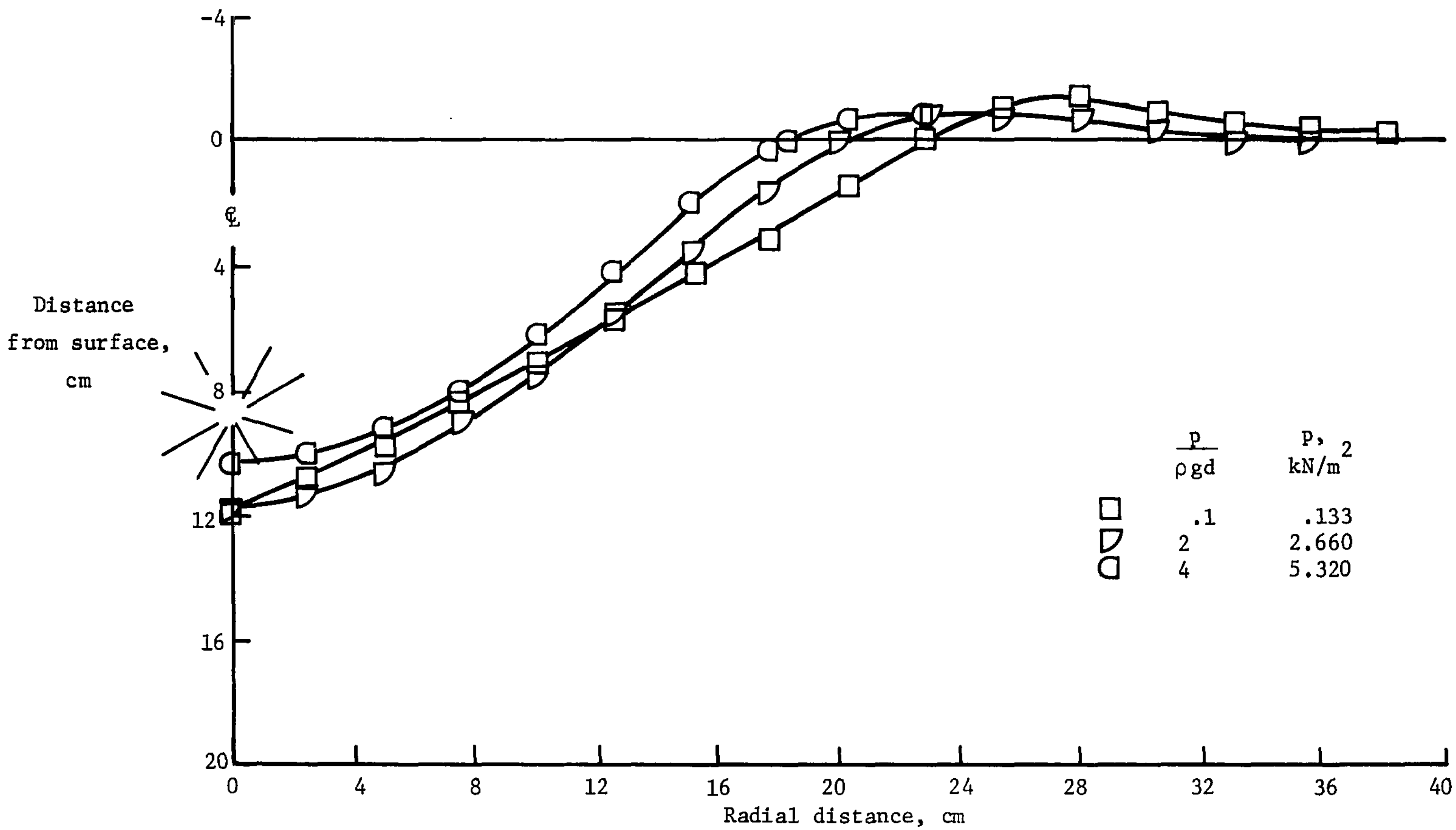

(c) Charge depth = 8.6 cm; $d\left(\frac{\rho g}{M}\right)^{1/4} = 5.7.$

Figure 17.- Continued.

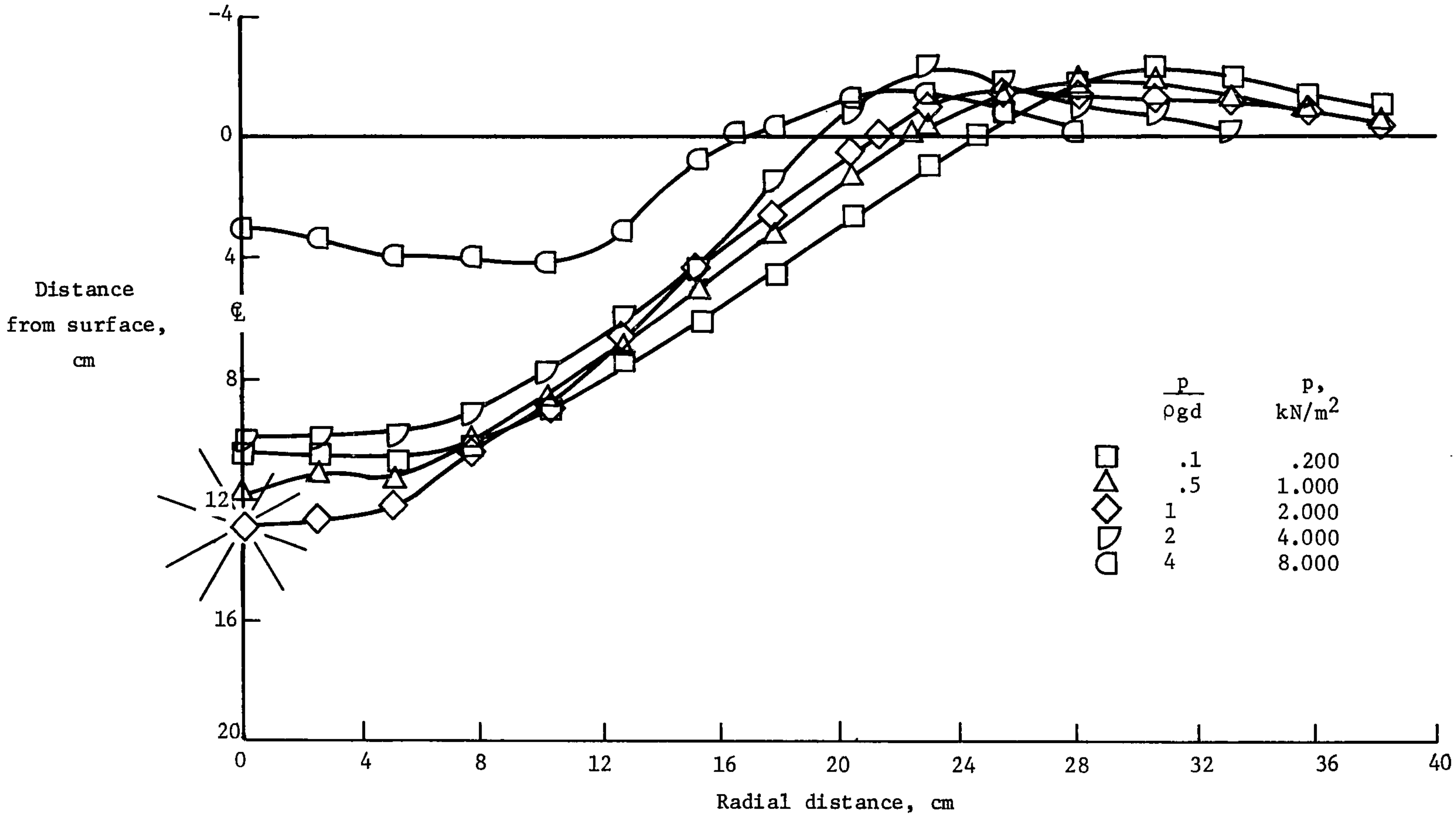

(d) Charge depth = 12.9 cm; $d\left(\frac{\rho g}{M}\right)^{1/4} = 8.6$.

Figure 17.- Continued.

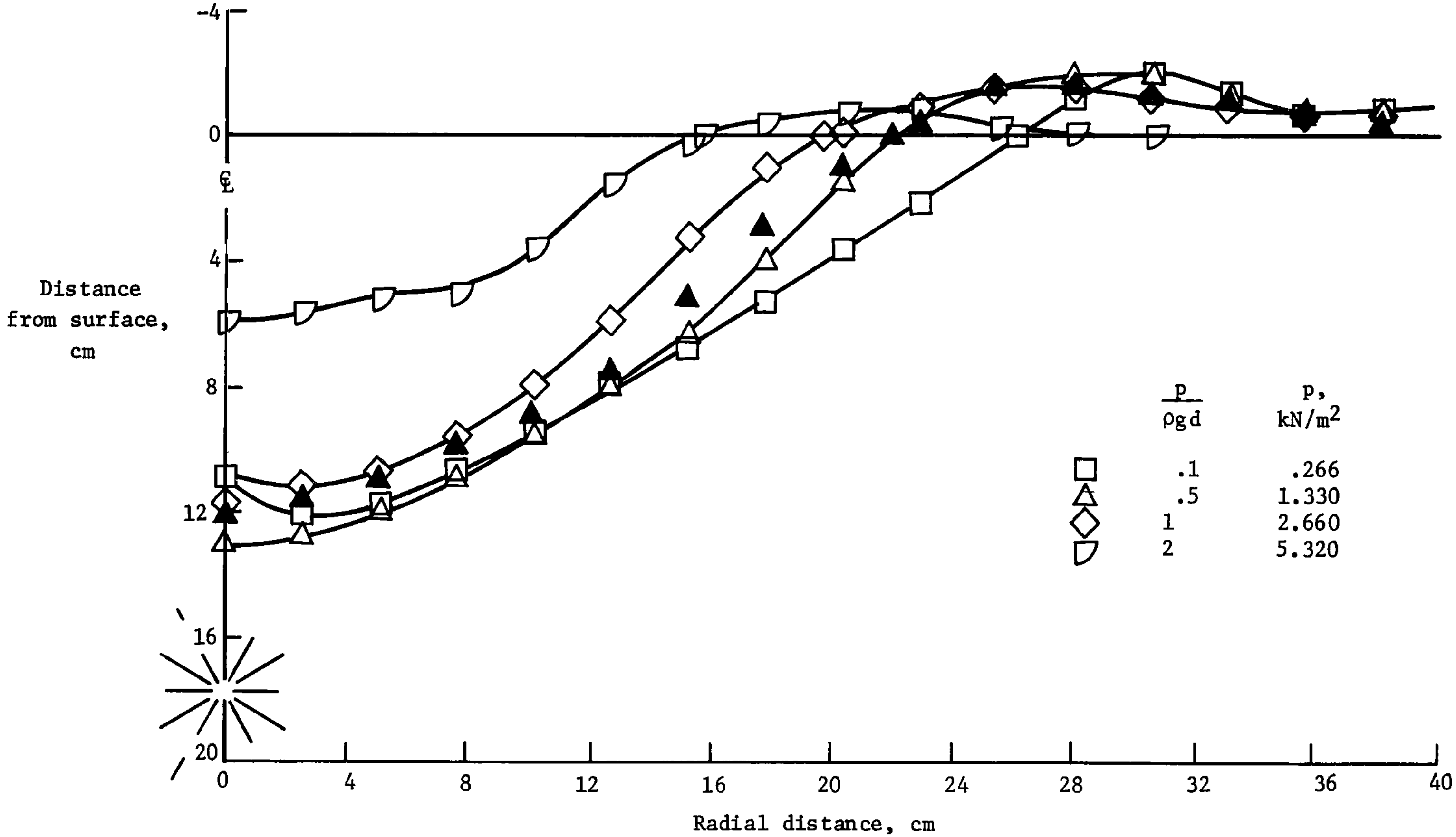

(e) Charge depth = 17.1 cm; $d\left(\frac{\rho g}{M}\right)^{1/4} = 11.4$.

Figure 17.- Continued.

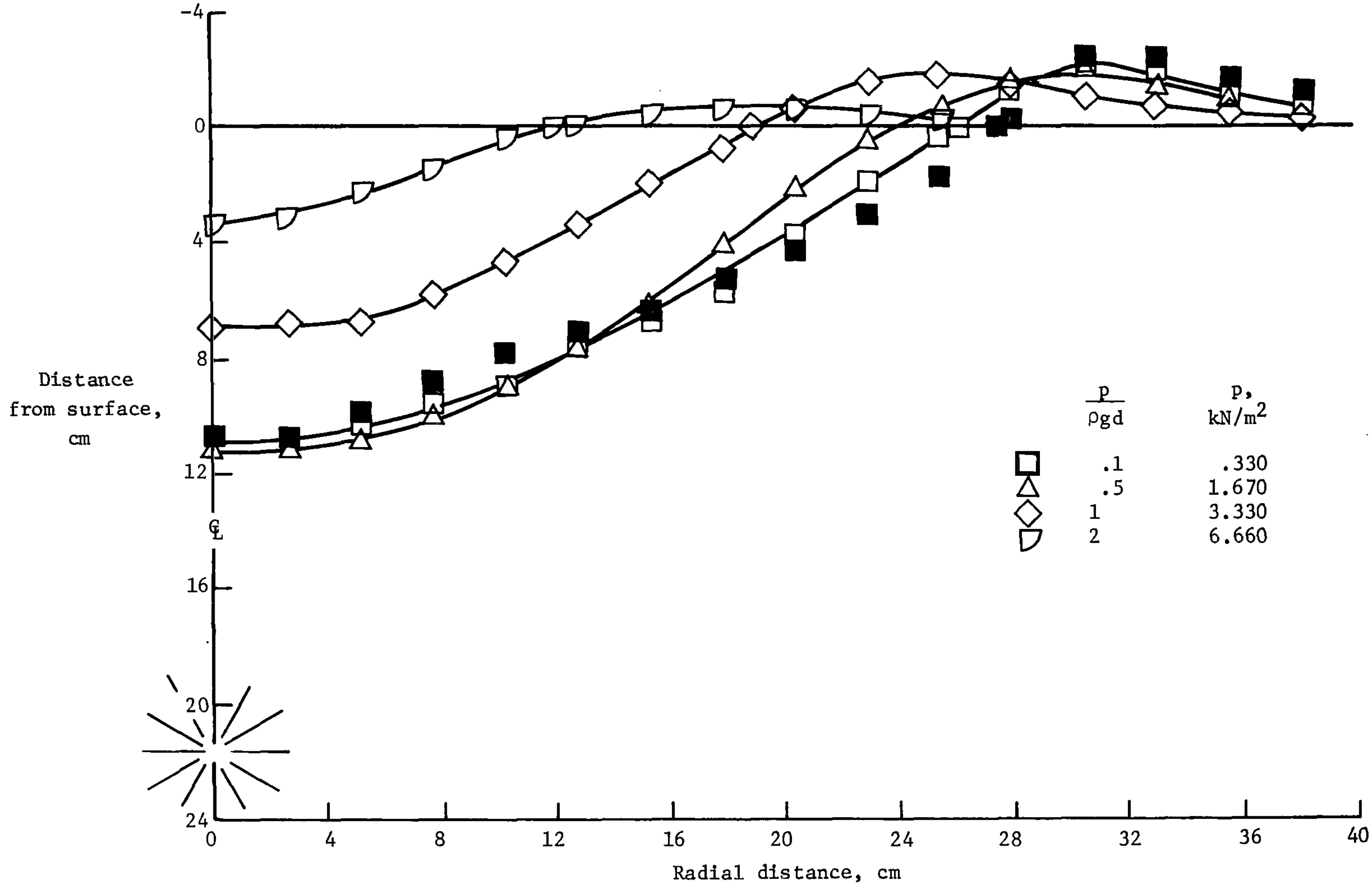

(f) Charge depth = 21.6 cm; $d\left(\frac{\rho g}{M}\right)^{1/4} = 14.4$.

Figure 17.- Continued.

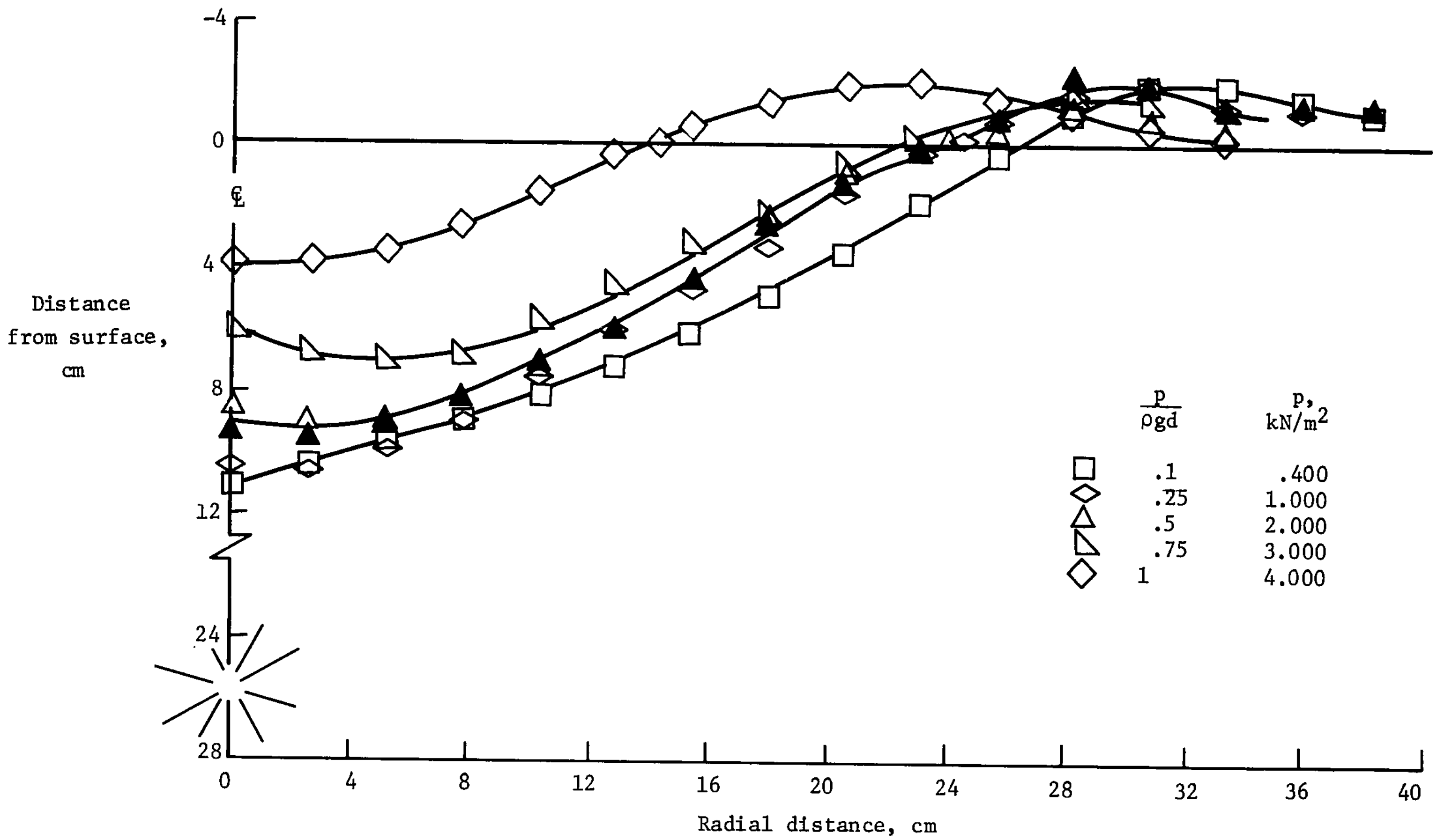

(g) Charge depth = 25.7 cm; $d\left(\frac{\rho g}{M}\right)^{1/4} = 17.1.$

Figure 17.- Continued.

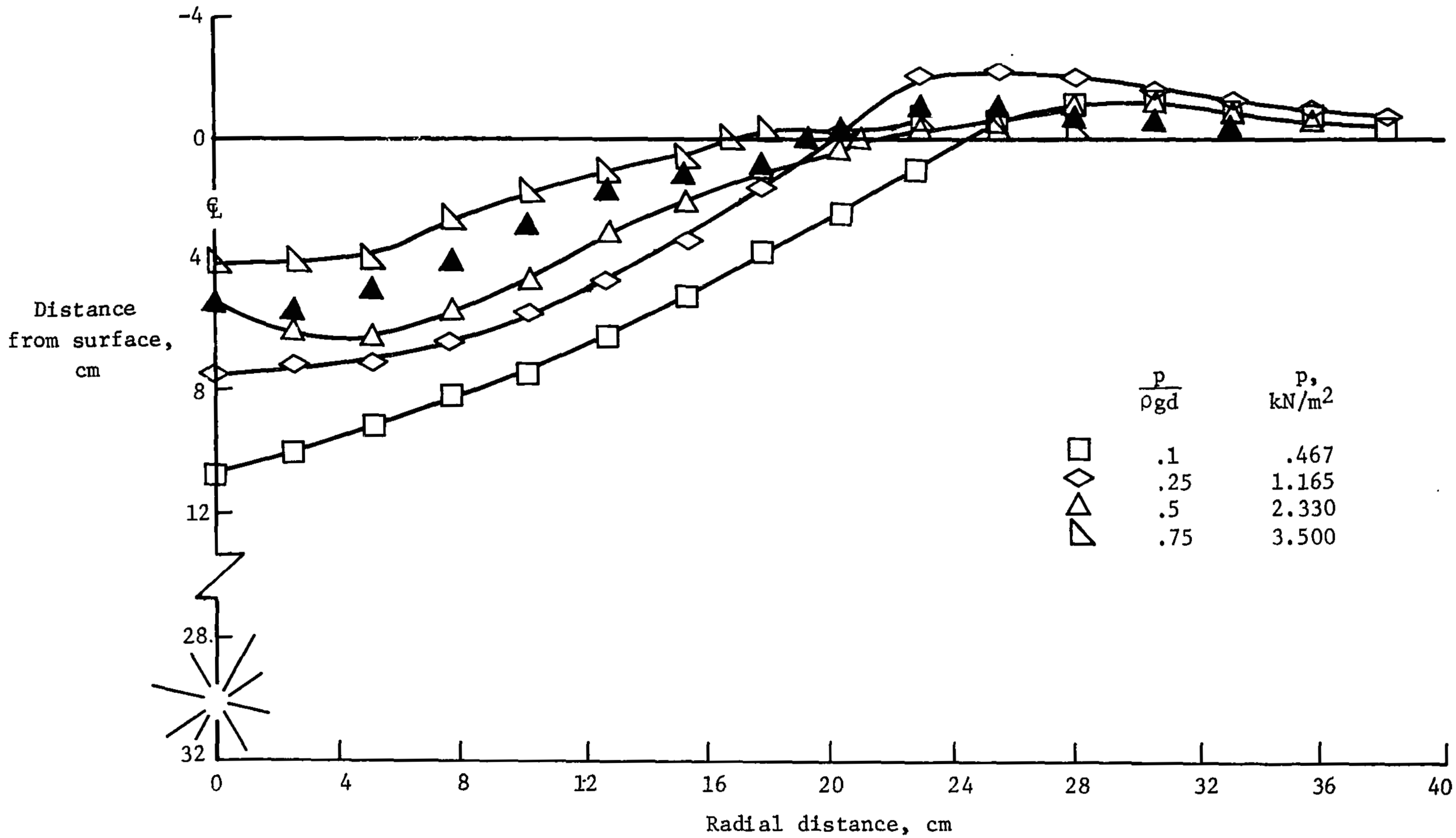

(h) Charge depth = 30.2 cm; $d\left(\frac{\rho g}{M}\right)^{1/4} = 20.1$.

Figure 17.- Continued.

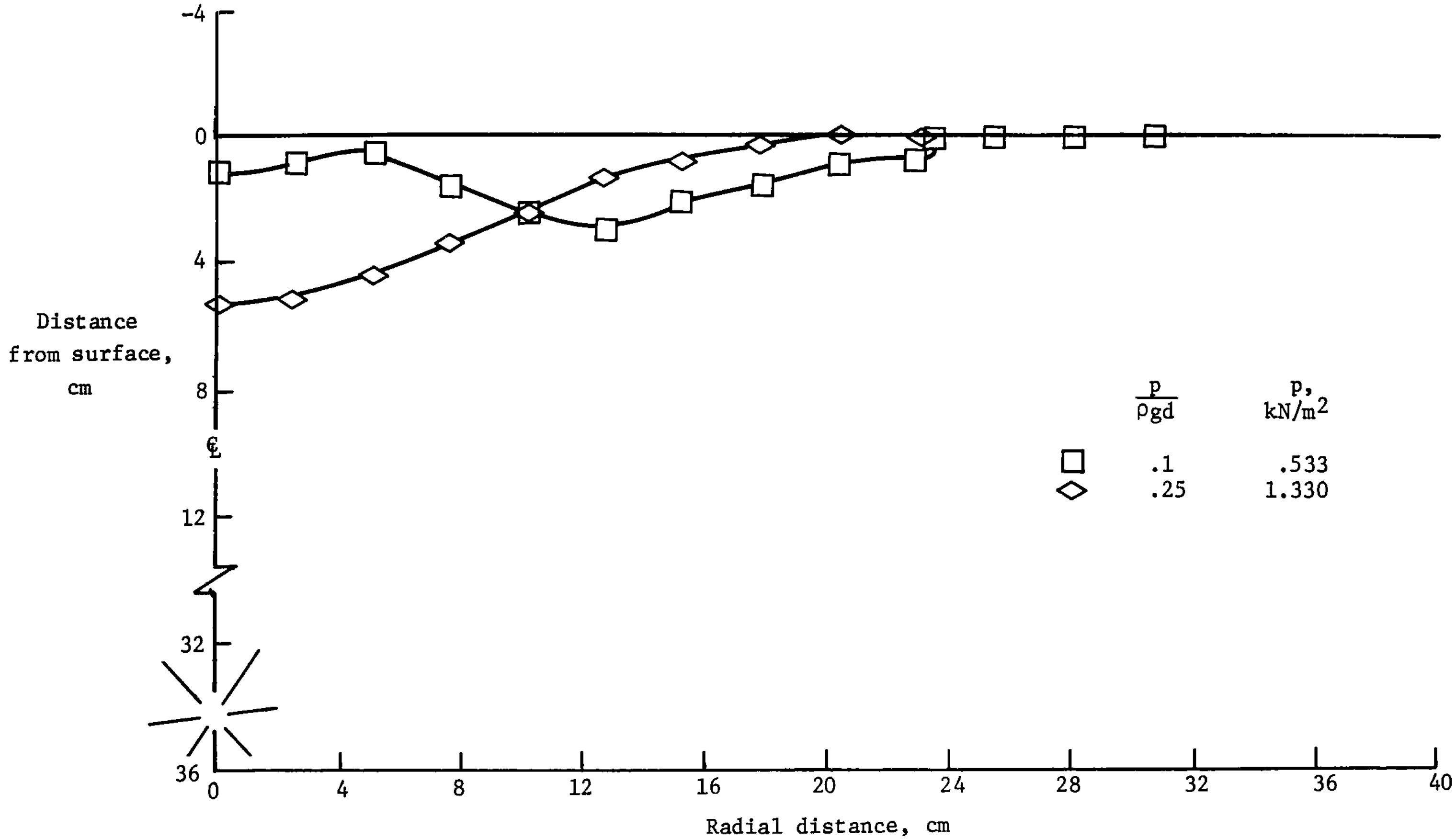

(i) Charge depth = 34.4 cm; $d\left(\frac{\rho g}{M}\right)^{1/4} = 22.9.$

Figure 17.- Concluded.

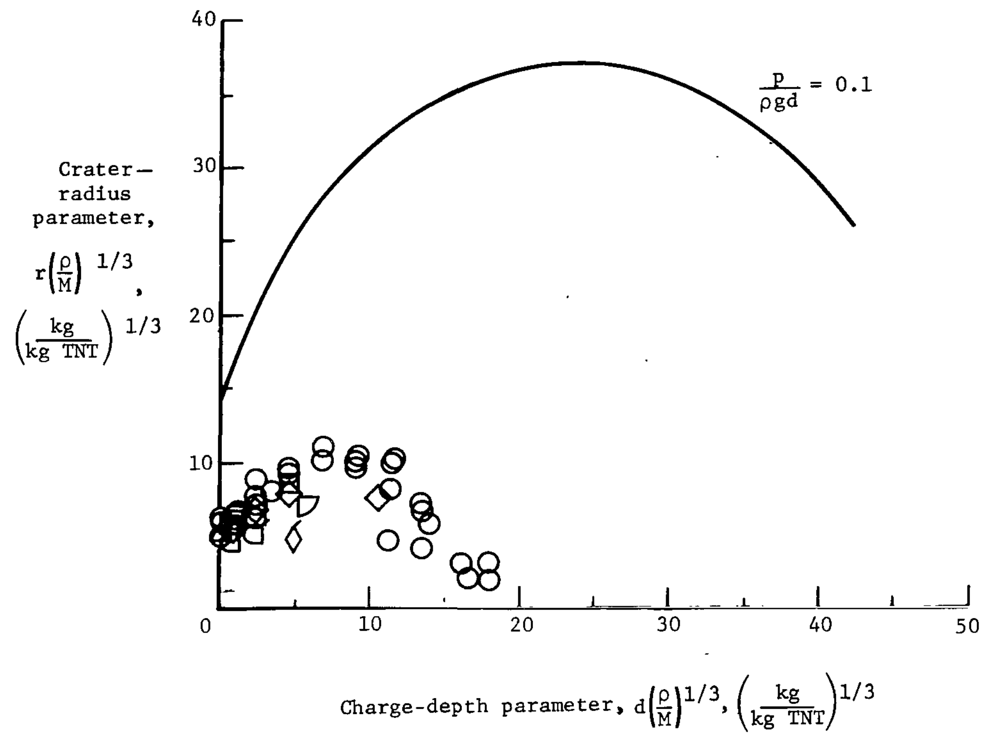

(a) Cube-root scaling.

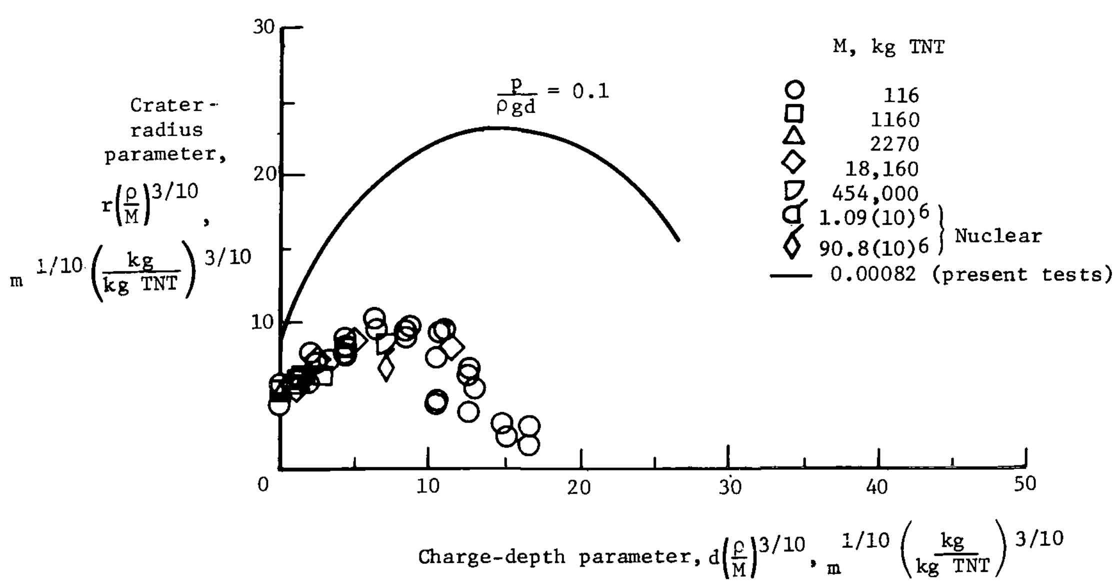

(b) Three-tenths power scaling.

Figure 18.- Comparison of the radii of small-scale craters in sand with large-scale craters in alluvium by cube-root and three-tenths power scaling.

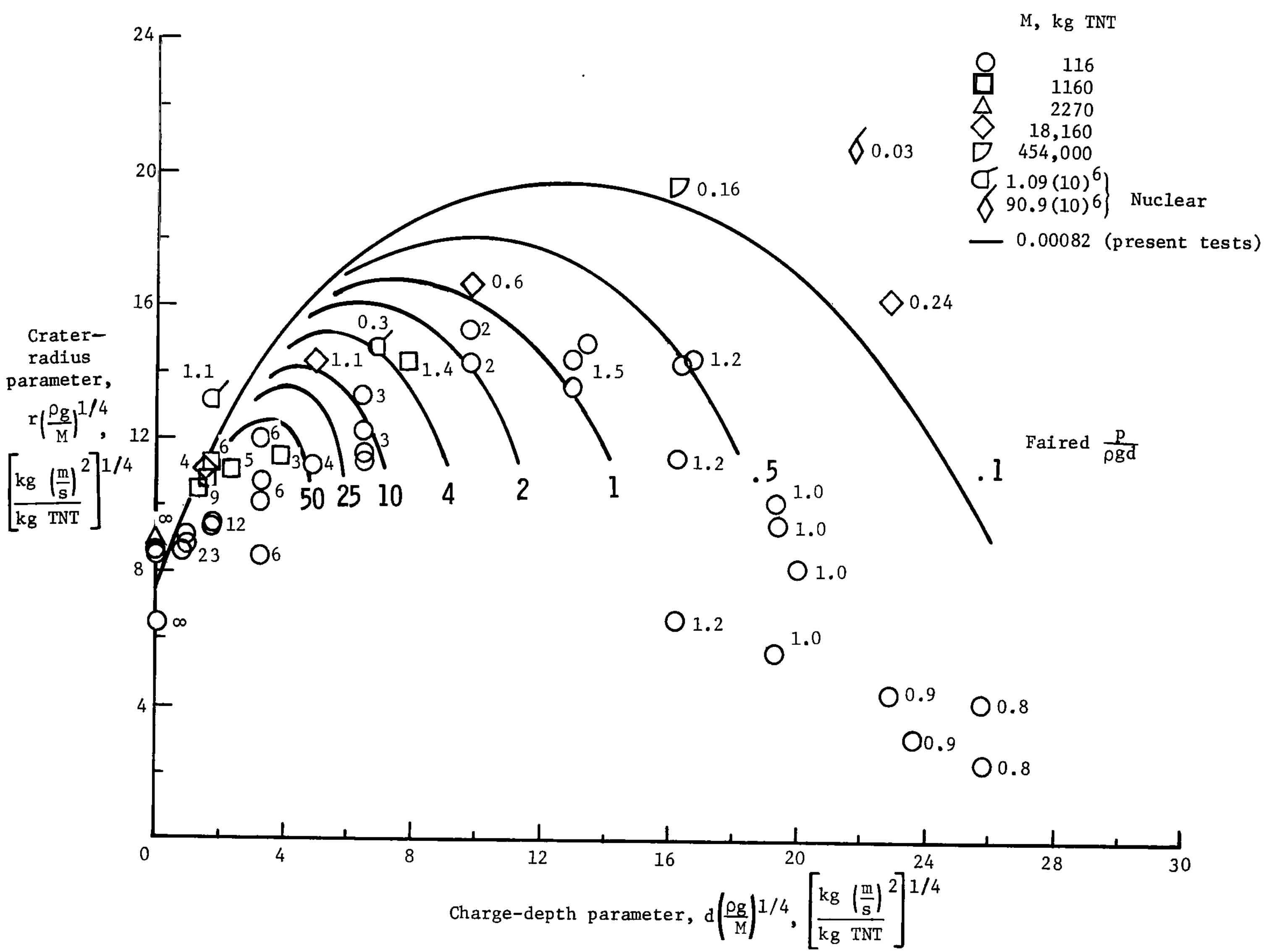

(a) Crater radius.

Figure 19.- Comparison of the dimensions of small-scale craters in sand with large-scale craters in alluvium by fourth-root scaling.

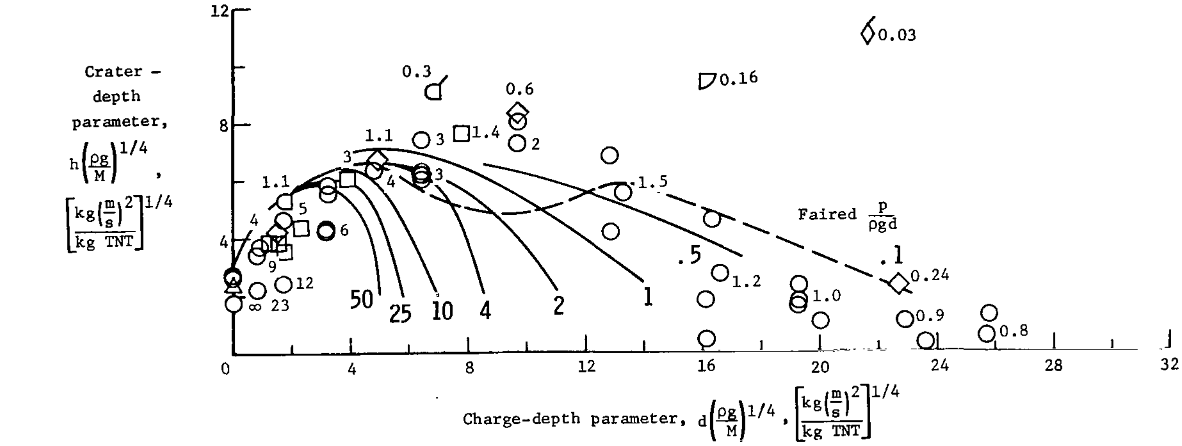

(b) Crater depth.

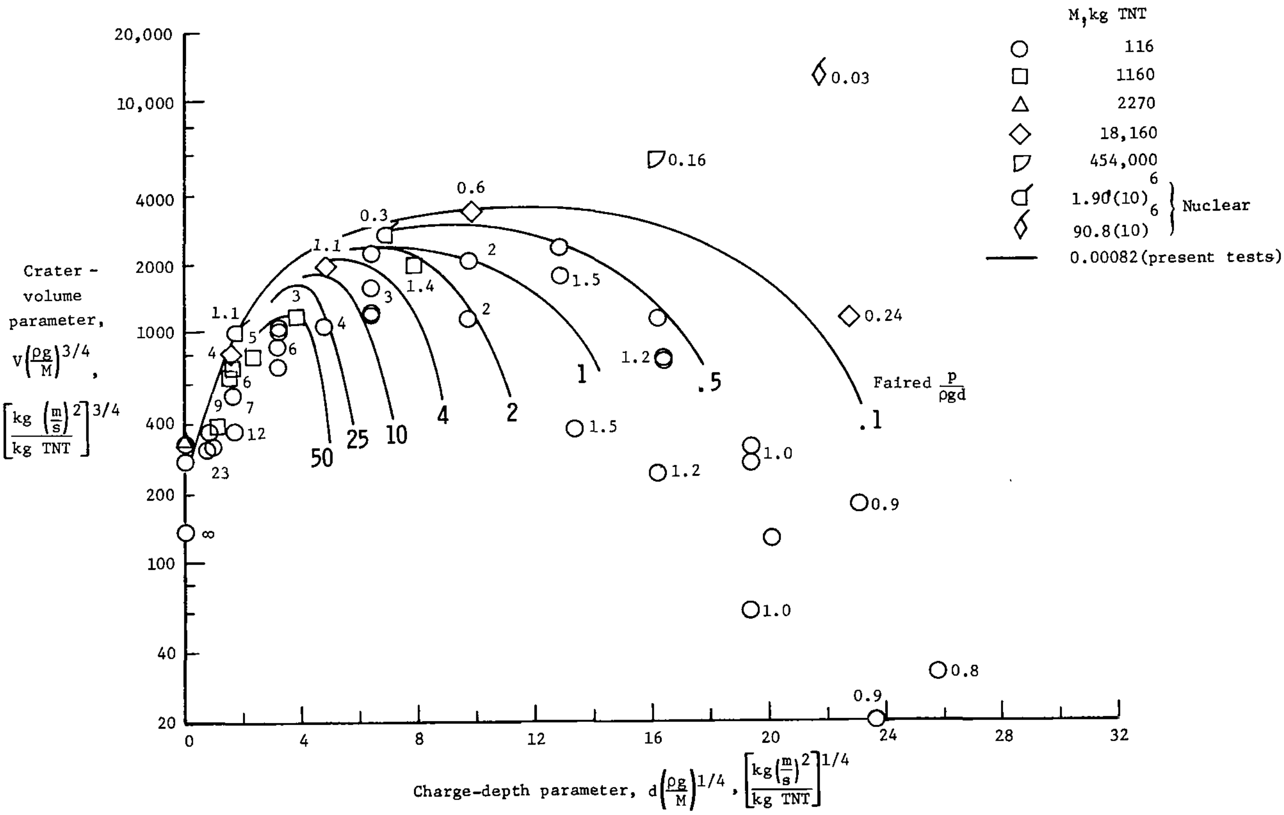

(c) Crater volume.

Figure 19.- Concluded.

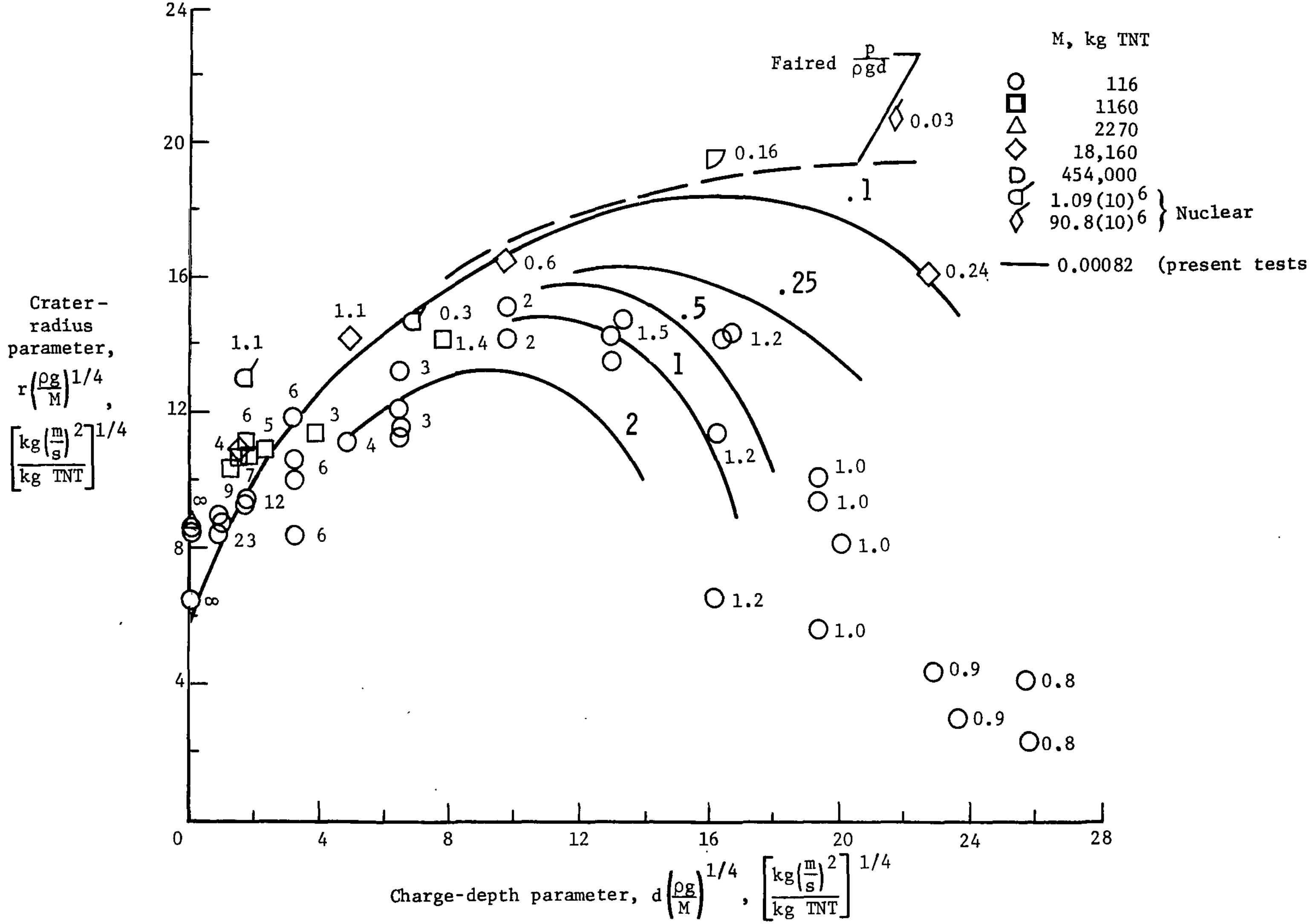

(a) Crater radius.

Figure 20.- Comparison of the dimensions of small-scale craters in ground limestone with large-scale craters in alluvium by fourth-root scaling.

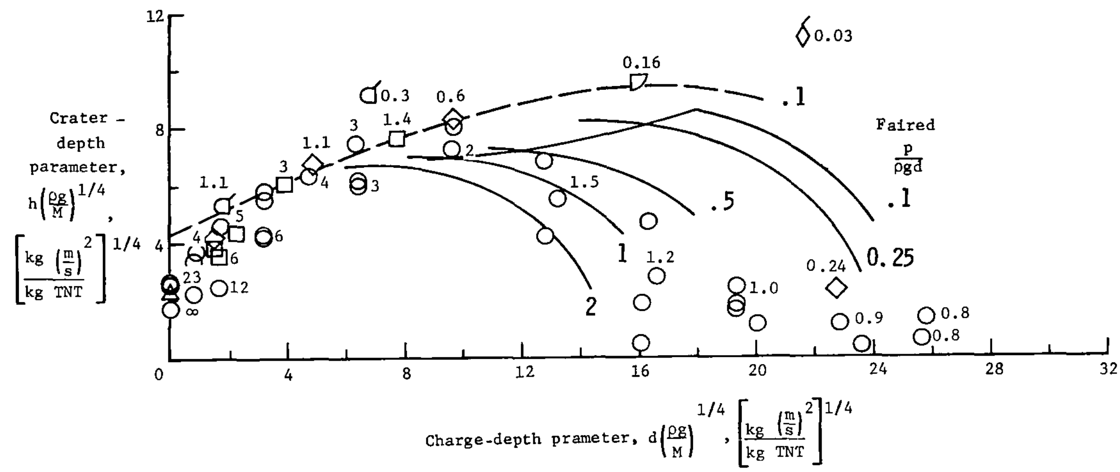

(b) Crater depth.

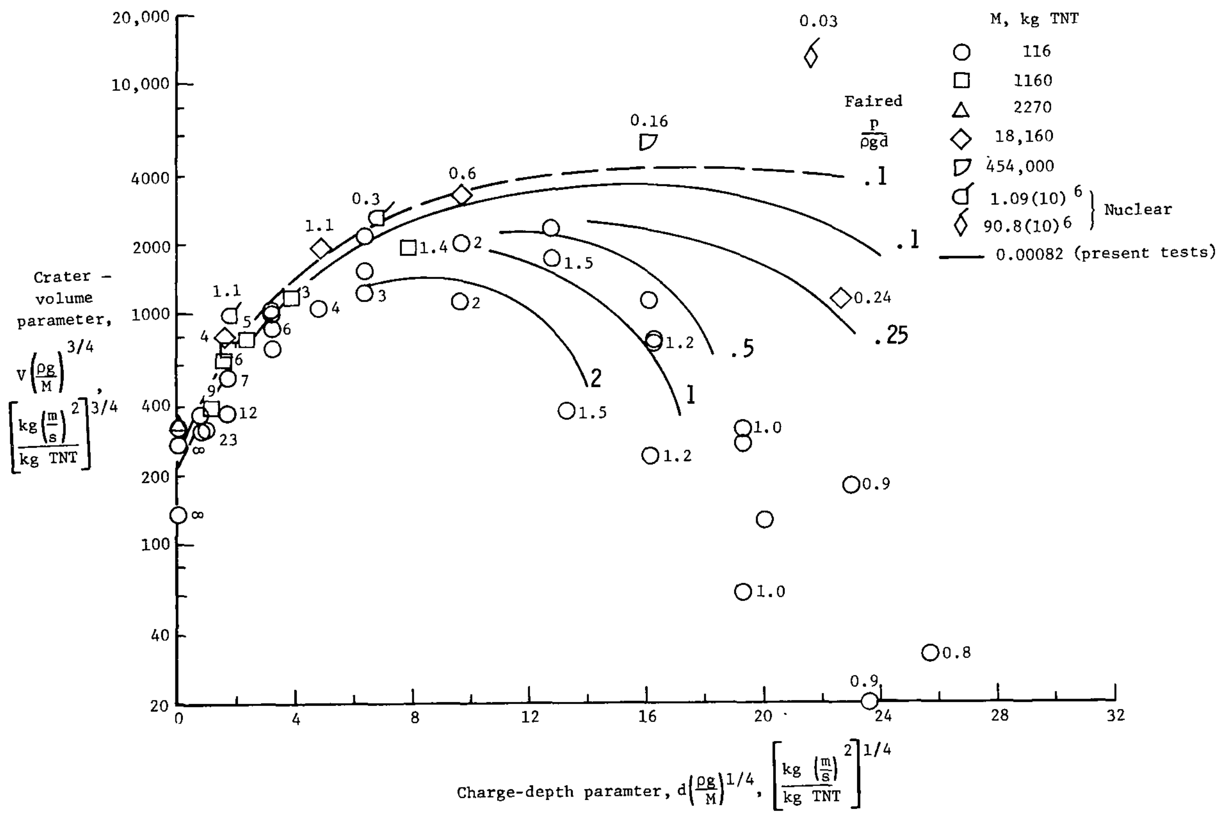

(c) Crater volume.

Figure 20.- Concluded.

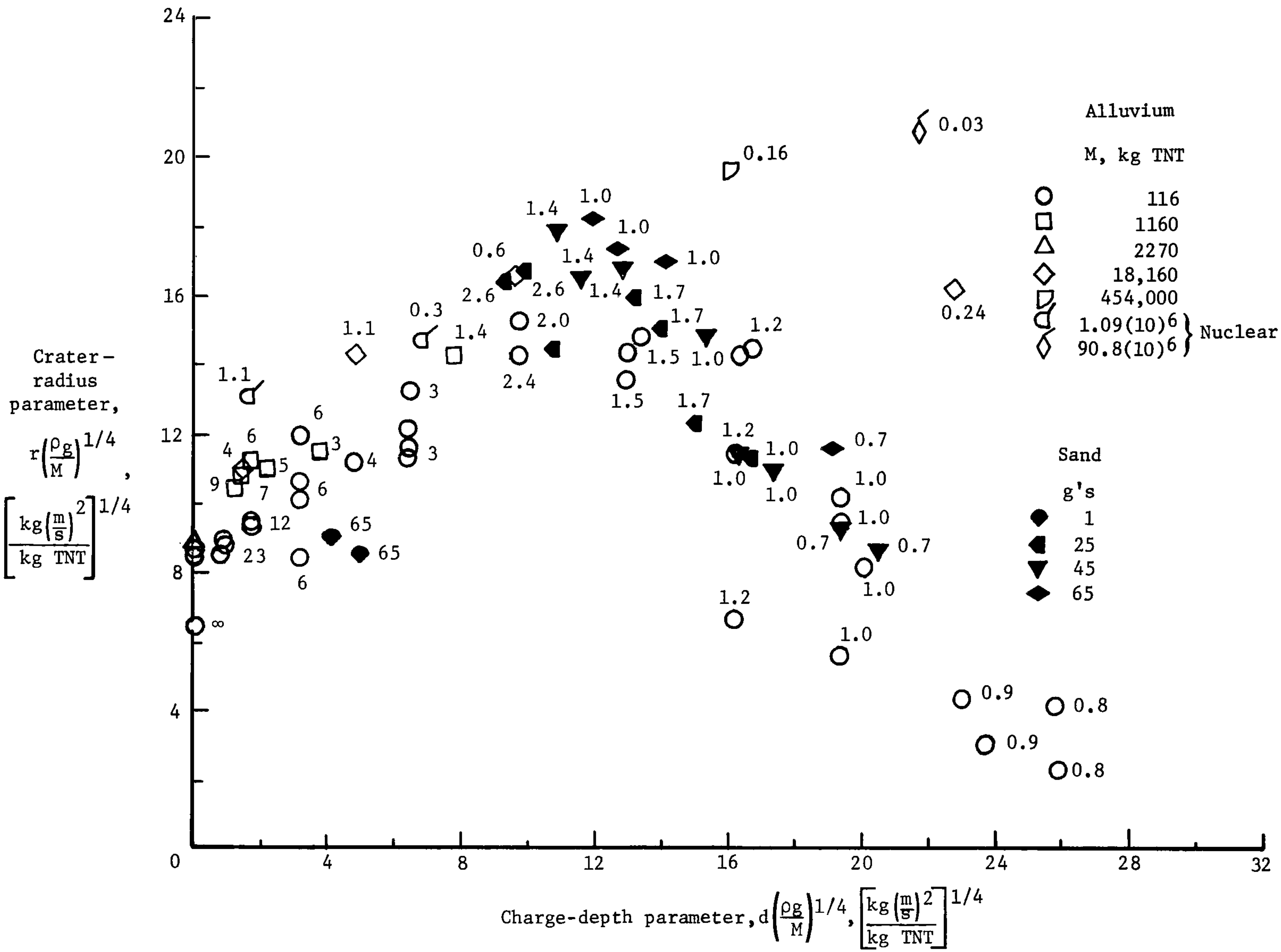

(a) Crater radius.

Figure 21.- Comparison of large-scale alluvium cratering data with small-scale, high-g data in sand of reference 3, where $\rho = 1650\ kg/m^3$ and $M = 0.0027$ to 0.008 kg TNT.

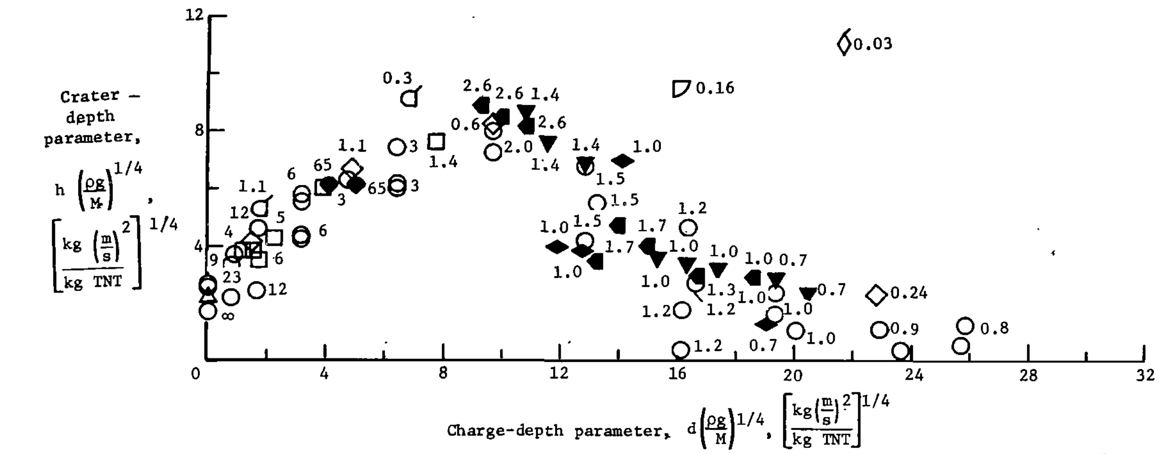

(b) Crater depth.

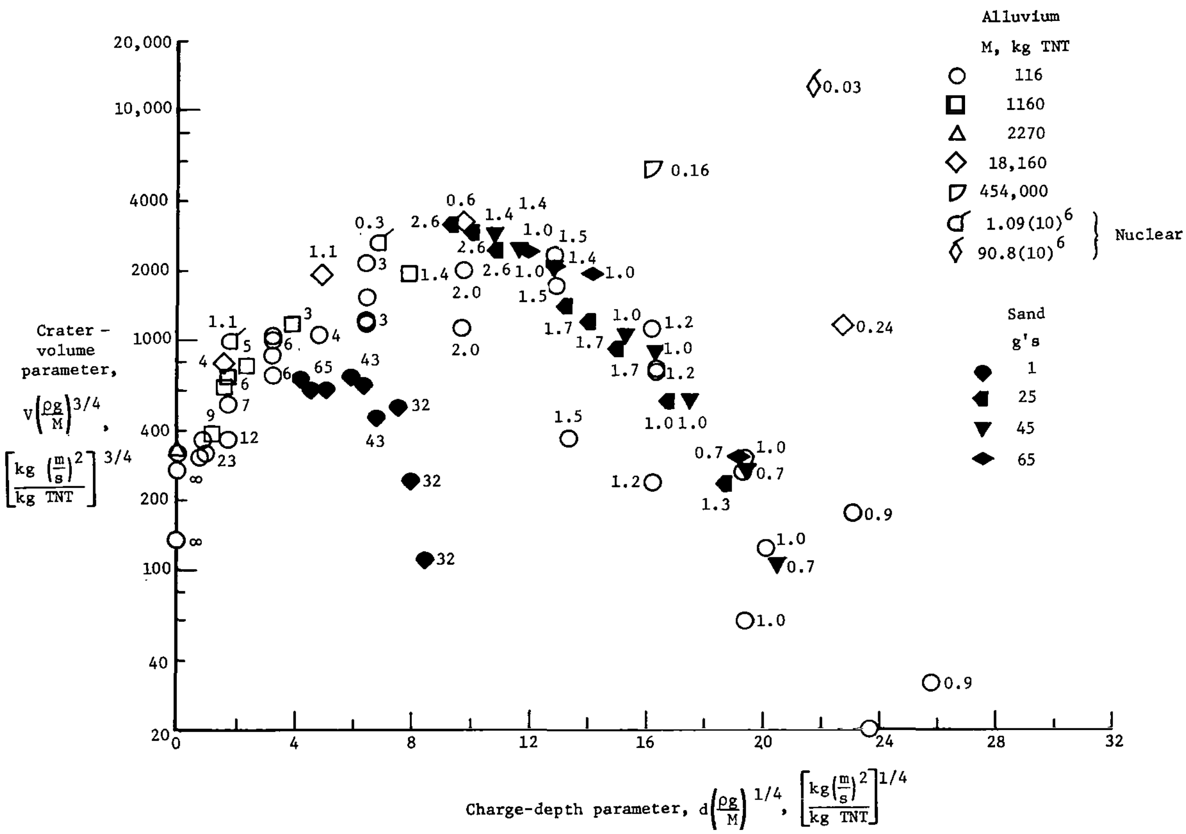

(c) Crater volume.

Figure 21.- Concluded.

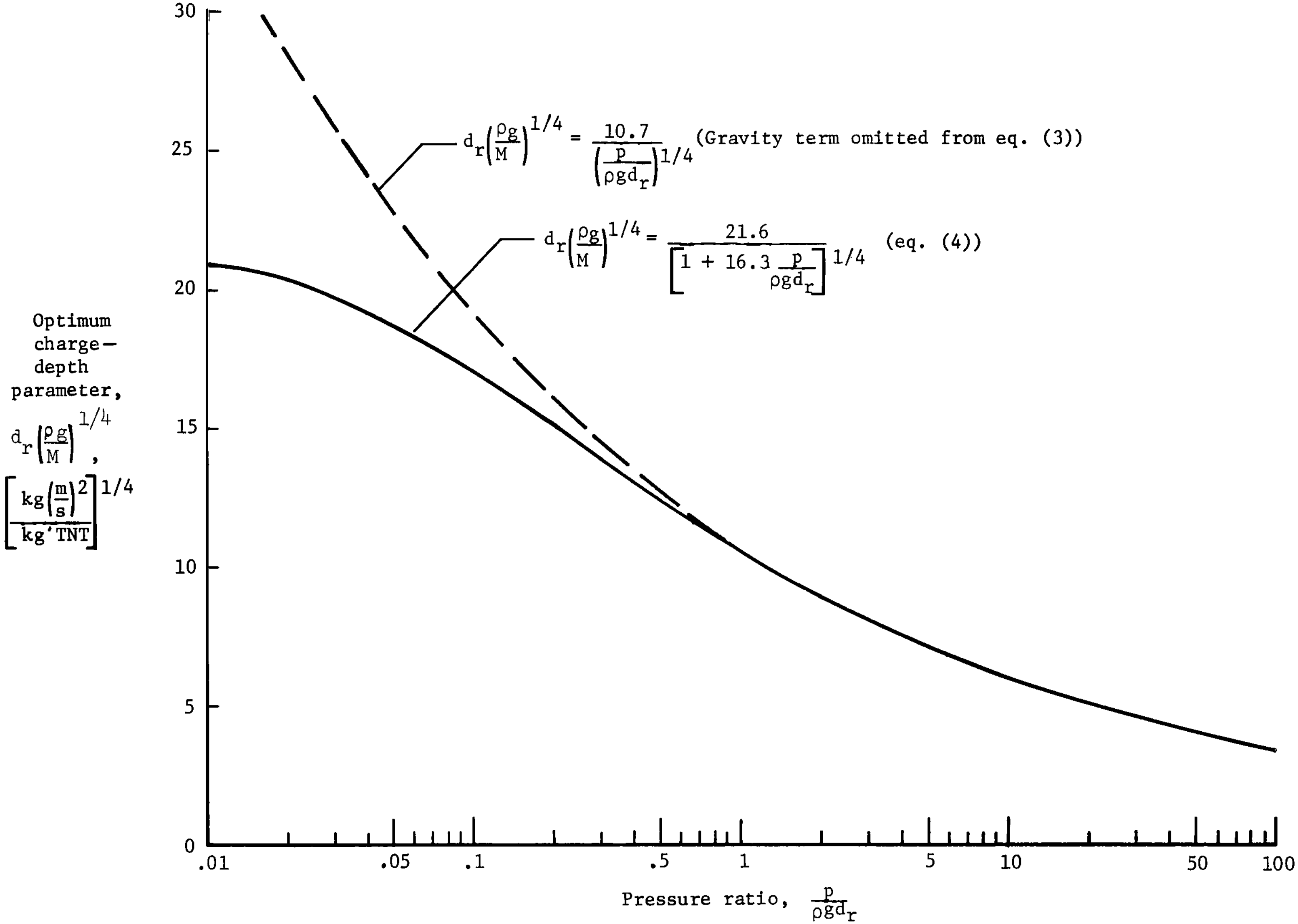

Figure 22.- Optimum scaled charge depth in dry particulate soil as a function of the ratio of the atmospheric to lithostatic pressure.

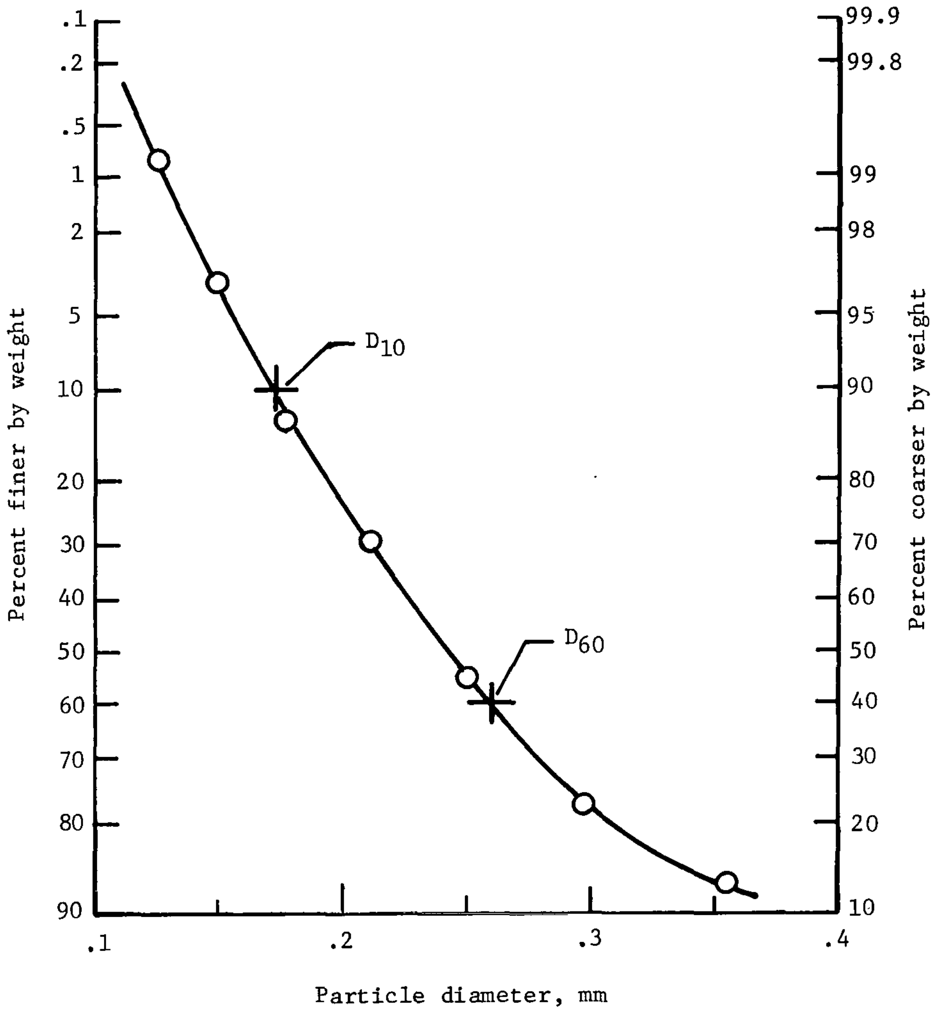

Figure 23.- Particle-size distribution curve for sand.

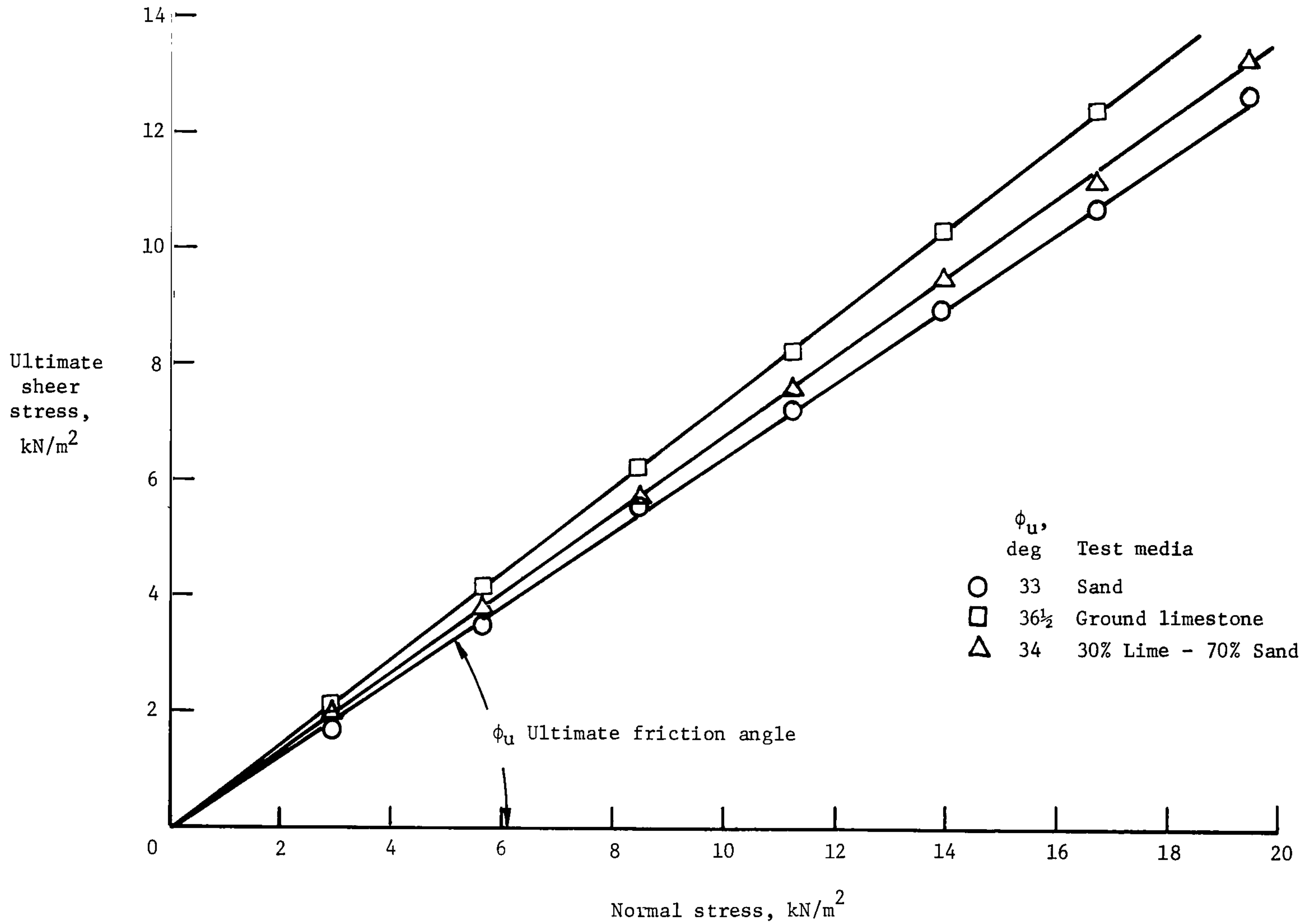

Figure 24.- Results of direct shear tests on test media.

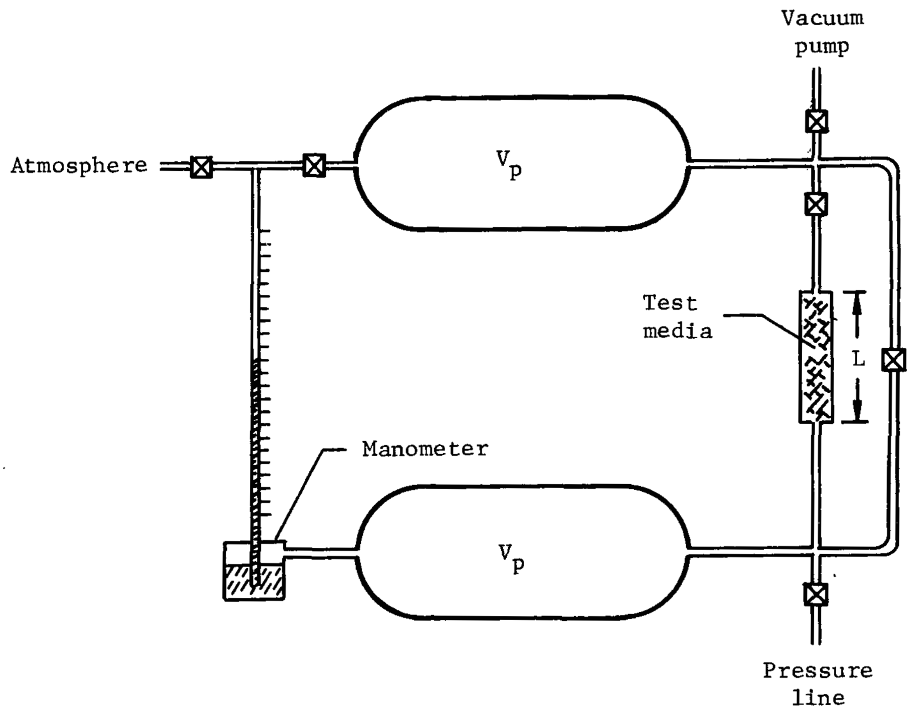

Figure 25.- Apparatus used for determination of permeability of test media to air.

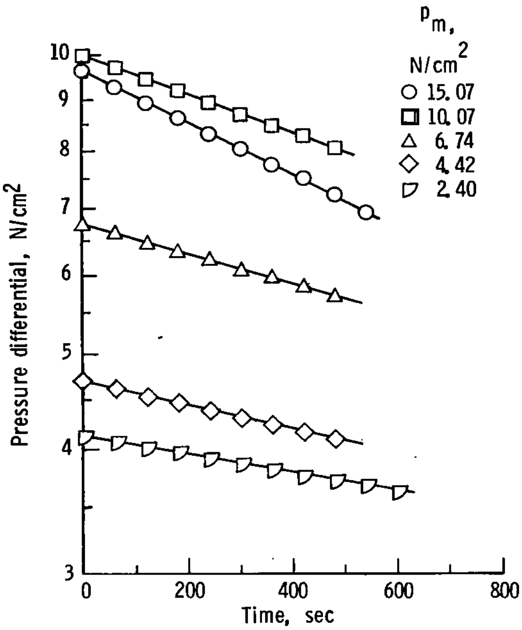

(a) Ground limestone; ρ = 1600 kg/m^3; L = 13.7 cm; A = 20.25 cm^2; V_p = 10 820 cm^3.

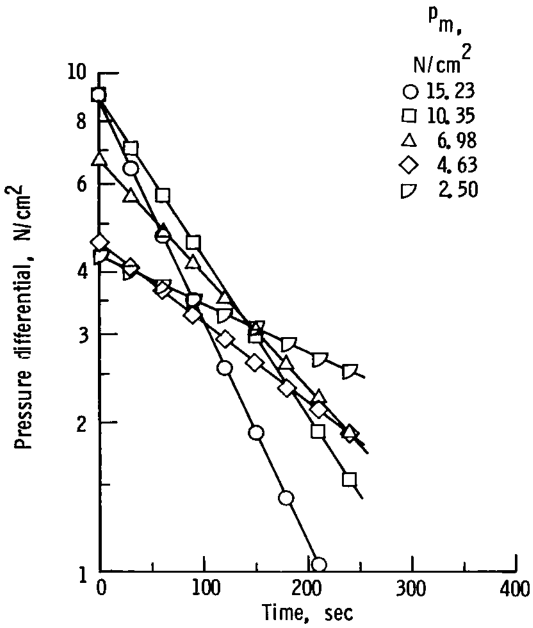

(b) Mixture of 30% limestone and 70% sand; ρ = 1680 kg/m^3; L = 13.7 cm; A = 20.25 cm^2; V_p = 10 820 cm^3.

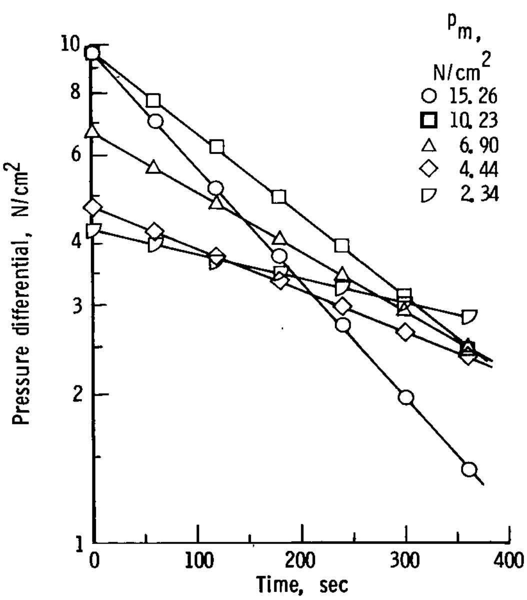

(c) Mixture of 30% limestone and 70% sand; ρ = 1680 kg/m^3; L = 2.54 cm; A = 1.98 cm^2; V_p = 10 820 cm^3.

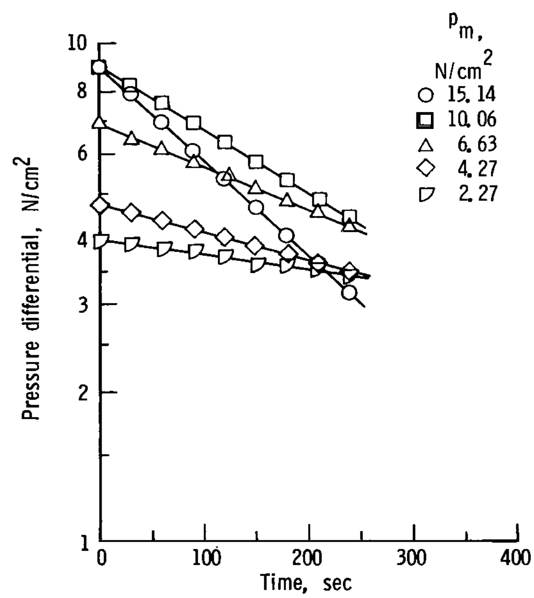

(d) Sand; ρ = 1655 kg/m^3; L = 142 cm; A = 1.98 cm^2; V_p = 10 820 cm^3.

Figure 26.- Pressure differential across samples of test media as a function of time for several values of mean pressure.

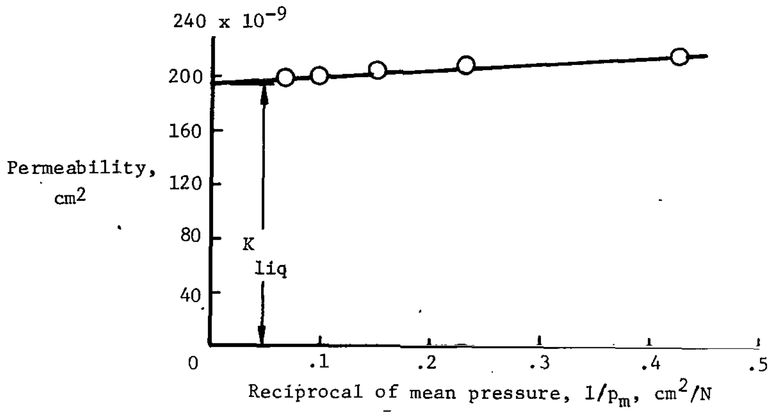

(a) Sand; ρ = 1655 kg/m^3; L = 142 cm; A = 1.98 cm^2; V_p = 10 820 cm^3.

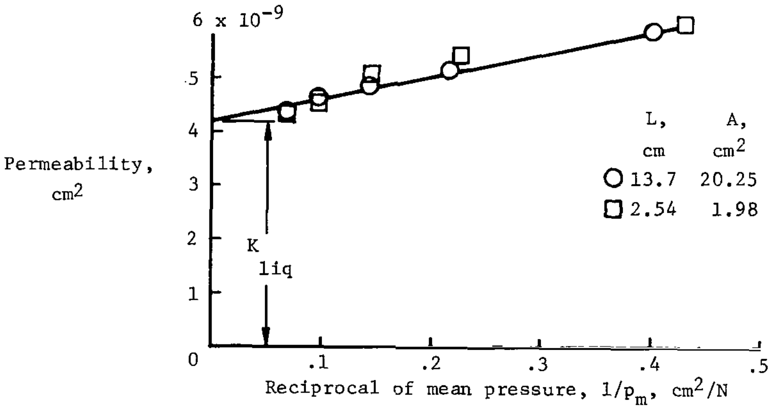

(b) Mixture of 30% limestone and 70% sand; ρ = 1680 kg/m^3; V_p = 10 820 cm^3.

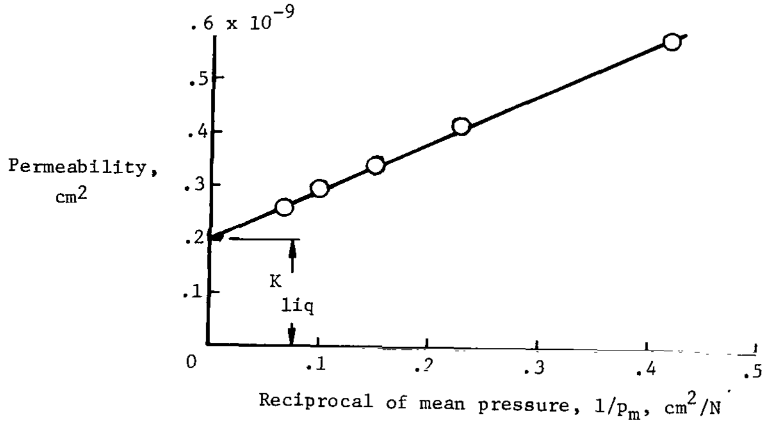

(c) Ground limestone; ρ = 1600 kg/m^3; L ≈ 13.7 cm; A = 20.25 cm^2; V_p = 10 820 cm^3.

Figure 27.- Permeability of test media to air as a function of the mean pressure.

NASA-Langley, 1971 —— 13 L-7380

NATIONAL AERONAUTICS AND SPACE ADMINISTRATION
WASHINGTON, D. C. 20546

OFFICIAL BUSINESS
PENALTY FOR PRIVATE USE $300

FIRST CLASS MAIL

POSTAGE AND FEES PAID
NATIONAL AERONAUTICS AND
SPACE ADMINISTRATION

022 001 C1 U 13 710903 S00903DS
DEPT OF THE AIR FORCE
AF SYSTEMS COMMAND
AF WEAPONS LAB (WLOL)
ATTN: E LOU BOWMAN, CHIEF TECH LIBRARY
KIRTLAND AFB NM 87117

POSTMASTER: If Undeliverable (Section 158 Postal Manual) Do Not Return

"The aeronautical and space activities of the United States shall be conducted so as to contribute . . . to the expansion of human knowledge of phenomena in the atmosphere and space. The Administration shall provide for the widest practicable and appropriate dissemination of information concerning its activities and the results thereof."

—NATIONAL AERONAUTICS AND SPACE ACT OF 1958

NASA SCIENTIFIC AND TECHNICAL PUBLICATIONS

TECHNICAL REPORTS: Scientific and technical information considered important, complete, and a lasting contribution to existing knowledge.

TECHNICAL NOTES: Information less broad in scope but nevertheless of importance as a contribution to existing knowledge.

TECHNICAL MEMORANDUMS: Information receiving limited distribution because of preliminary data, security classification, or other reasons.

CONTRACTOR REPORTS: Scientific and technical information generated under a NASA contract or grant and considered an important contribution to existing knowledge.

TECHNICAL TRANSLATIONS: Information published in a foreign language considered to merit NASA distribution in English.

SPECIAL PUBLICATIONS: Information derived from or of value to NASA activities. Publications include conference proceedings, monographs, data compilations, handbooks, sourcebooks, and special bibliographies.

TECHNOLOGY UTILIZATION PUBLICATIONS: Information on technology used by NASA that may be of particular interest in commercial and other non-aerospace applications. Publications include Tech Briefs, Technology Utilization Reports and Technology Surveys.

Details on the availability of these publications may be obtained from:

SCIENTIFIC AND TECHNICAL INFORMATION OFFICE

NATIONAL AERONAUTICS AND SPACE ADMINISTRATION

Washington, D.C. 20546